FINAL REPORT

CONTRACT NAS9-11934

MULTI MODE OPTICAL SENSOR

MMOS

SUBMITTED TO

NASA

JOHNSON SPACE CENTER

JUNE 1973

ITT Gilfillan
7821 Orion Avenue, P.O. Box 7713
Van Nuys, California 91409

6906

FINAL REPORT

MULTI MODE OPTICAL SENSOR
MMOS

SUBMITTED TO

NASA

JOHNSON SPACE CENTER

CONTRACT NAS9-11934

JUNE 1973

ITT GILFILLAN
7821 Orion Avenue, P.O. Box 7713
Van Nuys, California 91409

TABLE OF CONTENTS

TABLE OF CONTENTS
(Continued)

LIST OF FIGURES

LIST OF TABLES

1.0 INTRODUCTION

The development of a Multi-Mode Optical Sensor (MMOS) for use on the Space Shuttle Vehicle (SSV) has been completed. The delivery of the second engineering model in May 1973 culminates a program at ITT Gilfillan initiated in July 1971. During this 22-month program, ITTG developed, designed, built and tested two MMOS models. Also since April 1972, NASA/JSC has conducted extensive evaluation tests on the first MMOS (hereafter referred to as MMOS A). Based upon changes in the SSV concept and results of these tests on MMOS A, revisions, improvements and additions have been incorporated in a second MMOS (hereafter referred to as MMOS B).

Section 1.0 of this final report addresses the objectives, accomplishments and history of the program. Based upon the program accomplishments, a projection of MMOS performance is made in the form of recommendations as to where improvements can be realized.

Section 2.0 presents a detailed description of MMOS B. Since all the operational modes of MMOS A are provided by the second model, this also suffices to describe MMOS A. The difference between the two models is treated briefly in Section 2.4.

Section 3.0 is a collection of design studies, trade-off studies and test program results conducted during the program. In most cases, the results apply to MMOS B although in the area of turn-on stability and field

map accuracy, characteristics of MMOS A are included in order to emphasize the improvement achieved.

Section 4.0 is a description of the Acceptance Tests conducted at ITTG on each of the models.

1.1 PROGRAM OBJECTIVES

The Multi-Mode Optical Sensor is intended for possible application on the SSV. Its uses are expected to include alignment of an inertial reference unit (IRU) to known stars, and orbital and rendezvous navigation. To accomplish the function of orbital navigation, it was necessary to include a horizon profile radiometer mode in the sensor. With this capability, it is possible to align the IRU using the star tracker mode and then take an earth horizon profile measurement, reduce the data in an on-board computer and use the result to perform orbital position determination. Additional navigation capability by means of the landmark tracking mode might be afforded by use of correlation techniques to process real-time video from the MMOS.

For rendezvous navigation, full field acquisition and tracking of both cooperative and non-cooperative targets is provided. In the event of a priori position information, the on-board computer will command acquisition of the target vehicle, both cooperative and non-cooperative, by directing the re-acquisition search field to the expected angular position of the target. Use of the real-time video to obtain pictorial data for display to the flight crew could be of extra assistance in operational situations.

The objective of the MMOS program was to develop, design, build, test and deliver an engineering model SSV MMOS. Based upon its projected uses, the model was to have the following minimal capabilities:

- Full field acquisition of the brightest star
- Star tracking over the full field

- Re-acquisition of a star under internal and external control
- Radiometric indication of the ultra-violet horizon profile
- Full field acquisition, re-acquisition, tracking and identification of a xenon rendezvous beacon
- Full field acquisition, re-acquisition and tracking of an extended target
- Real-time video presentation for a full field star map
- Real-time video presentation for a full field with radiometric indication of scenes up to 10,000 ft.-lambert brightness
- Real time video presentation for a limited field with radiometric indication of bright scenes while accepting external control of the limited field location within the full field (landmark tracking).

Initially in the program there were two primary objectives; namely,

1) determine an optimum field-of-view dependent upon the tracking accuracy attainable over that entire field, and
2) determine the feasibility of combining the horizon profile radiometer with a star tracker.

As background information, analysis by NASA/JSC had indicated than an accuracy equal to or less than one arc minute was necessary to satisfy SSV requirements. A square field-of-view, 17 degrees on each side, is considered optimum, giving about a 60 percent probability of having a star brighter than third visual magnitude in the field for any random orientation. Since the ideal lens for the specific image dissector (F4012) would be an expensive custom design and since the accuracy

requirements were preliminary, NASA specified the field-of-view requirements generally while keeping accuracy requirements consistent with anticipated SSV requirements. Evaluation test data on the engineering model was to be used to extrapolate a final field-of-view for the flight configuration MMOS.

Use of a single component to perform star tracking and horizon profile readout provides advantages of less weight, volume, cost and less complexity of alignment and checkout. NASA had determined that within the spectral range of the optics and S-20 photocathode, there is a spectral range where the horizon radiance profile is sufficiently defined to serve as the SSV navigation reference. The spectral range was specified as $0.38 \pm .01$ microns.

It was an objective of the program then, to determine if a combination star sensor-horizon sensor was feasible. The penalties in performance, if any, to be paid in one or the other modes were to be determined. The risks of potential damage, temporary or permanent, due to viewing a source giving the sensor an irradiance of approximately 10^6 times that of the dimmest star to be tracked was to be determined.

Following test and delivery of MMOS A, the objectives in performance of MMOS B changed slightly. Although the feasibility of 1 arc minute map accuracy was proven on the initial model, accuracy remained of primary importance. With respect to accuracy, techniques were sought to improve the map even further and reduce a turn-on drift which became evident in testing of MMOS A.

Additional operational modes were also added to the MMOS B. Although the performances in these modes were primarily design goals, an objective was to provide this added capability without deleterious effects to the performance of the original modes.

The objectives stated in terms of MMOS performance parameters are given in detail in Section 4.0. The specified and demonstrated performance during Acceptance Tests is presented along with explanations as required.

1.2 PROGRAM ACCOMPLISHMENTS

MMOS B, delivered to NASA/JSC in May 1973, provided all the operational capabilities described in the preceding section. In Acceptance Tests, run prior to delivery, performance in the star tracker and horizon radiometer modes was comparable or exceeded that demonstrated one year earlier by the MMOS A model. Feasibility of one arc minute accuracy over the full field and compatibility of a star sensor-horizon sensor in an integral package had been demonstrated on MMOS A.

The full field of the MMOS is 10^{o} x 10^{o}. In combination with the optics this transforms to 0.35 inch x 0.35 inch linear dimension of the sensor photocathode. For the F4012 having a 0.7 inch usable diameter, this represents 70% of the photocathode (considering the field diagonal).

The major contributor to position output non-uniformity is the focus-deflection coil component. For economic and delivery reasons, an off-the-shelf design previously used on the ITTG Optical Data Correctors was used on MMOS A. Initial field map data displayed gradient non-linearities of up to $\pm 2.5\%$ at the field extremes. Electronic compensation circuitry was incorporated to reduce the field map non-uniformities. By this method, the peak error demonstrated by MMOS A was 1 arc minute. Subsequent tests by NASA/JSC indicated an RMS error of 35 arc seconds over the 10^{o} square field.

Although anticipated, the care in test methods and equipment use necessary to demonstrate arc minute accuracy over a large field was further established during the MMOS A testing program. In order to effect

stability, a mount was used that caused a temperature rise of 30°F to the model. During the temperature transition, the MMOS A exhibited position output shifts of approximately 1 arc minute. This drift was not included as a component for the accuracy stated.

Based on the MMOS A experience, a significant effort was made to:

1) improve the focus-deflection coil field uniformity, and
2) decrease the turn-on (or warm-up) drift

A coil was designed with parameters based on specific MMOS requirements. Three performance improvements were realized; namely,

1) a power reduction of 50%
2) a position uniformity improvement of 50%
3) improved video output uniformity.

An extensive test program of position output drift as a function of temperature was undertaken. Tests were conducted on both models. As a result of the tests (detailed in Section 3.6), a temperature compensation circuit was added on MMOS B.

Through the above efforts, MMOS B demonstrated improved accuracy over MMOS A. A peak error of 53 arc seconds was measured with a preliminary RMS error of 20 arc seconds. A turn-on drift of 10 arc seconds peak was measured, starting within 5 minutes after turn-on and extending for several hours.

It is noted that in addition to proving 1 arc minute accuracy, an improvement was effected on MMOS B. It appears certain that additional modifications could be made to the coil design such that even further improvements in accuracy and stability could be realized.

The incorporation of a UV horizon radiometer with a star sensor is possible by effectively reducing the sensor sensitivity for the radiometer mode. The method used on the MMOS was to optically attenuate

between the optics and photocathode and to reduce the tube gain. Some curve shaping of the tube video output was used to provide an output uniformity of ±3%.

In addition to proof of feasibility of the horizon sensor-star sensor concept, a significant step was taken on the Phase B model with respect to the filter insertion movement. The mechanism required to position the UV filter and the optical attenuator needed for several new MMOS B modes was designed and built with components that are adaptable for flight model usage.

1.3 RECOMMENDATIONS

Based on the work on the MMOS program and on test results of both engineering models, certain observations and recommendations can be made. These recommendations are general and address areas that should have consideration in building a flight model.

1.3.1 Package Size and Outline

Since the end result of this contract was an engineering model to establish the feasibility of performance outlined in the preceding section, the package size was not of prime concern. The package size used was as proposed originally. It became evident on MMOS A that not all board space was needed and the overall package size might be reduced.

It was decided to make MMOS B the same size as the initial model because of extra circuits needed for the additional modes and to allow use of the same mounting fixtures. Even with additional circuits, not all board space was needed. Dependent upon the final flight model requirements, it is probable that a decrease in package size and weight could be accomplished. The size reduction could be effected in either diameter or length. It is recommended, however, that the reduction be made in length.

In order to facilitate alignment and stability, the flight model should use a single flange near the MMOS center of gravity for mounting. The ring would contain 3 or 4 pads for mounting to ensure alignment (±5 sec) in two axes. In order to reduce the cantilever effect and minimize the buildup of vibrational resonances, the MMOS length should be minimized. It is noted that use of the Angenieux lens and F4012 image dissector set the minimum length at approximately 12 inches.

By reducing the package size, a corresponding weight reduction should also occur. However, this cannot be predicted until the mounting method has been specified.

1.3.2 Position Output Accuracy

A significant improvement in accuracy was made between MMOS B and MMOS A. A close examination of the uncorrected field map (refer to Figure 3-13) indicates that the accuracy of ±1 arc minute was attained without electronic correction for all but the peripheral test angles.

It is anticipated that the next generation coil assembly would again substantially improve field map uniformity. The basis for this is not only initial improvement of the MMOS B coil over the MMOS A coil but also that the MMOS B coil itself has much better linearity in the Y axis than the X axis. It is highly probable that a slight design change in the deflection coil would allow the X linearity to equal that already displayed in the Y axis.

From the MMOS B results, one might also project a field size over which the ±1 arc minute accuracy could be met. Based on using the same correction area size ($5/8^{\circ}$ x $5/8^{\circ}$) the field-of-view could be increased to 14° diameter. If correction were used only in that portion of the field necessary (annular ring from 10° to 14° diameter) no additional electronic correcting circuitry would be necessary.

Another goal of the second generation coil assembly should be stability with temperature. Position drift as a function of coil temperature was significant enough to measure. It is anticipated that better encapsulation would improve the stability.

The lens housing interface was also a large contributor to the temperature instability. It is projected that a different means of securing the lens into the adapter would effect a significant improvement.

1.4 PROGRAM HISTORY

Following is a brief chronological description of the MMOS Program.

June 30, 1971	Contract award
July 1, 1971	Preliminary design review at NASA/JSC. Radiometer implementation concept changed slightly by use of a mechanically driven UV filter rather than use of a permanent filter deposited on the tube photocathode.
October 4, 5, 1971	Critical design review at ITTG. No significant changes are made to the MMOS design.
December, 1971	Initial position output map taken. ITTG proposes to use electronic compensation to effect 1 arc minute accuracy.
February 18, 1972	Contract award of the B phase of the program.
March, 1972	Mounting instabilities become evident. This is in addition to a circuit intermittent and power line interference causing one month delay in Acceptance Tests.
April 17-20, 1972	Acceptance Tests on MMOS A completed. All specifications are satisfied with the exception of power and weight.

April 28, 1972	MMOS A delivered to NASA/JSC
May 12, 1972	Preliminary design review for MMOS B held at NASA/JSC. Minor changes made to the new modes. Possibility of landmark track mode is added for ITTG review. Possibility of building a completely new model is discussed.
June, 1972	Decision is made that MMOS B will be a new unit keeping MMOS A intact. Mode descriptions and operation are defined.
August, 1972	MMOS A is returned to ITTG for temperature tests. Tests are continued into September.
Sept. 14, 1972	Critical design review for MMOS B held at ITTG. No significant changes are made to the design.
December, 1972	Extensive testing is made to determine source of turn-on drift. A compensation circuit is designed to minimize position output drift.
January, 1973	Filter insertion mechanism altered to provide better registration of position. Acceptance testing delayed.
April 25 -27, 1973	Acceptance tests on MMOS B completed. Performance satisfactory with accuracy improvement over MMOS A.
May, 1973	MMOS B delivered to NASA/JSC.

2.0 MMOS DESCRIPTION

The Multi-Mode Optical Sensor (MMOS) is an electro-optical component designed to provide information to the Space Shuttle Vehicle (SSV). Orbital navigation of the SSV is effected by use of the MMOS star tracking capability to align an inertial reference unit and its ultraviolet radiometer capability to take an earth horizon profile measurement. Rendezvous navigation is effected by use of the MMOS extended target tracking capability for non-cooperative targets and its beacon tracking capability for cooperative targets. Assistance to the flight crew in operational situations is provided by a display of the MMOS video output in any of its mapping modes.

The operation of the MMOS with respect to its many modes is automatic or can be controlled by external commands. In the same manner, its operational status is provided and displayed to allow flight crew control.

2.1 FUNCTIONAL DESCRIPTION

Basically, the MMOS is a single integral electro-optical component designed to alternately function as

- a star tracker which acquires and accurately tracks radiative point sources,
- a UV radiometer which accurately measures the earth horizon profile,

- a target tracker which acquires and accurately tracks a cooperative Xenon beacon source,
- a target tracker which acquires and tracks non-cooperative radiative extended sources, and
- a camera which provides a radiative profile of the scene being viewed.

While operating in any of the modes, the MMOS provides its own protection to prevent permanent damage due to highly intense radiative sources. By sensing the image dissector anode current, a latching protection of two steps by attenuation in the optical path and decrease of the multiplier gain protects the image dissector. By sensing the resistance change of two photoconductive cells, a shutter insertion in the optical path and removal of the image dissector image section voltage protects the image dissector from the sun.

A general block diagram of the MMOS B is presented in Figure 2.1. The MMOS consists of three basic units; optics, sensor and electronics. The purpose of the optics is to collect and image radiant energy on the sensor element, i.e., the image dissector photocathode surface. The optical sensor field-of-view is a function of the optics focal length, and its sensitivity a function of the aperture of the optics.

The heart of the optical sensor is an image dissector tube. The photocathode forms an electron image of the optical image focused on its surface. Behind the photocathode is an aperture mask and secondary emission dynodes capable of amplifying a signal up to 10^7 times. The image dissector is constructed so that when an accelerating voltage is applied between the photocathode and a mechanical limiting aperture, only those electrons leaving a specific area on the photocathode will pass through the limiting aperture. This area is called the instantaneous photocathode dimension (IPD). When a target image is positioned on the photocathode by the lens, a small stream of electrons is formed by the

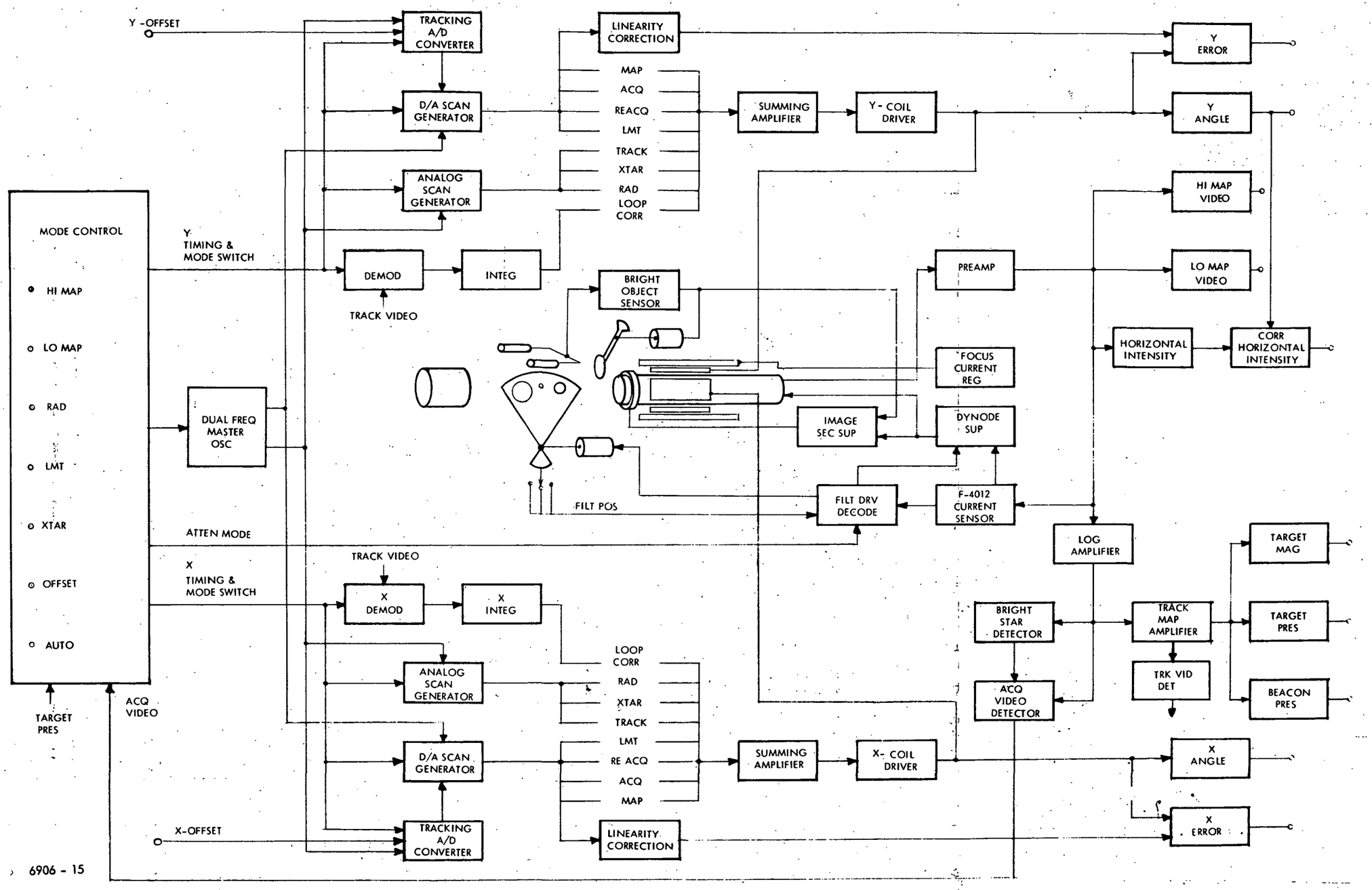

Figure 2-1. Multi-Mode Optical Sensor

electron optics of an electromagnetic focusing field. A deflection coil is positioned around the image section to provide magnetic deflection of the target image electron beam. Be applying proper deflection coil currents, the electron beam is swept back and forth across the limiting aperture, causing a modulation of the electron beam. The IPD, when projected through the optics, represents a region in space defined as the instantaneous field-of-view (IFOV). It is defined by the simple geometric relationship:

$$\tan \frac{\text{IFOV}}{2} = \frac{\text{IPD}}{2 \times \text{lens focal length}}$$

The region of space covered when scanning deflection currents are applied represents the total search or acquisition field-of-view (AFOV).

The electronics make up the majority of elements of Figure 2-1. They consist of both digital logic and analog circuits that perform:

Mode control logic
Search sweep generator
Track sweep generator
Horizon sweep generator
Video amplification and target selection
Track loop control
Output error filtering and amplification
Attenuator vane position decoder
Attenuator vane motor driver
Power conversion and regulation
Protection signal amplification and control
High voltage generation

2.1.1 Star Tracker Operation

As a star tracker, the MMOS is a two-axis, dual-mode star tracker designed to precisely measure the angle between its boresight

axis and the line-of-sight to a target. The MMOS provides target position information in two axes, mutually perpendicular to its boresight axis.

The MMOS has the unique features of previous ITT electric-optical trackers, namely:

- Ability to scan a large field-of-view
- Ability to select the brightest star in the field-of-view
- Ability to provide position information of excellent resolution and accuracy
- Automatic switching between track and acquisition mode of operation
- Provision for manual override of automatic functions
- Ability to search a limited field-of-view at loss of track.

Explanation in detail of the ITTG MMOS is best presented by describing the operational sequence normally encountered. Note that for the star tracker modes of acquisition, tracking and reacquisition, the horizon and map mode functions are disabled.

Acquisition - Initially, the MMOS is in the search or acquisition mode of operation. The search generator produces a digital raster scan covering the central portion of the phtocathode. With a two-inch focal length lens, the 10^{o} x 10^{o} angular dimension represents 0.35 inch x 0.35 inch linear dimension on the photocathode.

Upon receiving an AUTO command, a "brightest star selection" cycle is begun. As the search scan is executed, the video content at each dwell time is compared to the largest preceding video pulse. Any larger pulse causes an output from the comparator. The output of the comparator opens a set of logic gates in the search scan generator so that the search counter states are transferred into a parallel register.

Upon completion of one frame, the search scan register contains the digital address of the brightest target position. A reset pulse generated by the search scan counter at the end of one complete scan frame:

- Disables the CLOCK from the counter input
- Resets the counters to the digital address of the register
- Enables the CLOCK to trigger the miniscan counter
- Sets the logic circuits of the mode control so that any succeeding video pulses will change the operational mode to tracking.

A miniscan mode is required to compensate for any relative movement between tracker and target during the selection cycle. The miniscan utilizes a negligible portion of the total acquisition time.

Tracking. - Receipt of the first video pulse after the start of the scan about the original address causes the removal of the drive from the miniscan generator. Simultaneously, an analog cruciform scan is employed in the deflection coils and the track loop circuits (demodulator and integrator) are activated. These circuits are grounded during all search modes to preclude drift of the coil current.

The cruciform tracking scan causes pulsewidth modulation of the video signal. The signal is amplified and limited to produce a square wave output. Demodulator circuits develop analog error signals that are proportional to the distance (i.e., the angle) between the center of the cross scan and the center of the target. These error signals and their integral in time are fed to summing amplifiers that generate target position corrections to the initial cross scan position. The track mode is therefore characterized by closed loop control whereby any movement within the AFOV results in an automatic correction to the dc coil current so that the cruciform scan remains centered on the target image.

Target position signals are generated by sampling the actual deflection coil currents. These waveforms are filtered to remove the scan frequencies and then amplified to provide the desired volts per degree transfer function.

Track lock is maintained by noting the presence of the fundamental component in the video signal. This is the proper video frequency for the cruciform frequency and must be present for the tracker to generate meaningful position outputs. Loss of the target-presence signal automatically returns the tracker to the miniscan mode and then to the full acquisition mode.

Re-Acquisition. - Loss of the target-presence signal for any reason other than manual override (to initiate another mode) results in disabling the track loop circuits and initiating a miniscan centered at the last point of tracking. Reacquisition by miniscan rather than another complete selection cycle minimizes reacquisition time.

Since the target was inadvertently lost, and is assumed to be moving at a maximum rate of 0.5^{o} per second, its maximum displacement from the last tracking point is known. To search the immediate area, an 8 x 8 element miniscan covering 1.25^{o} x 1.25^{o} is employed. With a dwell time of 230 μ seconds, the resultant miniscan frame time is 15 milliseconds. Eight scans of the areaare made in search of a target, based on the threshold of the preceding target. If a target has not been acquired after eight scans (about one-eighth of a complete selection cycle), the entire AFOV is searched for the brightest target employing the normal acquisition sequence.

2.1.2 UV Horizon Radiometer

The MMOS radiometer mode does not use the sweeps and video processing circuits of the star tracking modes. When in the Radiometer

mode, the image dissector multipler gain is decreased. A UV filter with a 200 Å bandpass centered at 3800 Å is placed in the optical path between lens and tube. To restrict the optical energy, and to minimize the angle of incidence at the UV filter, the energy from the lens is limited to 0.175" diameter by an aperture in the UV filter holder.

The sweep of the horizon is an 0.2 Hz sawtooth with a $\pm 5^{\circ}$ amplitude in the vertical axis only. The video processing is an amplification of the energy in the IFOV.

2.1.3 Extended Target Tracking Mode

The extended target tracking mode is identical, functionally, to the star tracking mode. The tracking scan pattern is a cruciform as is used for star tracking. so that the modulation is equivalent. As a result, the tracker demodulator and tracking loop circuits are used.

The extended source subtends a maximum angle of 5.7° (100 ft. diameter object at 1000 ft.). The sweep amplitude in the extended target mode is set to 6.3° by controlling the gain of an amplifier. Note that the sweep amplitude is constant regardless of target size, thereby restricting tracking to within 3.2° of the edge of the total field-of-view.

With a constant sweep amplitude, the target size affects the track-video duty cycle. The duty cycle change in turn alters the open loop gain of the tracking loop, thereby changing the track dynamics and bandwidth. However, the output bandwidth of the MMOS is set by the error amplifier filter, and is not affected.

2.1.4 Beacon Tracking Mode

The beacon tracking mode utilizes the star tracking functions, and as a result the normal acquisition, track and reacquisition modes are common.

Additional circuits are activated to note the presence of the beacon modulation frequency. However, the beacon-presence signal is not used to automatically break or lock track on a target. This function or criteria is the target presence level. Breaking lock on a target if it is other than the beacon (determinable by noting the beacon presence signal), is at the discretion of the operator. Breaking lock can be accomplished by commanding any of the other modes momentarily.

The beacon itself has certain restrictions, necessary so that the target can be acquired and tracked without instrument damage. With a beacon modulation of 4.725 kHz $\pm$0.5%, the MMOS will give a beacon presence indication for a 25% modulation or greater. The minimum detectable target is equivalent to a third visual magnitude. The target range that can be accommodated is 10^3 times less than minimum detectable range. By means of sensing the video signal, the MMOS self protects over a 10^6 times signal intensity range.

Initially, to restrict the optical energy at the photocathode, an aperture is inserted between the lens and tube. A second protection is provided as required by reduction to the tube multiplier gain. Acquisition and tracking characteristics are unchanged by the status of the protection devices. The protection devices are latching, i.e., they will remain effective even if the source intensity is decreased below the potentially dangerous level. Removal of the devices occurs with a command to another mode.

2.1.5 Mapping Modes

The mapping modes are identical in some ways to the acquisition mode. The sweep generator produces a digital raster scan covering the central portion of the photocathode. The 10° x 10° field-of-view is scanned at 8 frames/second. The digital pattern is 64 x 64 thereby

providing a 30 microsecond dwell time per element. The output information is a video signal indicating the energy in the IFOV.

The MMOS can be commanded to either a high sensitivity or low sensitivity mode. The higher sensitivity is the same as the star tracking modes thereby allowing star field mapping capability. The lower sensitivity allows viewing of scenes up to 10,000 ft-lambert. It is noted that the self-protection described in Section 2.1.4 is operative in the mapping modes.

Included as a mapping mode is the landmark tracking mode. A 2.5^{o} x 2.5^{o} field-of-view is scanned at 30 frames per second. This is a lower sensitivity mode than can be used to restrict the field to view a prominent area of a particular scene. The restricted scan can be moved within the total 10^{o} x 10^{o} field by application of DC offset voltages. Video processing external to the MMOS may be used to maintain the restricted scan on a selected area thereby effecting landmark tracking.

2.2 OPERATIONAL DESCRIPTION

Following is a signal flow operational description of the MMOS when operating in the following modes:

1) AUTO
2) XTAR
3) MAP
4) LMT
5) RAD

An understanding of the MMOS operating characteristics will be aided by referring to the block diagram of Figure 2-1.

2.2.1 Automatic (AUTO)

When commanded to AUTO, the mode control initially sets the MMOS to the ACQ mode causing a scan of the full 10^{o} x 10^{o} field-of-view. The dual frequency master oscillator operates at its lower frequency of 8.7 kHz. The 8.7 kHz signal is scaled and shaped to produce the basic 4.35 kHz clock pulse rate. Various clock pulse rates are used to drive the acquisition counters to produce a variety of digital type MAP, ACQ, RE-ACQ and LMT scans. The acquisition scan is a 64 x 64 element digital step pattern with a dwell time of 230 microseconds at each step position. During this dwell time, the video is analyzed for the presence of a target. The scan generator deflects the 11 arc minute instantaneous field-of-view in 9.4 arc minute increments providing a 16% overlap. As the instantaneous field-of-view (IFOV) intercepts the target, photo current flows within the F4012 image dissector tube and is amplified by the phototube dynodes. The signal current flow can be followed by referring to the block diagram of Figure 2-1. The F4012 low level anode current is amplified and converted to a low impedance output voltage by the PREAMPLIFIER. The signal voltage is processed by the LOG AMP which accommodates a 50 dB dynamic range and linearizes the TAR MAG output. The signal voltage is sensed by the BRIGHTEST STAR and ACQ VIDEO detectors. The signal pulse triggers the ACQ VIDEO comparator while the brightest star detector senses the peak level of the signal and adjusts the ACQ VIDEO comparator threshold to this voltage. Having sensed a target, the acquisition video pulse triggers the address memory system to store the digital address of the X and Y deflection angles. If more than one target is in the field-of-view, a new acquisition pulse is detected and a new address stored only if the new pulse amplitude exceeds the threshold level set by the previous brightest target. The step scan sequence continues until all areas of the field-of-view have been sampled. A total of 0.94 seconds is required to

complete the 4096 step field search. A bistable latch is used during the field search to sense the detection of any target. A "reset" latch mode indicates that no target has been sensed, therefore, the field search starting address is parallel loaded into the acquisition counters and the full field scan repeats. If at the end of the field search, the latch has been set, the acquisition counters are commanded to the logic address contained in the storage registers. This returns the IFOV to the angular position where the target was last sensed and the mode is switched from ACQ to RE ACQ.

In the RE ACQ mode, the digital to analog scan generator continues to generate a step type scan but restricted to an area immediately surrounding the target's position. The limited search scans in a triangular step pattern, 8 steps in azimuth by 9 steps in elevation. This is equivalent to a far field angle of 1.25° in X by 1.40° in Y. The limited field is scanned at 60 fields per second. With this REACQ scan, target acquisition is accomplished within 1.5 field scans (24 milliseconds). If zero relative motion has occurred between the MMOS and the target since the initial acquisition, the switch from ACQ to RE ACQ to TRACK will appear to be instantaneous. If target motion exceeds 0.5° per second, the target may not be positioned within the RE ACQ field-of-view and will not be sensed. If no target detection occurs during the REACQ scan, the scan will continue for 7.5 fields. The mode is then returned to ACQ by the mode control logic and the full field scan is reinitiated. Detection of a target while in the RE ACQ mode, results in an immediate switch to the TRACK mode.

When the mode is switched to TRACK, the mode control enables the ANALOG SCAN GEN to generate a TRACK scan. The ANALOG SCAN GEN is a multifunctioned generator consisting of a logic controlled four channel integrated circuit operational amplifier. Through logic selection of its four channel internal amplifiers it generates the TRACK, XTAR and RADIOMETER scans as required. In the TRACK mode a .3V p-p

cruciform scan is generated as shown in Figure 2-2d. As shown in the block diagram of Figure 2-1, the track scan voltage generated by the ANALOG SCAN GEN, is "summed" to the ACQ scan voltage which has the IFOV deflected to the target's coarse position (within $\pm 1/2$ ACQ steps. A deflection coil current proportional to the sum of the input voltages is generated by the summing amplifier-coil driver circuit. The resultant coil driving current, dithers the IFOV about the target position resulting in a modulated signal voltage referred to as TRACK VIDEO. Referring to the block diagram Figure 2-1, the video signal flows from the sensor tube, through the pre amp, log amp, track video amp and is detected by the TRACK VIDEO DETECTOR. Subsequent to detection, the track video is pulse position and width-modulated. The video pulse train is synchronously demodulated and provides a voltage proportional to the angle between the target and the center of the cruciform scan. This tracking loop correction voltage is summed to that of the ACQ and TRACK SCAN voltages resulting in a very precise repositioning of the IFOV on the target. The tracking loop bandwidth is 12 Hz.

In the process of scanning the IFOV on and off the target with the 270 Hz track scan, the video signal fundamental frequency component is 1.08 kHz. The TARGET PRESENCE circuit is comprised of an active bandpass filter and diode detector. The filter is sharply tuned to 1.08 kHz and senses the presence of the track video signal's 1.08 kHz component. Subsequent to detection of the 1.08 kHz signal, the TAR PRES status output is high. Target tracking continues as long as a target is present having an intensity $\geq$ 3rd visual star magnitude. If the target is lost, the loss of TAR PRES triggers the logic control which returns the mode to RE ACQ. Mode sequencing is then switched as previously described, dependent on the presence or absence of a target.

The track video, having been non-linearly amplified, is detected by the TARGET MAGNITUDE amplifier. The output voltage produced by the TAR MAG amplifier is approximately proportional to the log of the target intensity. A plot of the output voltage-target magnitude transfer function is provided with each MMOS.

Acquisition and tracking of a Xenon beacon target is accomplished upon command to AUTO. The automatic sequencing between ACQ, RE-ACQ and TRACK is identical to that described for star tracking. If the beacon is intensity modulated at 4.725 kHz, it is identified by the BEACON PRESENCE DETECTOR. As seen in the block diagram (Figure 2-1) the signal voltage is amplified by the preamplifier and then sensed by a bandpass filter and peak detector. If the beacon source has an intensity ≥ a 3rd magnitude star and has been intensity modulated at a frequency of 4.725 kHz to a level which is ≥25% of its intensity, the modulation will be amplified and detected by the BEACON PRESENCE detector. When beacon modulation is sensed, the BEACON PRESENCE status is high. All other mode functions and status indications are identical to those generated when star tracking. It is noted that the return to RE-ACQ from TRACK is not dependent upon presence of the beacon modulation but upon TAR PRES.

In the TRACK mode, voltages present at the X and Y ERROR outputs, represent the target position in a 5 Hz bandwidth at a gradient of 1V per degree. Coil currents, proportional to the X and Y angular deflection of the IFOV, are sensed across the coil drivers sampling resistors. The sampling resistor voltage is then summed to a field linearity correcting voltage, at the summing junction of the X and Y ERROR amplifiers. The correction system consists of a read only memory (ROM), programmed to store the digital error correction voltages, and X and Y D/A converters, which convert the digitally encoded position

corrections, to X and Y analog correction voltages. The sum of the IFOV deflection voltage and the deflection linearity correcting voltage, at the output of the X and Y ERROR amplifiers, represent the target position in the 10^{o} x 10^{o} FOV to an accuracy of ± 1 arc minute.

When a target is within the MMOS having a brightness $\geq$ -4 visual magnitude star, automatic attenuation is inserted into the light path to prevent damage to the F4012 photocathode and to extend the MMOS dynamic operating range. Referring to the block diagram Figure 2-1, the PRE AMP output voltage is used to drive the F4012 CURRENT SENSOR. The sensor is comprised of a voltage comparator and a dual latch. When the comparator's threshold is first exceeded by the signal voltage the #1 latch is set. This commands the FILTER DRIVE DECODER to insert an attenuating aperture between the Angenieux lens and the image dissector tube. The limiting aperture is 0.067" in diameter and attenuates the signal by 40 db. When the signal again reaches a level which exceeds the comparator threshold, the second latch is set. The second latch reduces the image dissector dynode voltage to attenuate the signal an additional 37 db. A command to the LO MAP holding mode resets the attenuation latches, once energized. Continuous protection is provided the MMOS by both optical and electrical attenuators, either dynamically or by a command, depending upon the operating mode. The position of the optical attenuator is sensed to establish the attenuation status. This is shown in the block diagram Figure 2-1 as a single pole 3 position switch that provides an input to the filter drive decoder. The switch is, in fact, three photo optical limit switches driven by an encoding disc. The encoding disc is attached to the attenuation vane drive. The attenuator is motor driven through a worm and spur drive system to a commanded position. As the attenuator reaches the selected position, a slot (or slots) in the encoder disc operates one or more limit switches and the motor drive is removed. The worm-spur gear type drive requires no detenting and eliminates overshoot.

2.2.2 Extended Target (XTAR)

The XTAR mode extends the MMOS tracking capability to include the acquisition and tracking of sources which subtend an angle much greater than the IFOV. As described in the AUTO track mode, the IFOV is deflected ±one acquisition step as it is scanned on and off the target to produce a modulated track video. If the taret diameter subtends an angle in the MMOS FOV of ≥2 acquisition steps, the target would be in the IFOV continuously, thereby precluding accurate tracking. In the XTAR mode, the IFOV deflection is adjusted to assure scanning off the target. A 6.3V p-p track scan waveform is generated by the multichannel ANALOG SCAN GEN (see Figure 2-1). All modes sequences (ACQ, RE-ACQ and TRACK) are identical to the AUTO mode. The extended track scan is generated by logic selection of a multichannel amplifier having a gain which is adjusted to 21 X the AUTO track scan amplitude. The 6.3^{o} extended track scan permits tracking not only large diameter, uniformly illuminated sources, but also sources which are asymmetric in shape. Targets ranging in diameter from 0.5^{o} to 4^{o} were tracked during the acceptance tests.

2.2.3 MAP

Command to either HI MAP or LO MAP modes provides both video and deflection outputs which can be used as a graphic aid to display the target information contained within the MMOS FOV. When commanded to LO MAP, which is the most sensitive of the two modes, a star field can be displayed to show star position and relative brightness over the total FOV.

In the map modes, phototube anode current is amplified by the PRE AMPLIFIER (see Figure 2-1). It is then amplified in similar integrated circuit amplifiers of 20 Khz bandwidth but different closed loop

gains. The gain ratio of the LO MAP to HI MAP amplifiers is approximately 30 db. The LO MAP video transfer function has been recorded for stellar targets of -1 to +4 visual magnitude during acceptance tests. The HI MAP video-transfer function has been recorded for scene brightness up to 10,000 ft-lamberts.

The full field mapping scan is generated at a rate that utilizes the full bandpass capabiltities of the MMOS deflection system. When commanded to either map mode, the dual frequency MASTER OSCILLATOR is set by mode control to oscillate at 8 x f_o (69.7 kHz). The 8x clock pulse rate generated drives the digital to analog generator producing a field scan at a rate of 8 fields per second. The 34.8 kHz step rate of the x scan is rate limited by the reactive components of the x deflection system. This results in the smooth triangular waveform in the X-axis as shown in Figure 2-2a. The increased field scan rate is used in both mapping modes to enhance the image as viewed on a display monitor.

In the LO MAP mode, automatic attenuation occurs if the target intensity exceeds the attenuator threshold. At that signal level, the LO MAP status becomes low and the ATTEN status becomes high. If the target intensity continues to increase, both the LO GAIN and HI MAP status will become high. The status now indicates HI MAP even though the LO MAP had been commanded.

For viewing of bright scenes up to 10,000 ft-lamberts, the MMOS must be commanded to HI MAP mode. This command immediately effects insertion of the optical attenuator and lowering of the dynode gain without regard to the call for attenuation by sensing the image dissector output.

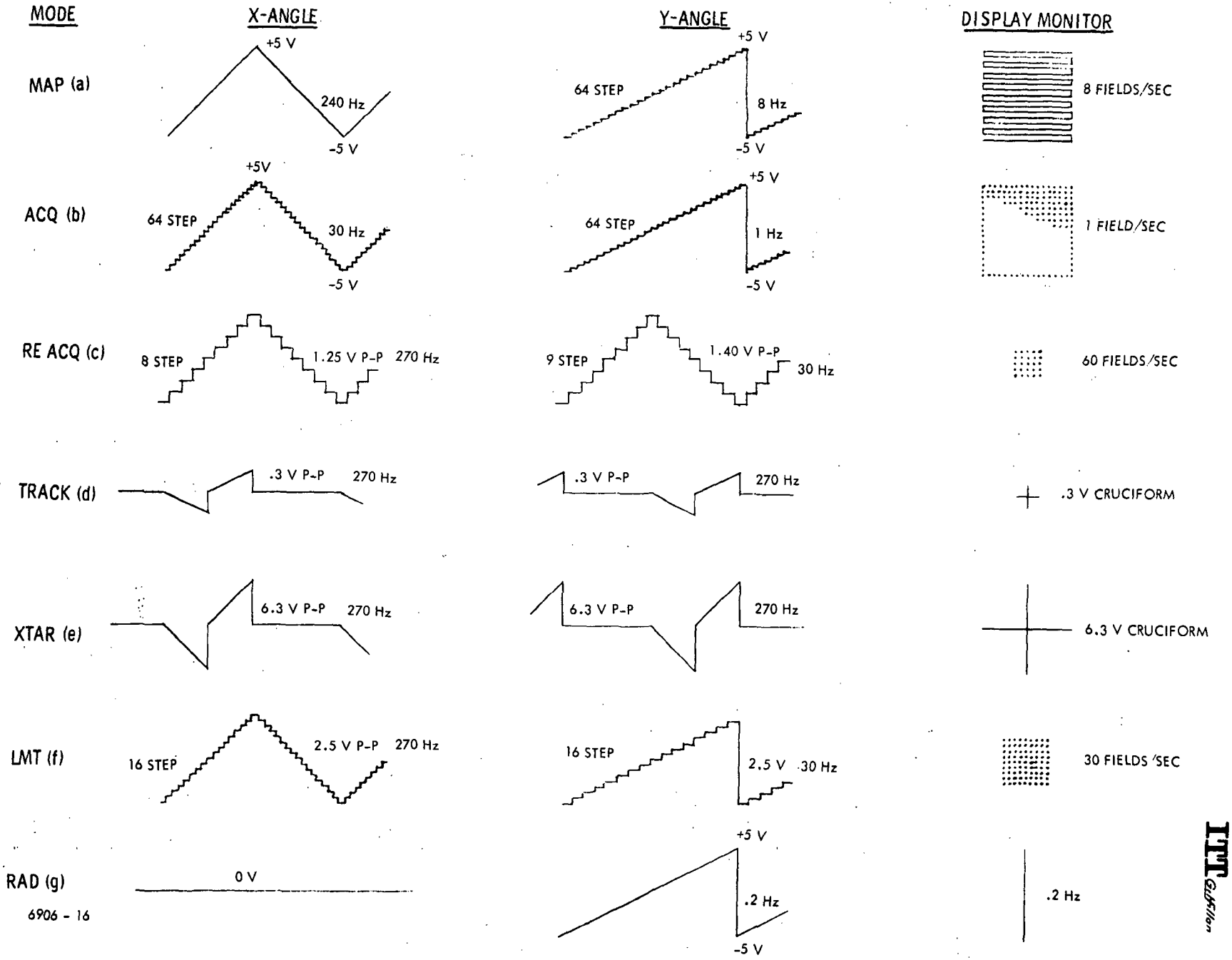
MODE
X-ANGLE
Y-ANGLE
DISPLAY MONITOR
MAP (a)
+5 V
240 Hz
-5 V
64 STEP
8 Hz
8 FIELDS/SEC
ACQ (b)
64 STEP
30 Hz
1 Hz
1 FIELD/SEC
RE ACQ (c)
8 STEP
1.25 V P-P
270 Hz
9 STEP
1.40 V P-P
30 Hz
60 FIELDS/SEC
TRACK (d)
.3 V P-P
270 Hz
.3 V CRUCIFORM
XTAR (e)
6.3 V P-P
6.3 V CRUCIFORM
LMT (f)
16 STEP
2.5 V P-P
2.5 V
30 FIELDS/SEC
RAD (g)
0 V
.2 Hz

6906 - 16

2.2.4 Landmark Track (LMT)

In addition to HI and LO MAP modes, a third map mode is generated by the MMOS when commanded to the LANDMARK TRACK mode. In the LMT mode, a field is scanned similar to the MAP modes but covering a reduced area of 2.5^{o} x 2.5^{o}. The step type scan waveforms are similar to those of the MAP modes but limited to 16 steps in X by 16 steps in Y (see Figure 2-2f).

The LMT scan has a stepping rate of 8.7 kHz. The limited FOV frame rate is 30 fields per second. X is scanned in a serpentine fashion using a 16 step, 30 Hz sawtooth. The LMT field starting position is updated to the X and Y OFFSET voltage at the completion of each field scan. In this manner, a landmark may be mapped and tracked over the entire 10^{o} x 10^{o} FOV.

The intensity levels to be encountered in LMT are comparable to that of the HI MAP mode. For this reason, both optical and electrical attenuators are inserted when commanded to the LMT mode. The video bandwidth in this mode is step rate limited by the X step scan frequency to 4.35 kHz. The maximum number of horizontal or vertical bars produced by step scanning the LMT field, is 8 black and 8 white. This pattern can be displayed by Z-axis modulation of a display monitor by the HI VIDEO output.

2.2.5 Radiometer

In the RAD mode, the MMOS provides a voltage output (HOR INT) proportional to the UV energy in the IFOV as it is scanned $\pm 5^{o}$ in the Y axis. At the command to RAD, a 0.38 micron UV filter and limiting aperture is positioned in the MMOS light path between the Angenieux lens and the image dissector. In addition, the dynode gain is set to its low level in order to provide the proper HOR INT transfer function.

When commanded to RAD, the X-axis ±5 volt .2 Hz sawtooth waveform. (See Figure 2-2g.) During generation of the RAD scan, the Y-axis D/A SCAN GEN and the tracking loop are mode controlled to generate zero volts at the input to the Y-deflection coil summing amplifier. The tracking loop and both digital and analog scan generators are held to 0 volts at the X-axis summing amplifier. This results in a sawtooth scan which deflects the Y-axis only.

Further scan versatility is obtained in the RAD mode by a switch to RAD $\overline{\text{OFFSET}}$. Grounding the normally high RAD $\overline{\text{OFFSET}}$ control line switches control of the Y-axis deflection from the ANALOG SCAN GEN to the Y-OFFSET input. Thus, an externally generated OFFSET voltage can be used to control the Y-axis deflection.

The HOR INT output in the RAD mode has a radiant energy-voltage output transfer function of 5.78 volts output at an intensity level of 1.5×10^{-6}w cm^{-2} $steradian^{-1}$ $angstrom^{-1}$. The HORIZON INTENSITY output bandwidth is 20 Hz in both RAD and RAD $\overline{\text{OFFSET}}$ modes.

2.2.6 Sun Sensor

The MMOS is protected from excessive light levels by the BRIGHT OBJECT SENSOR. A bright object, such as the sun, will be sensed at a minimum angle of 65° with respect to the optical axis. The large angle of acceptance is achieved by the use of wide angle optics coupled to two Cd Se photo sensors. When a bright object is sensed, the voltage is removed from the F4012 tube's image section thus preventing excessive dynode current flow. Simultaneously, a rotary solenoid is driven to position a shutter in the optical path directly in front of the image dissector tube to protect the tube's photocathode. The electrical and mechanical protection is non-latching and normal operation will resume as the exposing source is removed from the sensor's FOV. The dual photo

sensors are parallel connected to the BRIGHT OBJECT SENSOR circuitry to provide an AND/OR drive. This connection precludes sensing failure due to obscuration of either sensor by the lens barrel.

2.3 MECHANICAL DESCRIPTION

2.3.1 Structure

The structure of the MMOS is similar to that of other ITTG sensors. The basic backbone of the instrument is a central tube with end fitting brazed to it. This brazement technique has been used in a number of ITTG sensors and results in a light, yet surprisingly rigid structure. It is symmetrical and symmetry is vital in an electro-optical device if stability is to be achieved.

The four component boards are mounted via mounting bosses machined into the basic brazement. The connector is located on the rear flange, and the front flange is precision machined to accept the lens adapter via a close tolerance pilot diameter. The bright object sensors, lens, and filter vane assembly are all located in this adapter. The entire sensor body has a simple cylindrical cover over the electroncs.

2.3.2 Filter Vane and Drive

The filter vane and drive is a self-contained assembly located in the lens adapter. A stepper motor drives a worm and wheel mesh to position the filter vane. The position of the vane is determined by the encoding of three optical switches and an encoding disc. Slits in the disc readout the position of the vane. One distinct advantage of the worm and wheel drive is the self-locking aspect of these gears. When power is removed from the stepper motor, the vane is effectively locked in position and cannot be moved unless the stepper motor is energized.

A consideration in the design of the vane and drive mechanism is that this type of drive is easily implemented in a flight type instrument. The stepper motor is brushless and is available in space-qualified versions. The worm and wheel drive requires only that one member of a non-metallic, self-lubricating material. The dynamic loads on the drive are low enough to preclude any requirement for high strength gears. The only remaining area of concern is in the bearings for the vane and worm wheel shaft. These can either be specially treated ball bearings, suitable for flight application; or merely non-metallic bushings of a material such as nylatron (molybdenum disulphide impregnated nylon). The optical switches utilized for position encoding are reliable components and can be acquired in hi-rel quality. In essence, the design and preliminary testing of a flight type vane and drive have been accomplished.

2.3.3 Electronics

The majority of the electronic subsystems is fabricated on four 3.5" x 9" circuit boards. Fabrication and wiring were completed by the Micro Technology division of Sterling Scientific Industries.

High density circuit board packaging is achieved by the use of a welded wire technique called stitch wiring. Point-to-point wiring avoids typical PC board problems of parallel runs, crossovers, etc. To stitch wire, a machine welds a continuous 30 gauge wire to gold-plated terminal pins. A single wire is welded from terminal to terminal as required by the circuit.

Gold plated leads of integrated circuit flat packs can also be directly welded to the circuit board terminals using the same technique. The circuit boards are made of 1/16" blue glass epoxy, type FLGE per MIL-P-13949. Both component and wiring sides of the circuit boards are

coated with a 2 ox. solder-plated co pper. The VCC plane is typically on the component side of the boards while the ground plane is on the wiring side.

The circuit distribution is on the four boards as follows:

Board #1

1. Preamplifier
2. HI and LO MAP amplifiers
3. Target Magnitude
4. Beacon Presence detector
5. Brightest Star detector
6. Over-Exposure detector
7. Horizon Intensity amplifier

Board #2

1. Analog Scan generator (Track, XTAR and RAD scans)
2. X and Y Tracking loops
3. X and Y deflection coil drives
4. X and Y Angle and ERROR amplifiers

Board #3

1. Digital type step scans (ACQ, RE-ACQ, LMT and MAP)
2. Mode control logic
3. Offsetting A/D converters
4. Target address storage

Board #4

1. Command mode isolation
2. X and Y Linearity correction
3. Attenuator Filter drive
4. Temperature compensation

The boards are mounted around the periphery of the cylindrical housing. Input and output terminations are made at the end of the boards, at the rear of the housing. Mounted inside the center cylinder is the image dissector tube and deflection coil assembly. To the rear of the tube coil assembly is the dynode and image section power supplies, the focus current regulator and the protective shutter drive electronics. The power supplies and control circuits are a subassembly consisting of three circuit boards and a mounting plate. Both dynode and image section power supplies are mounted to a 3" diameter x 1/4" aluminum plate. The same plate provides a heat sink and mounting surface for the focus current regulator pass transistor. Ahead of the mounting plate is a circuit board which contains the high voltage filter and image section voltage regulator components. Two boards providing protective shutter and power supply control circuits are located to the rear of the mounting plate. Access to the rear circuit board and associated pins is obtained by removal of the MMOS rear cover.

Mounted to the MMOS backplate is the low voltage power supply which converts the 28 VDC primary source voltage to ±15 VDC and +5 VDC. The power supply consists of four modules fabricated by Powercube Corp. which are electrically isolated but thermally coupled to the back plate mounting surface. The back plate therefore acts as a heat sink and thermal radiator for the power supply. The entire back plate - power supply unit is mechanically attached to the cylindrical housing by four Allen screws.

Attached to the front of the housing is the lens adapter which houses the lens, bright object sensors and the filter attenuator assembly. A wire bundle, passing through a hole in the housing front flange, connects the adapter electronics to their appropriate circuits.

2.3.4 Lens

The optics of the MMOS is an Agenieux 50mm f/0.95 refractive lens. The lens provides the following features to facilitate the design.

- light-weight (less than 1.5 pounds)
- good MTF on and off axis
- off-the-shelf
- sufficient back focal length to allow room for magnetic shielding, the attenuator vane, and the sun shutter
- can be ruggedized for flight use

2.3.5 Image Dissector

The MMOS image dissector is an ITT F4012RP. The tube is a ruggedized design and has successfully met flight level environment requirements.

General parameters of the F4012 are:

- 1" dia. x 6.5" long
- 0.7" dia. usable photocathode
- electromagnetic focus
- electromagnetic deflected

Specific parameters of the MMOS image dissector are:

- S-20 spectral response photocathode
- remote processed photocathode
- 0.0065" square internal mechanical aperture
- 9 stage box and grid multiplier

2.3.6 Focus and Deflection Coil

The focus and deflection coil used on MMOS B was built to ITTG specifications by Washburn Laboratories. The coil assembly includes the

the focus and deflection coils in an integral package with shielding material to properly form and contain the magnetic fields.

The coil assembly parameters were chosen to be compatible with the MMOS A package (package outline changes were not desirable), to improve field uniformity, to improve video output uniformity and to minimize power requirements. Pertinent assembly parameters are as follows:

FOCUS COIL:

Resistance:	90Ω
Inductance:	No requirement
40 gauss current:	100 ma

DEFLECTION COILS:

Resistance:	140Ω
Inductance:	<50 mHy
Deflection Sensitivity:	50 ma/inch

2.4 MMOS A DIFFERENCES

The preceding discussion described the operational modes of MMOS B. MMOS A provided the following modes:

ACQ

RE ACQ

TRK

AUTO

OFFSET

RAD

The detailed operation within these modes is identical to that described for MMOS B.

In order to facilitate testing and evaluation of performance, MMOS A could be commanded to and held indefinitely in the ACQ, RE ACQ or TRK modes. This cannot be done on MMOS B.

UV filter insertion on MMOSA is accomplished with a rotary solenoid rather than a stepper motor. The rotary solenoid is identical to those used on both units as the drive for the sun shutter. It is noted that MMOS A does have self protection for highly intense sources other than that afforded by a sun sensor and shutter.

3.0 DESIGN STUDIES

In order to fulfill the performance objectives of the MMOS program, studies of various design approaches and concepts were made. These studies included feasibility investigations, breadboard tests, trade-off analysis, and previous sensor parameter review. The following section is a collection of design studies conducted during the program.

3.1 EFFECT OF NIGHTGLOW ON STAR TRACKING

In anticipation of testing to be performed at NASA/JSC, the effect of nightglow on MMOS star tracking performance was of interest. In determining the nightglow that can be tolerated for tracking a third visual magnitude star consider initially the signal current from the star.

$$I_{spc} = H A_1 T_1 T_a G$$

where

I_{spc} = PC - signal current

H = 3^M Class AO star irradiance

A_1 = Optics diameter

T_1 Optics transmission

T_a = Atmospheric transmission

G = PC responsitivity

therefore

$$I_{spc} = 1.27 \times 10^{-14} \text{ amps}$$

The background current is

$$I_{bpc} = \frac{N}{F^2} \frac{\pi}{4} T_1 \quad G \quad (IPD)^2$$

where

I_{bpc} = P.C. background current

N = background radiance

IPD = instantaneous P.C. dimension

therefore

$$I_{bpc} = 7.14 \times 10^{-6} N$$

The shot noise due to this signal is

$$\overline{I_{bpc}} = \sqrt{2e\, I_{bpc}\, \Delta f}$$

where

Δf would be the amplifier BW of 10 Khz

therefore

$$\overline{I_{bpc}} = \sqrt{2 \times 1.6 \times 10^{-19} \times 10^4 \times 7.14 \times 10^{-6} N}$$

$$= 1.5 \times 10^{-10} \sqrt{N}$$

IF I_{spc} is equal $\overline{I_{bpc}}$ a false alarm rate sli ghtly greater than 10% will result. Therefore

$$N = \left(\frac{I_{spc}}{1.5 \times 10^{-10}} \right)^2$$

$$= \left(\frac{1.27 \times 10^{-14}}{1.5 \times 10^{-10}} \right)^2$$

$$= .72 \times 10^{-8} \text{ w/cm}^2\text{/ster}$$

$$= 1.3 \times 10^{-2} \text{ ft. lamberts}$$

The model used assumes a uniform background. It is nearly a certainty that the background will not be uniform. False alarms will occur when the spatial change (in an increasing direction) in background is equivalent to the signal received from a third magnitude star.

The dc background current for the background radiance N calculated is

$$I_{bpc} = 5.1 \times 10^{-14} \text{ amps}$$

$$= 4 I_{spc}$$

At this background level the non-uniformities would increase the false alarm rate calculated above. It is noted that once acquisition is achieved, tracking a star will be successful in even brighter backgrounds, although the noise angle of the error signals will increase slightly.

In conclusion, the tracking of a 3 magnitude star with nightglow of 0.01 ft. lamberts will be possible. Acquisition will be possible although a longer acquisition time should be anticipated.

3.2 UV FILTER POSITION CONSIDERATIONS

In order to achieve an accurate profile of the horizon, a stable spectral range of the horizon radiance must be sampled. The MMOS is specified to respond to the 0.38 ± 0.01 micron wavelength of the horizon.

The initial design concept was to insert a bandpass filter between the optics and F4012 photocathode. The filter to be used is a UV interference filter with a bandpass of 0.02 micron centered at 0.38 micron. It is a characteristic of an interference filter to change its transmission peak wavelength as a function of the angle of incidence of the incoming radiation. For small angles, the wavelength shift is given by

$$\lambda_{\varphi} = \lambda_{o} \left(1 - \frac{\sin^2 \varphi}{n^2}\right)^{1/2}$$

where

λ_{φ} = Peak Wavelength

λ_{o} = Peak Wavelength when φ is zero

φ = Angle of incidence

n = Effective index of Refraction of the Filter

Positioning of the filter between lens and tube means that it is in an f/0.95 light cone with the maximum angle of incidence being 30 degrees. The resulting wavelength shift is approximately .02 micron which is the bandpass itself. Several alternatives were considered to minimze the shift:

1) Use of Absorption Filters - Unlike interference filters, the absorption type filter does not have wavelength shift. However, in order to get cutoff characteristics at the wavelength required, the filter would become quite thick; possibly .2 inches. The resulting problems of extra weight and focal plane shift would be more difficult than the original.

2) Use of the Interference Filter in Front of the Lens - This would reduce the angle of incidence to 5 degrees and wavelength shift to 0.0005 micron. However, eventual use of the MMOS on spacecraft would rule out this configuration because of weight and size requirements.

3) Aperture Stopping or Field Stopping in the Lens - Due to the excessive radiant energy available in the radiometer mode, this approach offers the best solution of minimizing the peak wavelength shift. The optimum method would be to operate an iris (within the lens at its nodal point), thereby increasing the lens f-number and reducing the maximum angle of incidence. Another method which does not require the iris (and motor to drive it) is to place an aperture as near as possible to the lens back element. This is the method to be used on the MMOS. An illustration of the positioning is shown in Figure 3-1.

The aperture will be 0.175" in diameter. The filter will be inserted into aperture and be a part of the plate. By positioning the plate within 0.125 inches of the back element the average angle of incidence for the image at 5 degrees from boresight is 0.002 micron. Therefore, the average center wavelength shift is from 0.3775 to 0.38 micron for an image from 5 degrees to 0 degrees (boresight).

This method does indeed decrease the HORIZON INTENSITY signal-to-noise ratio. However, there is sufficient signal to provide a ratio of 500 to 1 with a bandwidth of 200 Hz. Since the sweep frequency is 0.2 Hz (5 second sweep time), a bandwidth of 20 Hz will be sufficient to preclude any error due to lag.

By reviewing Figure 3-1 of the lens-filter-tube interface, the defocusing due to insertion of the UV filter can be calculated. Assuming

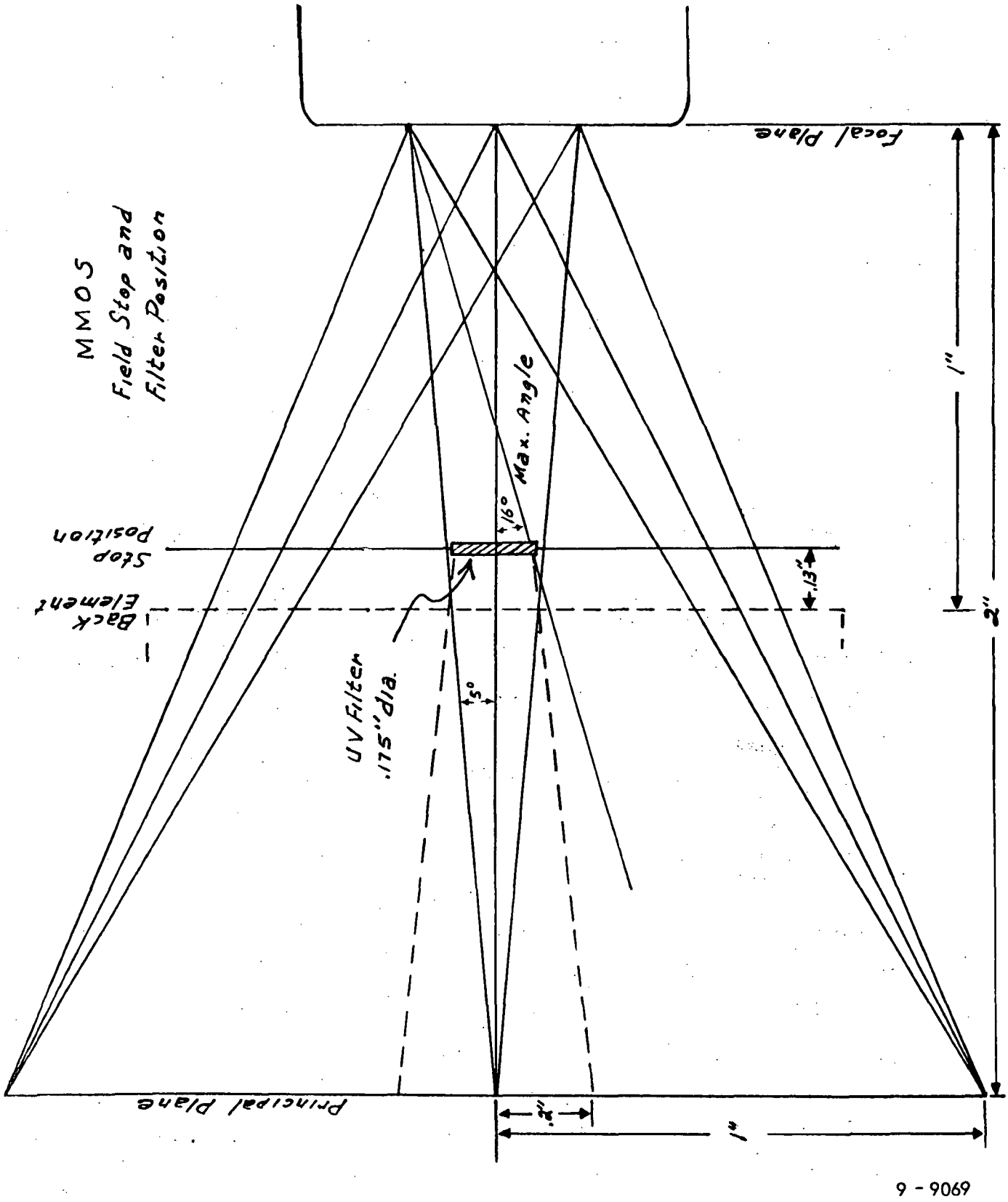

Figure 3-1. MMOS Field Stop and Filter Position

that the optical focus is optimum in the star tracking mode with an air path between tube and lens, then the filter insertion stretches the focal length by

$$d = \frac{n-1}{n} (t)$$

d = amount of stretch

n = filter index refraction

t = thickness of the filter

Since n is 1.5 minimum and t is .030 inches, d equals .010 inches. Using a cone half angle of approximately 5^{o} from Figure 3-1, the image size at the photocathode would have increased by 0.0018 inches. This corresponds to .05 degrees angle. It is certainly not implied that an error of this magnitude will result or that a corresponding amount of signal is lost. The effect would be a blurring of the object which would be noticeable only, if at all, at the ends of the HORIZON INTENSITY output.

3.3 OPTICAL ATTENUATION TECHNIQUES

Several of the modes on MMOS-B necessitate the use of an attenuator in the optical path in order to prevent F4012 photocathode (PC) damage. In the high range of the VIDEO mode, referred to as the HI MAP mode for full field map and LMT for limited field map, the MMOS will be required to view a sunlit earth or equivalent. In the BEACON mode, the MMOS will be required to acquire and track a Xenon beacon to within a range of 1000 feet. In the Extended Target (XTAR) mode the MMOS will be required to track sunlit targets at close range. In these modes, the optical power density within the S-20 spectral bandwidth will cause PC current densities greater than the maximum allowed for the F4012.

It is shown in a design study of the Xenon beacon (Section 3.4) that an attenuation of 100 is sufficient at close ranges for a 150 watt beacon. An attenuation of 100 is sufficient for viewing sunlit clouds.

Two methods were considered to provide the optical attenuation needed; namely,

1) use of a small aperture near the rear lens element to effectively stop the lens. This was used successfully to provide attenuation in the radiometer mode on MMOS A,
2) use of a neutral density filter between the optics and sensor photocathode.

If the attenuation is in the form of a neutral density filter, several optical effects must be considered. Specifically, the filter transmission as a function of angle of incidence and the focal length increase must be considered.

The transmission variation as a function of the angle of incident will not be a problem with a neutral density. Since the transmission characteristic extends beyond the S-20 spectral region on both ends, any shift would have little if any effect. (This shift had to be accounted for in the case of the UV filter.)

As with the UV filter, the ND2 filter will be of the interference type. An interference filter attenuates or blocks by reflection. The reflective coating is deposited on a substrate such as glass. Therefore, relative to an absorption filter, the interference filter can be quite thin. This is necessary in order to minimize the stretch of the focal length.

The general formula for increase in focal length due to glass in the air path is

$$\Delta f = T\left(\frac{\eta-1}{\eta}\right)$$

where

Δf = increase in focal length

T = glass thickness = 0.0015"

η = glass index of refraction = 1.5

However, this formula is an approximation based on small angles of incidence so that $\alpha \simeq \tan \alpha$. A sketch of the optical elements and path is shown in Figure 3-1. Note that with a fast lens, the angle of incidence is not small. The f/0.95 system results in an angle of incidence of approximately 27°. The exact formula for focal length increase is

$$\Delta f = T \left[1 - \frac{\cos \alpha}{\sqrt{\eta^2 - \sin^2 \alpha}} \right]$$

Using $\alpha = 27^{\circ}$, $\Delta f = 0.0057"$ for a filter thickness of .015". This filter thickness is selected as a minimum so that it will not become too delicate to handle. The standard thickness is 0.040" meaning that the 0.015" component is a special part.

With an f/0.95 system, the depth of focus is practically non-existent. The image size increase due to the focal length change is approximately 1:1. Therefore, the image size is 0.0057" which is nearly equal to the 0.0065" aperture size. This amount of defocus could probably be tolerated as far as noise angle in BEACON mode and contrast in the HI MAP mode is concerned. A more significant influence might be noted on the absolute position accuracy. By positioning the neutral density filter close to the back element as opposed to placing it near the photocathode, effect of filter inhomogeneity and substrate imperfections are minimized. The field accuracy should be affected uniformly such as would be experienced by a gradient change.

Use of a neutral density filter would necessitate the use of a clear glass insert in the open position (for star tracking modes) in order to maintain reasonable focus between modes. Although not impractical to implement the neutral density attenuation method has disadvantages. For this reason, initially the small aperture attenuation was tried on MMOS B. Tests made determined that results were predictable and performance with respect to other parameters did not deteriorate. This method was used, therefore, to effect optical attenuation on MMOS B.

3.4 BEACON MODE SENSITIVITY

MMOS B will acquire and track a Xenon beacon target. The target range will be 300 nautical miles (1.8 million feet) maximum and 1000 feet minimum. The target will be modulated such that during the tracking mode a BEACON PRESENCE signal can be generated by sensing the modulation frequency component in the image dissector video. The purpose of this analysis is to establish the Xenon beacon requirements based on signal conditions under which the MMOS A performance was demonstrated. The specified performance was demonstrated on a third visual magnitude Class A0 star. For this input the image dissector current was 32 nanoamps.

$$I_A = 32 \times 10^{-9} \text{ amps}$$

$$I_{PC} = \frac{I_A}{G\, g_m}$$

where G = dynode gain = 2×10^6

g_m = mesh gain of the F4012 = 0.5.

$$I_{PC} = 32 \times 10^{-15} \text{ amps}$$

$$P_I = \frac{I_{PC}}{k}$$

where P_I = optical power in the image

k = S-20 responsivity = 0.04 amp/watt

$$P_I = 8 \times 10^{-13} \text{ W}$$

$$H = 6 \times 10^{-14} \text{ w/cm}^2$$

These values will be used as the minimum sensitivity level for MMOS B.

Based on preliminary Xenon lamp specifications, the optical power output in the S-20 bandpass will be 20% of the power input to the lamp contained in one steradian solid angle. Modulation of the optical signal will vary the signal power sinusoidally about its nominal level. Initially consider the nominal level requirements only.

$$J = 0.2 \, P_{XI} \text{ w/ster}$$

and

$$H = J \times \frac{1}{R^2}$$

$$= 0.2 \, P_{XI} \, \frac{1}{R^2}$$

where

J = source S-20 radiant intensity

P_{XI} = power input to the Xenon beacon

R = source to MMOS range

From these formulae, several parametric curves can be constructed. Figure 3-2 is a plot of Xenon input power as a function of range. Figure 3-3 is a plot of beacon irradiance (S-20 wavelength) as a function of range. The minimum signal locus is based on the parameter values given above. The photocathode damage locus is based on an F4012 specification limit of 10 μa/cm^2 photocathode current. The locus also assumes the target image size is 0.002 inches diameter.

The 1000 feet to 1,800,000 feet (300 nautical miles) range interval implies a 3.24 x 10^6 signal dynamic range. The MMOS will accommodate a 10^6 dynamic range. Design of the image dissector voltage distribution and the video amplifier provide a signal dynamic of 100. The 10^{-6} range is present for

a) nominal configuration

b) insertion of optical attenuation of 100 times in the optical path, and

c) image dissector gain reduction of 100 plus the optical attenuation insertion

It is noted that the optical attenuation provides the necessary protection to allow use of a 150 watt Xenon beacon. Based on minimum signal requirements of the MMOS a 1 KW beacon will be required to provide the irradiance necessary for acquisition and tracking to 300 nautical miles.

As stated previously, the beacon signal will be modulated such that it can be distinguished from a continuous stellar signal. Based upon in-house studies the modulation frequency should be 4.725 kHz ±1%. The modulation is a sinusoidal oscillation about the nominal output with a peak amplitude of at least 25% of the nominal output. The MMOS is required to sense the modulation only during tracking of the beacon. While tracking, the video signal is 50% duty cycle as shown in Figure 3-4.

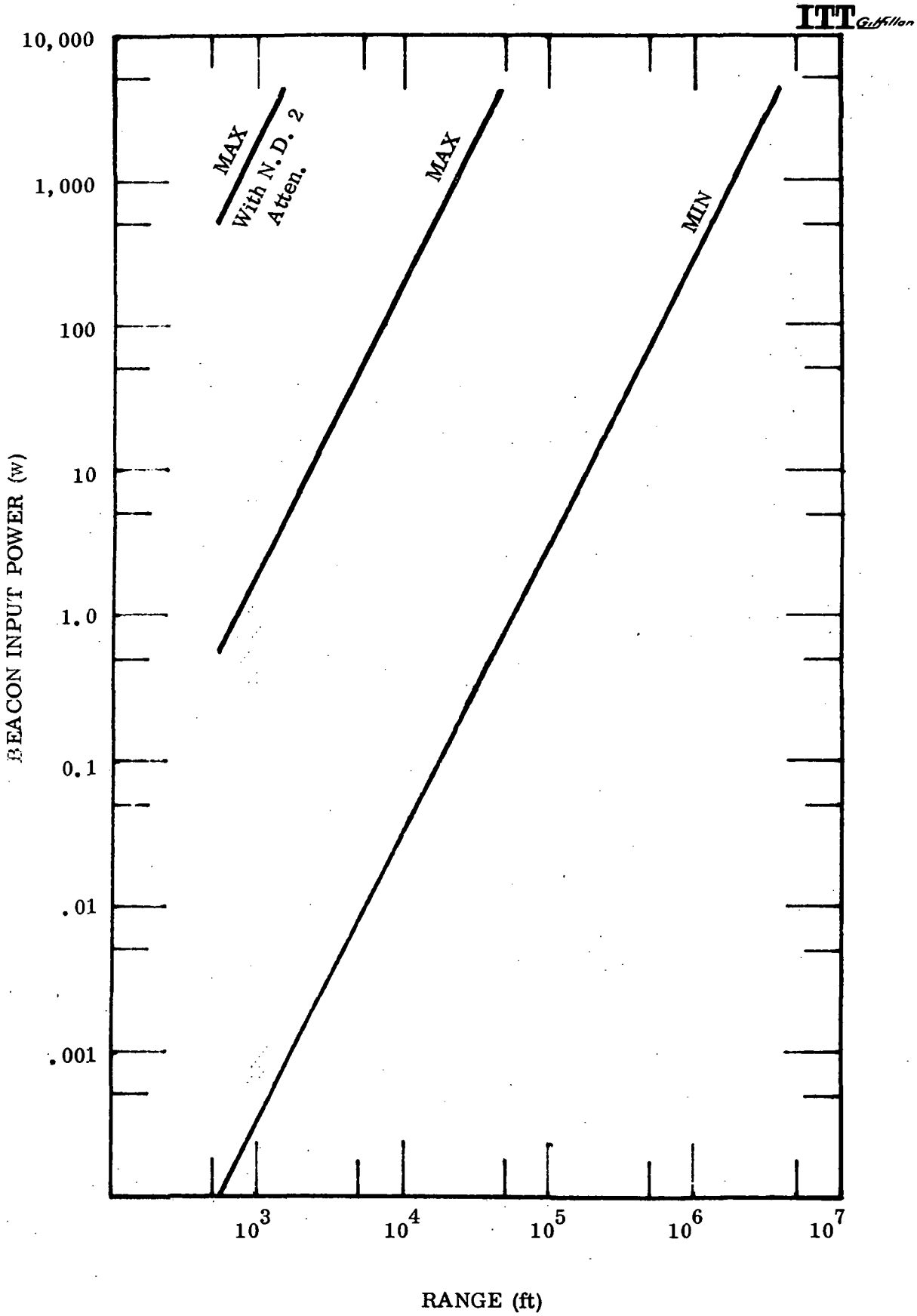

Figure 3-2. Beacon Input Power

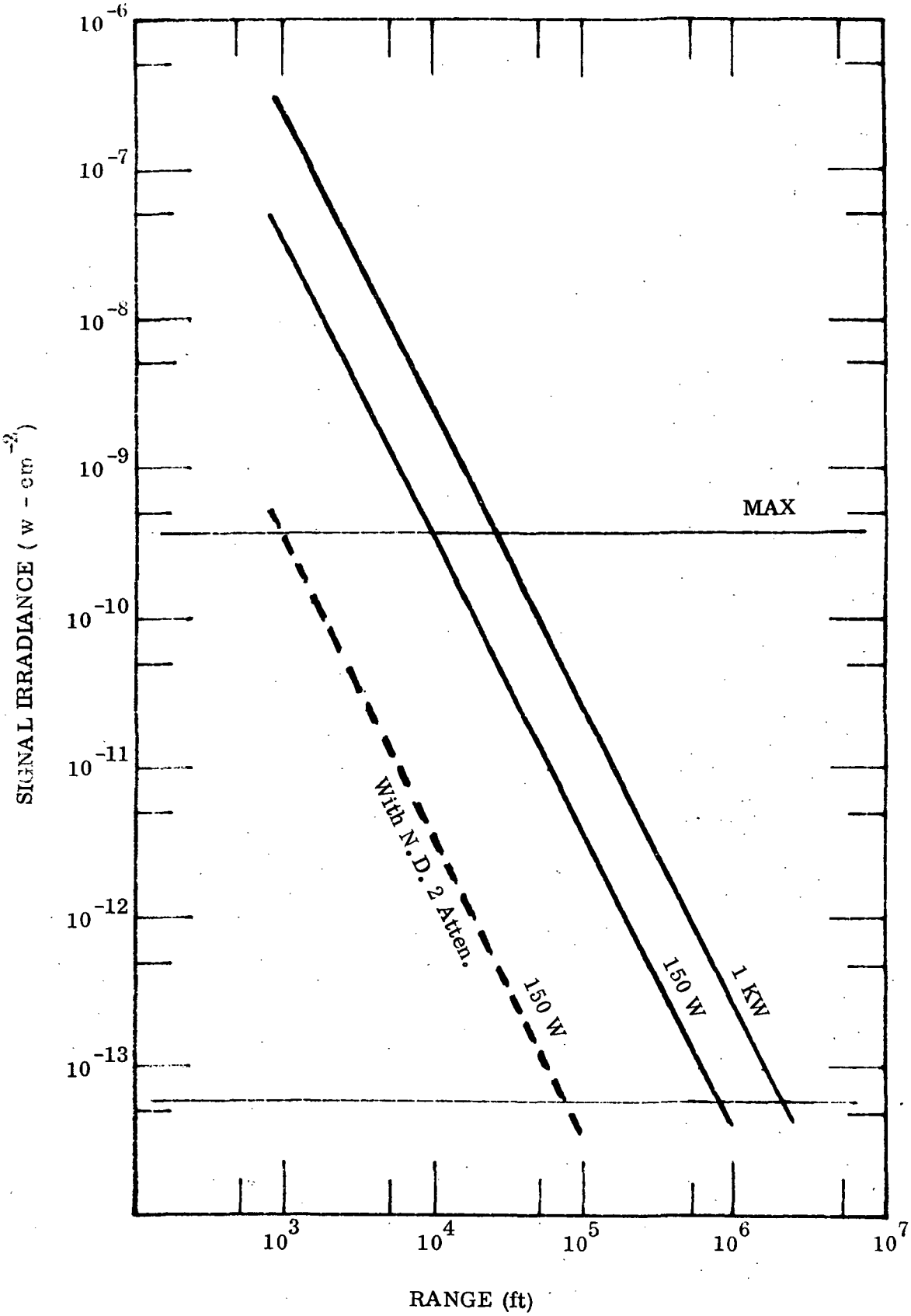

Figure 3-3. Beacon Signal Irradiance

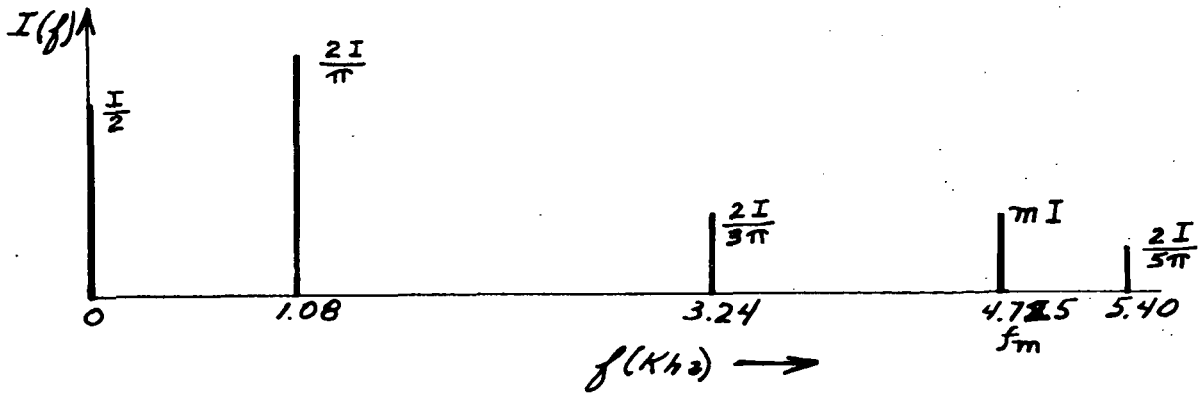

Figure 3-4. Video Signal Duty Cycle

The frequency components of a square wave and a sine wave, such as the waveform shown are given in Figure 3-5.

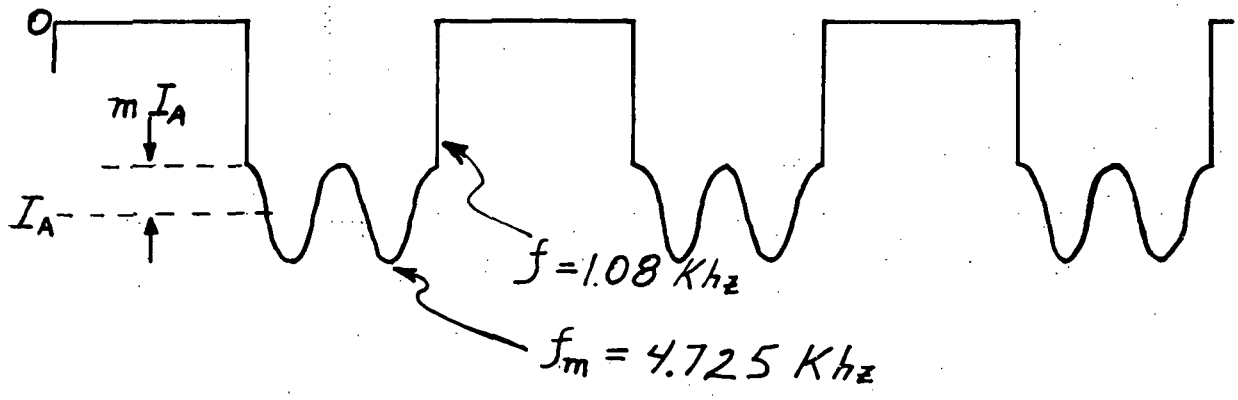

Figure 3-5. Square and Sine Wave Frequency Components

The following calculations are used to analyze the MMOS performance when tracking a modulated beacon. The modulation signal component must be compared to the signal shot noise in the bandpass of the detection circuit. Consider the S/N at the image dissector output; i.e., the input to the modulation detection circuit.

$$\overline{I_A} = \left(2e \frac{\sigma}{\sigma-1} G^2 g_m I_{PC} \Delta f\right)^{1/2}$$

where

$\overline{I_A}$ = RMS shot noise on the anode current

e = electronic charge = 16×10^{-19} coulombs

σ = individual dynode gain = 3

G = multiplier gain = 2×10^6

g_m = F4012 mesh gain = 0.5

Δf = modulation detection circuit bandwidth

I_{PC} = signal current at the PC

$$= \frac{.2\, P_{XI}}{R^2} A_L T_L k \quad \text{(established previously)}$$

The amplitude of the modulation frequency component is m I (the peak to peak value is 2m I but is reduced by 2 due to a 50% duty cycle).

Therefore

$$(S/N)_m = \frac{mI_A}{\overline{I}}$$

$$= \frac{mGg_m I_{PC}}{\left(2e \frac{\sigma}{\sigma-1} G^2 g_m I_{PC} \Delta f\right)} 1/2$$

$$= m \left(\frac{g_m I_{PC}}{2\, e \frac{\sigma}{\sigma-1} \Delta f}\right) 1/2$$

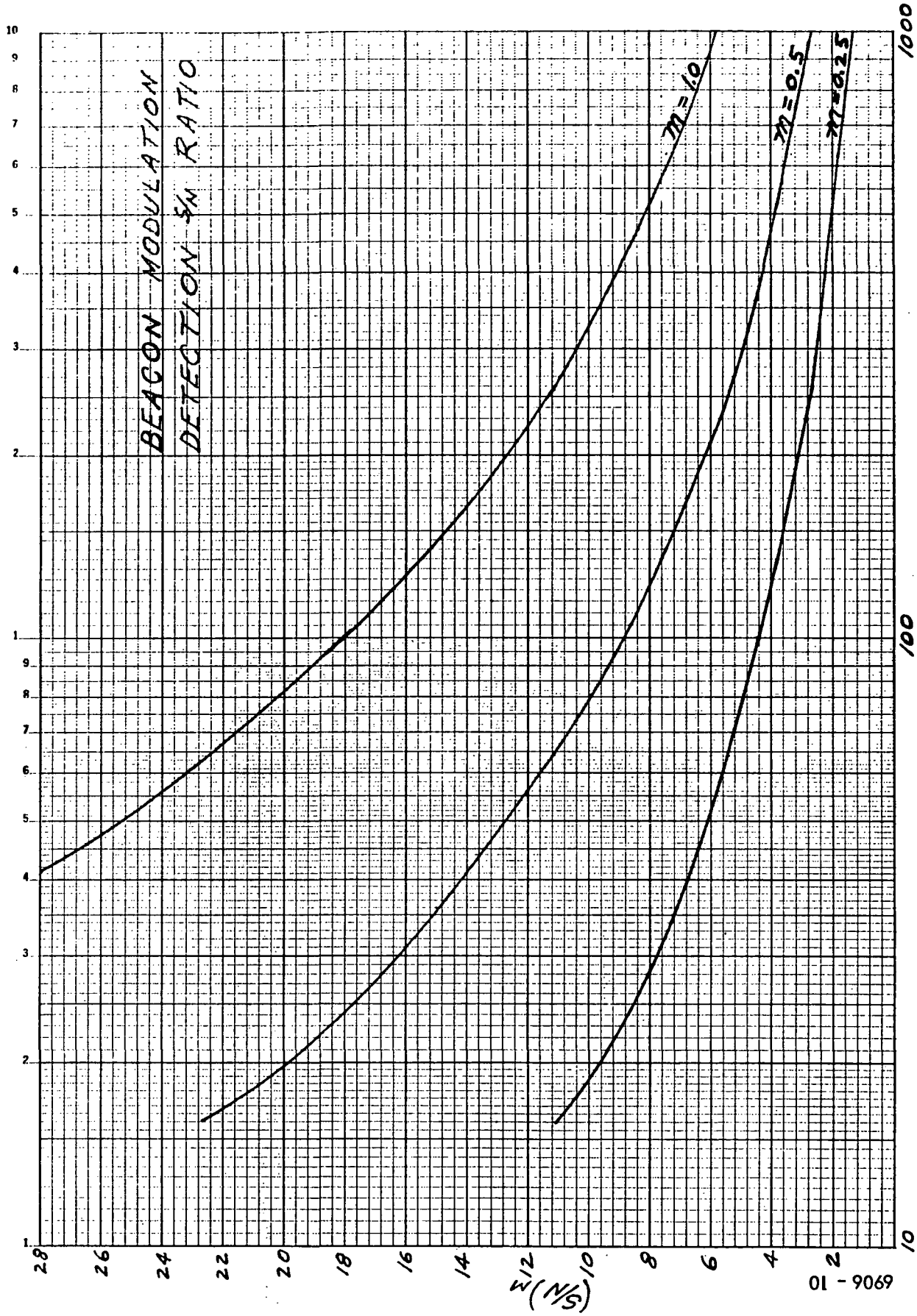

Figure 3-6. Beacon Modulation Detection S/N Ratio

Using minimum signal, i.e., $I_{PC} = 32 \times 10^{-15}$ a

$$(S/N)_m = 183 \frac{m}{(\Delta f)^{1/2}}$$

This formula is used to construct a graph, shown in Figure 3-6, of $(S/N)_m$ as a function of Δf for several values of m. The detection circuit will consist of a bandpass filter, rectifier, and comparator. The S/N ratio of 4 is adequate. Initially, the modulation frequency stability was specified as 4.725 kHz ±1%, If the center bandwidth tolerance of the detection circuit is also ± 1%, then a ± 2% bandpass is necessary. This would correspond to a S/N of 3 which is marginal. Consider the following plot in Figure 3-7.

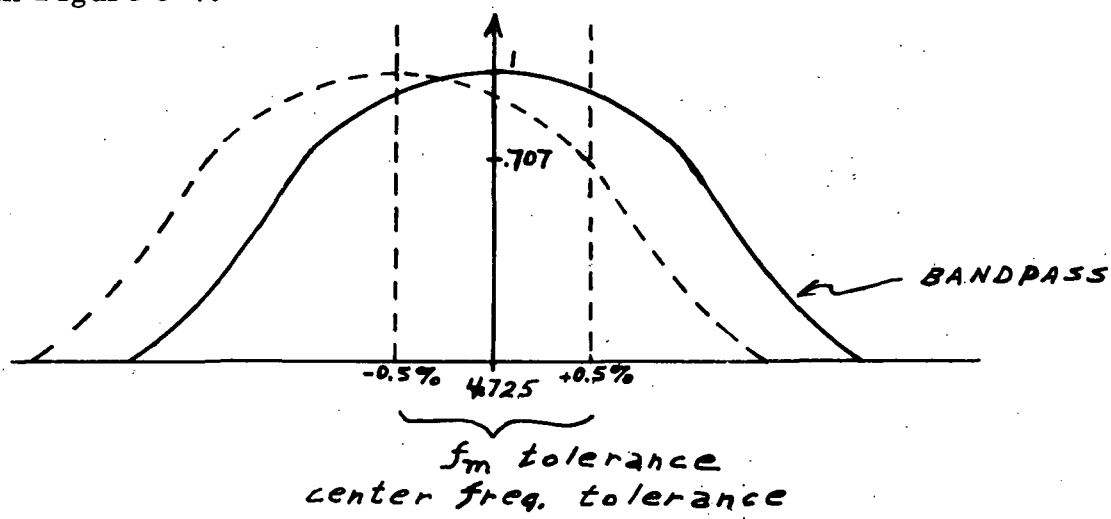

Figure 3-7. Center Frequency Tolerance

By reducing the modulation frequency tolerance to ±0.5% and the center bandwidth to ±0.5%, a bandpass of ±1% is sufficient to insure the modulation frequency component is selected. The S/N ratio is nominally 4.5 and decreases to 3.2 ($\sqrt{2}$ 4.5) at the tolerance extremes conditions. It should be noted that above calculations are on minimum condition signals. As the range is decreased, the $(S/N)_m$ ratio increases proportionately.

As a summary, based on the assumptions noted herein, the Xenon beacon must

1. be 1 KW to allow acquisition and tracking to 300 nautical miles
2. be limited to 150 W at ranges of less than 10^5 feet to preclude MMOS damage
3. be amplitude modulated at 4.725 kHz ±0.5%. The modulation amplitude is to be no less than 0.5 of the nominal signal output.

Actual tests on MMOS B were not implemented to check sensitivity with respect to range. Sensitivity in terms of irradiance was found comparable to third visual magnitude star irradiance. The BEA PRES indication was positive for 15% modulation.

3.5 LOW MAP SENSITIVITY

The initial concept of the VIDEO mode was to sample the 10° x 10° field by means of the search scan normally used for star acquisition. The video output was to be synchronized with the scan waveforms such that a real time presentation of the field scene could be effected.

The search scan for the 10° x 10° field is a 64 x 64 element format. The per step dwell time is 230 microseconds thereby making approximately a 1 Hz frame rate. The selection of these parameters was made in the initial proposal and was based on correct star selection within one second of time. The Phase A MMOS demonstrated specified target selection and a sensitivity of a 4.25 visual magnitude star.

In the VIDEO mode, computer processing of the video is required in order to achieve a usable presentation. Even then, the presentation quality would be poor due to any MMOS - target motion. In order to minimize this effect, a higher frame rate was discussed at the preliminary

design review. Since that time tests on a breadboard MMOS have shown that the frame rate can be increased to 8 Hz. With this increase, the sensitivity in any one frame has decreased proportionately.

Considering the sensitivity of the MMOS A as 4.25 magnitude, the MMOS b is 8 times less sensitive due to the decreased dwell time. Therefore the MMOS B sensitivity should be specified as second visual magnitude. The limit on sensitivity is primarily switching and processing transients within the MMOS. Even with design practices such as decoupling of the voltage inputs at individual boards and signal line shielding, this noise is predominant.

Based on signal shot noise alone, a greater sensitivity can be anticipated. The following discussion addresses what should be achievable and could be considered a design goal.

The VIDEO mode is now made of two modes and the name itself is no longer used. The two modes are LOMAP, for dark background stellar targets or equivalent, and HIMAP for scenes with brightness levels to 10,000 ft-lamberts. Both modes will incorporate a 8 Hz frame rate. Sensitivity is a concern only in the LOMAP mode since attenuation is necessary for HIMAP mode operation.

From Phase A MMOS performance data, the F4012 photocathode current for a third visual magnitude star was:

$$I_{PC} = 32 \times 10^{15} a$$

From this

$$n = \frac{I_{PC}\, t_d}{e}$$

where

n = number of electrons

t_d = dwell time = 26×10^{-6} seconds

e = electronic charge = 1.6×10^{-19} coulombs

therefore

$$n = \approx 6 \text{ electrons}$$

Based on the maximum dark current per the F4012 specification sheet, the comparable dark count would be 1 electron per sample period. The emission of the electrons is random and their occurrences obey the Posson probability equation:

$$P(x) = e^{-\lambda} \frac{(\lambda)^x}{x!}$$

where

$P(x)$ = probability of exactly x events occurring

λ = mean rate of events occurring per unit time

The video signal output for the third magnitude star will be a voltage proportional to the 6 electron sample. The voltage amplitude will fluctuate, dependent on the number of signal electrons emitted in a particular sample period. Amplitude fluctuations due to noise electrons will also occur. The graph of Figure 3-8 is based on Poisson distributed terms using a signal rate of 6 electrons and noise rate of 1 electron.

Since the MMOS video output is merely an amplification of the electrons, both signal and noise, the graph indicates possibilities of processing the output voltage for display. As an illustration, assume that a comparator is set to threshold at the voltage proportional to 4 electrons. Then the probability of third magnitude detection is 85% while the probability of false target indications is 2.5%. Although this probability of false indications seems low, 102 false targets per frame (4,096 elements) would be seen.

It is noted that the processing internal to the MMOS cannot be changed to enhance the signal to noise ratio. Improvement would be effected by increase in PC quantum efficiency or decrease in dark noise.

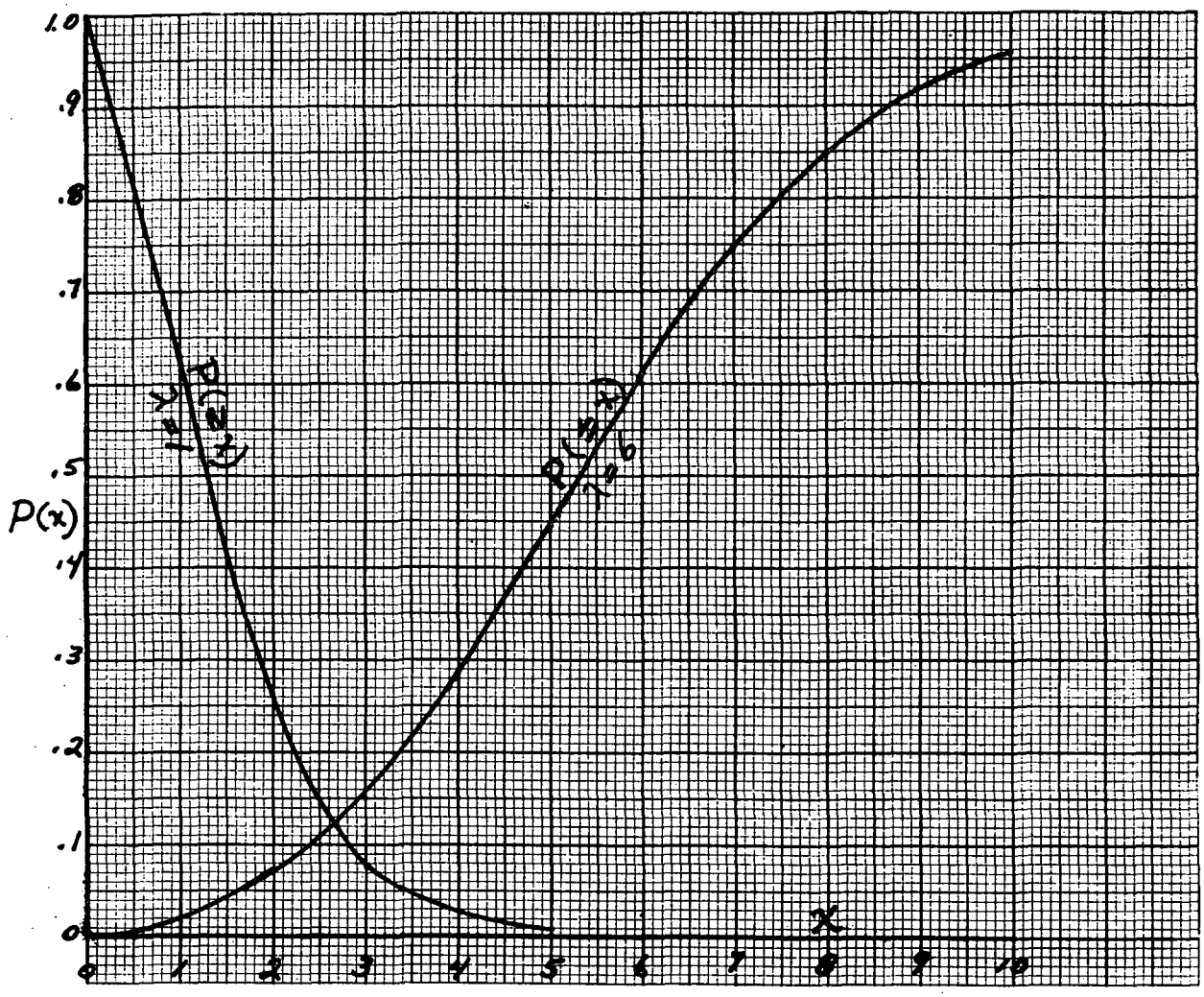

Figure 3-8. LO MAP Detection False Alarm Probability

Due to the decreased dwell time, the video amplifier BW is increased. Even with this BW increase the amplifier input resistance noise is negligible. Consider

$$t_d = 26 \times 10^{-6} \text{ second}$$

If the amplifier output pulse is to be within . 1 of a final value

$$BW = \frac{0.35}{26 \times 10^{-6} \text{ second}}$$

$$= 13.4 \text{ kHz}$$

Then

$$I_N^2 = \frac{4\,K\,T\,BW}{R}$$

where

I_N = Johnson noise

K = Boltzman constant = 1.38×10^{-23} joules/^oK

T = temperature = 300^oK

R = input impedance = 10K ohms

$I_N^2 = 2.22 \times 10^{-20}$

$I_N = .15 \times 10^{-9}$

This is 30 times less than the F4012 dark noise maximum and therefore negligible.

To summarize, the LO MAP sensitivity should be specified as second visual magnitude. This is an extrapolation from the "A" MMOS performance and is essentially a direct trade-off for frame rate.

3.6 POSITION OUTPUT STABILITY AS A FUNCTION OF TIME AND TEMPERATURE

In the laboratory testing of MMOS A in preparation for formal Acceptance tests, it became evident that the position outputs drifted following turn-on. The drift was significant in that it prevented getting any consistent position output maps from data taken within two hours following warm-up. The drift problem was especially noted following a change in mounting fixtures. The second mounting fixture enclosed the MMOS and caused a 30^oF temperature rise to the sensor.

Many time-temperature test runs were made prior to the Acceptance tests in April 1972. A typical position output MMOS housing temperature profile is shown in Figure 3-9. Included on the graph is a time mark. It is noted that the majority of drift occurs within two hours after turn-on. At that time, the temperature is approximately 92°F. Since the 1 arc minute accuracy requirement did not include turn-on drifts, demonstration of this accuracy followed a two-hour warm-up interval. However, a primary objective of the MMOS B performance was to provide 1 arc minute accuracy after a 15 minute warm-up time.

No further investigation of the MMOS A drift was made at this time. The unit was ready for formal rests and further isolation of the drift source(s) would require dis-assembly and time. Instead, the component selection and fabrication of MMOS B would take into account all potential drift sources. Some items of consideration were:

- focus coil current regulation
- image section voltage regulation
- focus/deflection coil construction
- image dissector-focus/deflection coil interface
- tube/coil assembly-magnetic shield interface
- tube/shield assembly-housing interface
- lens stability
- lens/housing interface

A focus/deflection coil design change had already been made to improve position output uniformity. This was also anticipated to be a more stable design than the MMOS A unit. The regulator circuits were checked in temperatures and no changes were made to the original design. Build-up of MMOS B in the lens, tube, and coil subsection was to be done at a step-by-step level so that drift could be checked as components were added.

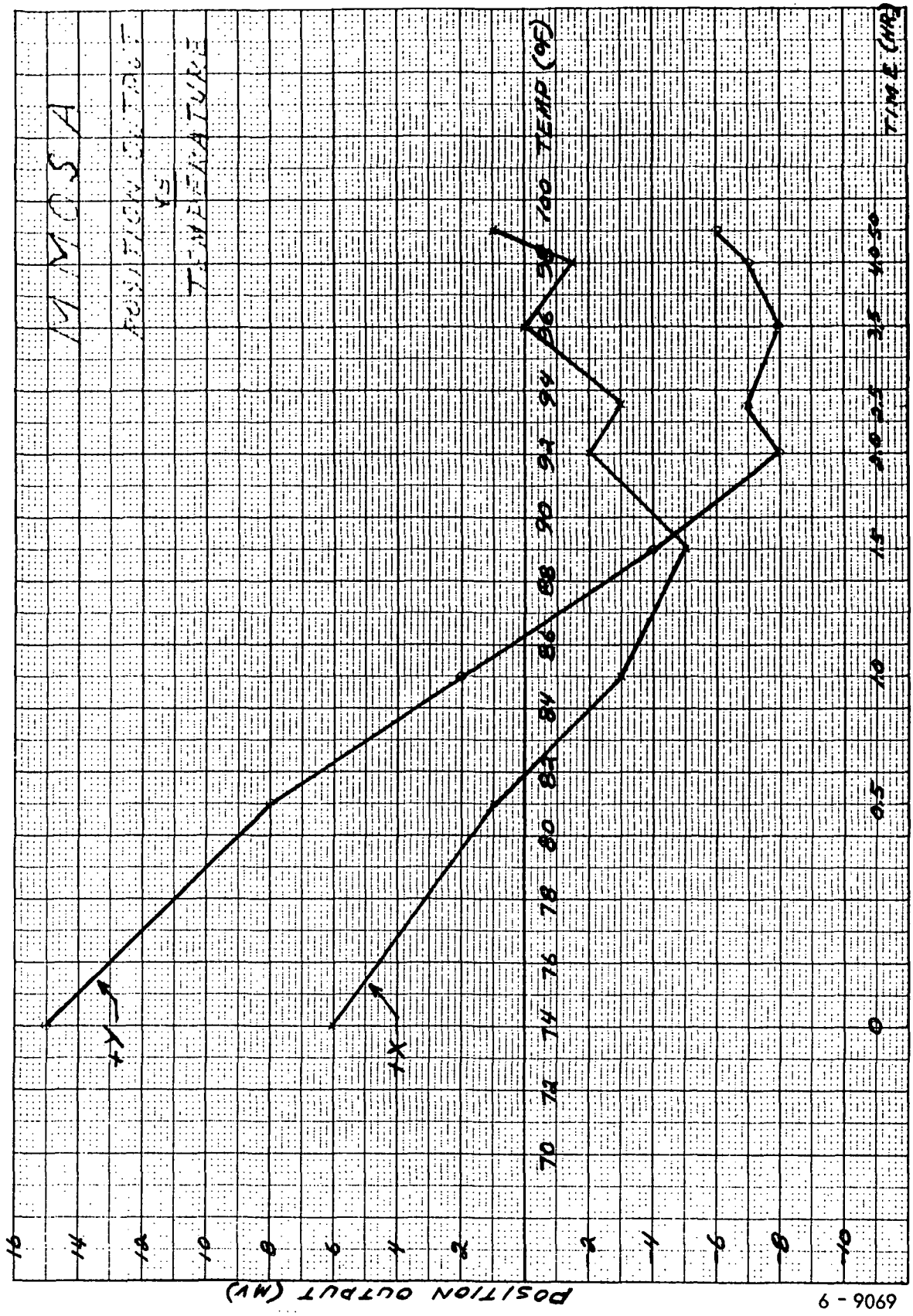

Figure 3-9. MMOS A Position Output vs Temperature

The MMOS A was returned to ITTG in August 1972 so that further tests could be made in search of potential drift source(s). From these tests changes to MMOS B could still be made since it was in early stages of construction.

Conclusions from results of MMOS A tests were:

1. Drift magnitude and direction were approximately the same as before shipment, i.e., 1.5 arc minutes in Y and 1.0 arc minutes in X.

2. Any drift due to heating and cooling of electronics circuits either individually or simultaneously was negligible.

3. The amount of drift stated above occurred regardless of the starting temperature of the entire unit.

4. The drift source could not be further isolated than the lens-housing-shield, focus/deflection coil-tube subsystem. The magnitude of the drift is equivalent to less than 10^{-3} inches on the photocathode.

These test results emphasized the importance of proper tube-coil-lens interface in MMOS B. As these components were brought together, drift tests were made to note any significant additions to drift.

Initial tests were run with the tube placed within the coil but not the shield. The coil was mounted in a saddle clamp which was independent of the lens holder. With this setup independent rotations of tube, coil, and lens could be quickly made. The temperature rise of the coil was nominally $5^{o}F$ within 1.5 hours after turn-on. Regardless of the relative positions of the components, the drift was nominally +8 millivolts in Y and +12 millivolts in X with polarity referenced to the coil. It was therefore concluded that there is a drift internal to the coil which must be compensated for. Even when starting at an elevated temperature, there was additional positive drift upon turn-on although not of the same magnitude.

The tube-coil shield assembly was potted in early December 1972. In this manner, the MMOS B could be tested in its final configuration except that the electronics boards were not mounted on the housing. The power dissipated by these boards was simulated by applying power to nichrome wire wrapped around the center tube of the housing. The temperature could be raised to well over 100°F and then returned to the mid-80's by fan cooling.

Typical drift curves for the sensor are shown by the #2 curve in Figure 3-10 and Figure 3-11 for X position and Y position outputs, respectively. The Y drift slope in the 72°-77° interval is nearly the same as measured previously. However, the X drift slope is now -1 mv/°F whereas previously it was measured as +2 mv/°F.

As a check on the tube-coil again, a unique test setup was used. The lens was removed and a .002" diameter aperture placed on the tube photocathode. A narrow beam HeNe laser was pointed to fill the small aperture. In this manner, the drift within the tube-coil assembly could be determined. Typical drift curves are shown by the #1 curve in Figure 3-10 and 3-11. Again, the Y drift corresponds to previous measurements in the region below 78°F. Although the X drift slope is 7 times less than pre-potting measurements, it is in the same direction.

The data of Figure 3-10 and 3-11 point out the complexity of the drift problem. It is now obvious that the lens-tube interface contribute a drift component comparable to the coil drift component. The composite drift seems to be primarily a function of temperature rather than time as evidenced by the return path of drift as the temperature is decreased. The temperature was monitored at the shields near the tube photocathode. Since there are several drift components, the temperature at each source probably differs and causes hysteresis in the return path.

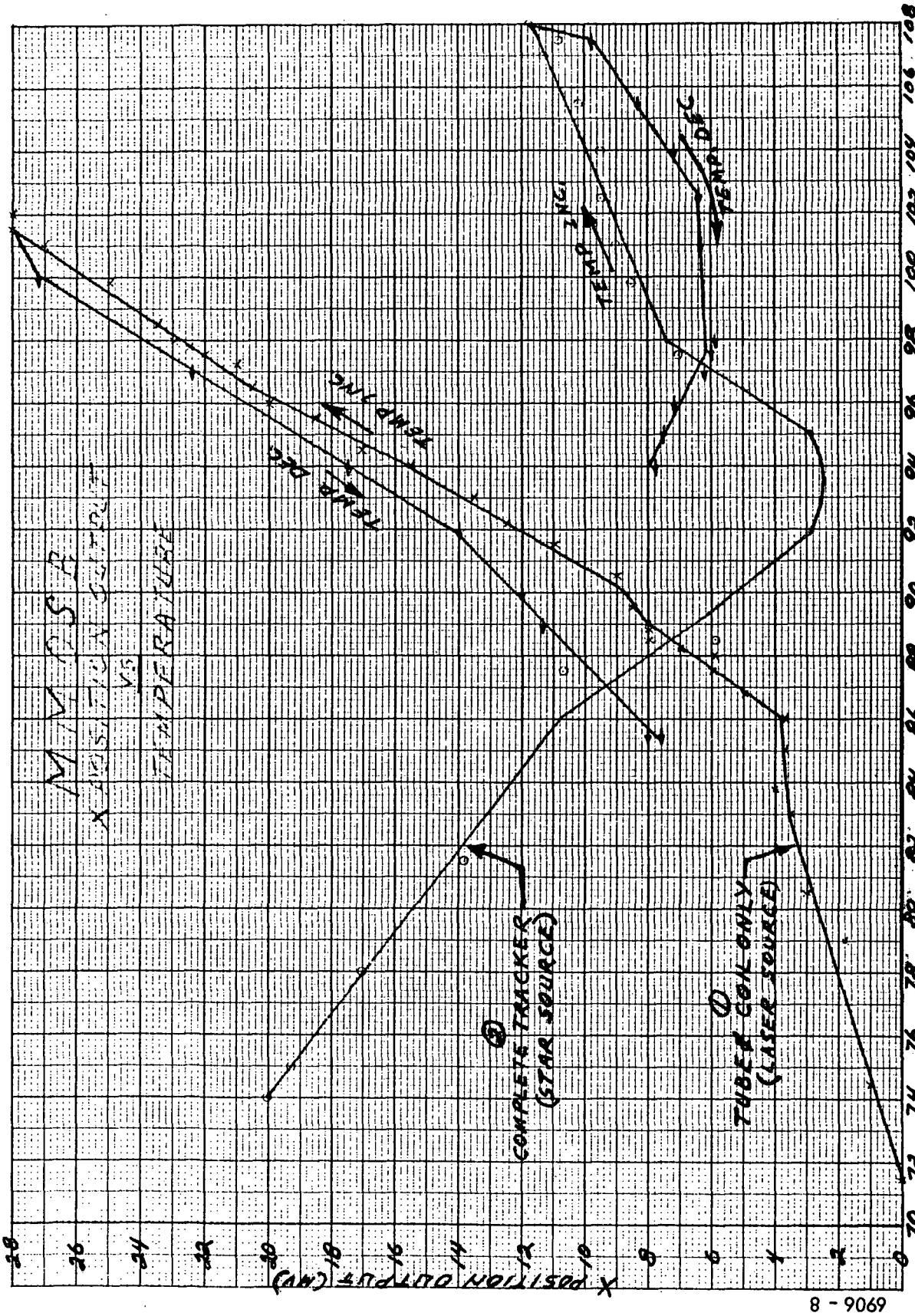

Figure 3-10. MMOSB X Position Output vs Temperature

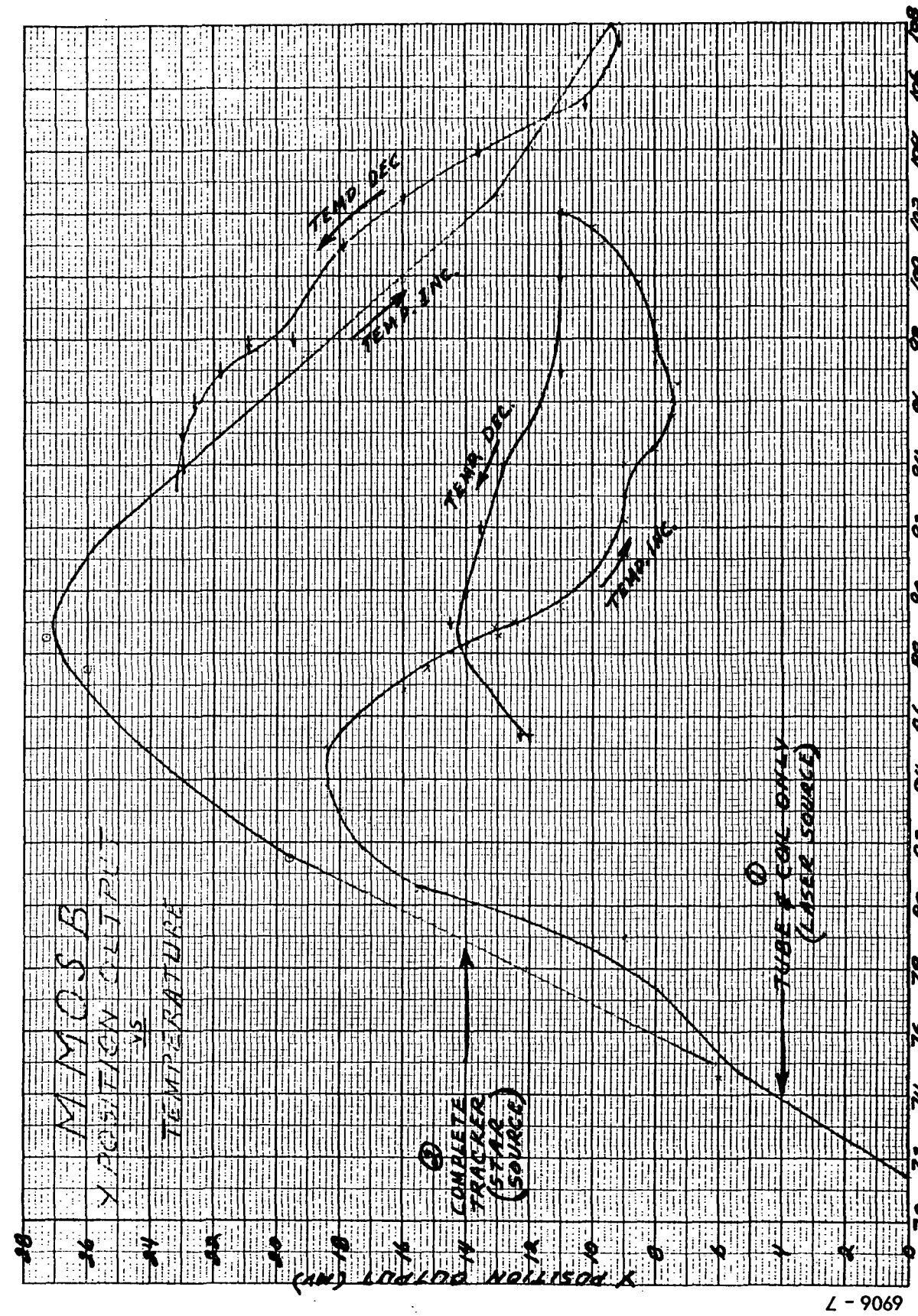

Figure 3-11. MMOS B Y Position Output vs Temperature

Further isolation of the drift components could not be made. Return of the lens to the MMOS B and use of the star source resulted in drift closely correlated to the #2 curves of Figure 3-10 and 3-11. Based on the repeatability of the drift, schedule, and economic reasons, it was decided to compensate the drift electronically.

Compensation is generated in shaping circuit which senses the MMOS B temperature by the signal from a resistive bridge whose one branch is a thermistor. A thermistor is used for each X and Y. These components are attached to the magnetic shields near the rear of that component. The compensation circuits were tailored prior to formal Acceptance Tests. The turn-on drift measured during acceptance tests was less than 5 millivolts.

3.7 FIELD-MAP ACCURACY

The primary source of inaccuracies in the MMOS is the field map non-uniformities. The field map is a plot of the X and Y position outputs as a function of target positions within the 10° x 10° field-of-view.

3.7.1 MMOS A Field Map Accuracy

Initial position accuracy tests on MMOS A indicated that an accuracy of ±1 arc minute was being met only within 3° of the boresight. Outside of the 6° diameter circle, errors due to geometric, optical and electronic aberrations were such that 6 arc minute inaccuracies at the field extreme were being measured. An initial position output map is given in Figure 3-12.

Several alternatives to the problem were discussed with NASA:

1) specification relief of the accuracy requirements of MMOS A
2) addition of electronic correction - either analog or digital,
3) addition of optical correction, and
4) use of a new deflection and focus coil design.

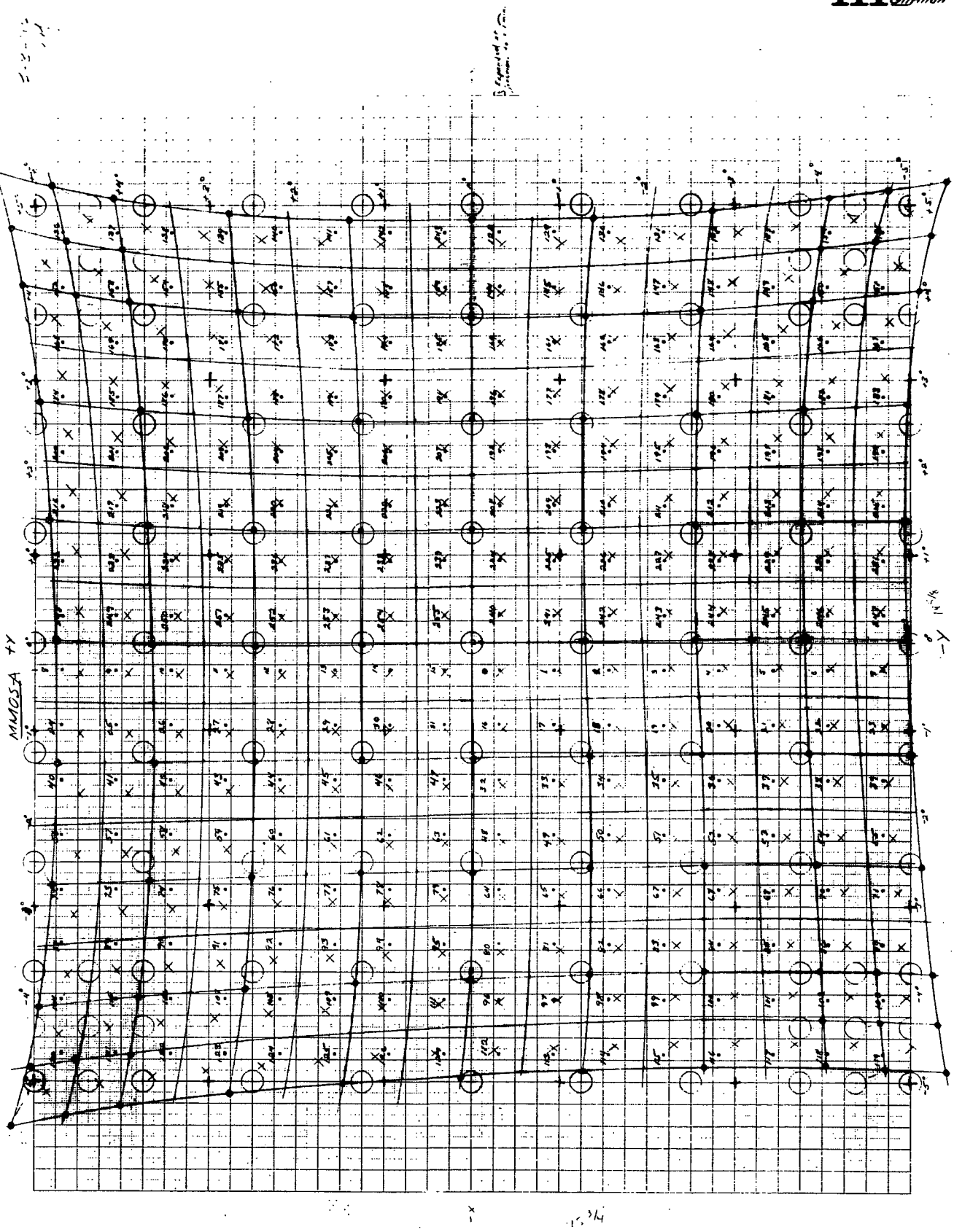

Figure 3-12. MMOS A Field Map

Because of the importance of the accuracy requirement in the MMOS application, the specification relief could not be granted. The importance prompted a study into all other alternatives.

The initial baseline approach to effect the specified accuracy on MMOS A was to use an electronic correction with 64 area corrections in the $10^{o} \times 10^{o}$ field. The primary components of the correction circuits are a re-programmable read only memory (ROM) and two D/A converters. Final programming of the ROM and circuit tailoring would be done just prior to acceptance testing.

Simultaneous with the generation of electronic correction, a new deflection and focus coil assembly was ordered. It is anticipated that this assembly would decrease the field plot distortion such that further corrections electronically would be easier or require fewer elements. The new coil assembly would be used on MMOS B.

Initially, it was thought that some correction would be available by use of a compensating field "distortion" lens in the optical path of the MMOS. Tests of this method indicated it would not be practical on MMOS A. Any optical correction should be an integral part of the optics design for a lens of this speed.

Therefore, correction of MMOS A field map shown in Figure 3-12 was to be all electronic. After initial study, it became evident that a 16 x 16 matrix would be required to provide accuracy of ±1 arc minute over the entire field.

3.7.2 Correction Area Granularity

Two major factors determine the size of the discrete areas to be corrected. They are the angle accuracy to which the target position must be defined and the magnitude of distortion contained within the field. The percentage distortion increases as the angle of deflection increases.

Therefore, when correcting a square FOV, the corner areas are the most distorted and must be analyzed to establish the correction area granularity. Second order factors which influence the determination of the size of areas to be corrected are: size and availability of memory (ROM) used to retain the correction-address and magnitude, and the circuit and operational complexity involved with correcting a map to the next higher order.

Referring to the uncorrected field map of MMOS A, it is seen that distortion magnitudes are nearly equal in both axes, thereby establishing equal correction increments for both X and Y.

The following rules are used as a guide to establish the correction area granularity:

1. The best accuracy attained for positioning a worst case point is 1/2 the smallest correction increment, ΔC.

2. The best fit for all angles of any given correction area is 1/2 the dimensional difference (each axis) between the ideal and the actual dimension, ΔD.

3. The best fit for all points within a correction area is equal to the sum of the above of $1/2\ \Delta C + 1/2\ \Delta D$.

With an angle error output accuracy specification of ± 1 arc minute, it follows that $1/2\ \Delta C + 1/2 \Delta D \leq 2$ arc minute. The uncorrected field map is, therefore, analyzed for the largest ΔD. This exists at the field corners. In plotting the uncorrected map, the error voltages have been expanded at the correction junctions to enhance analysis as related to the accuracy requirement. Actual target test positions are encompassed by a circle of radius equal to 1 arc minute and the angle errors are plotted in minutes of error from ideal. In analyzing the map, it is seen that areas of $5/8^{\circ}$ square have ΔD's which fulfill the requirement stated in 3 above, providing ΔC is $\leq 1/4$ arc minute. Correction areas of $5/8^{\circ}$ square are generated when the MMOS $10^{\circ} \times 10^{\circ}$ FOV is divided into 16 increments along the X and Y axes.

The 16 x 16 correction memory requirement is fulfilled by the use of an INTEL model 1702, field reprogrammable ROM. It is arranged in a 256 word by 8 bit pattern and can be field erased and reprogrammed. The reprogrammable feature affords the user the capability of adjusting the map corrections as required. To reprogram the ROM, a high intensity UV light is used to erase the existing program through a quartz lid. In this manner, the device can be reprogrammed as many times as required.

The ROM 8 bit output is divided into X and Y corrections of 4 bits each. The least significant bit (LSB) of the 4 bit correction is adjusted in magnitude to produce a voltage equivalent in angle to 1/16, the sum of the largest positive and negative errors over the 10^{o} x 10^{o} FOV. In analyzing the map of Figure 3-12, all errors are found to be within ± 2 arc minutes of desired (with the exception of the $+5^{o}$X, $+5^{o}$Y corner point) therefore, a LSB correction equal to 15 arc seconds was used as the basic correction unit.

3.7.3 Field Correction Procedure

A typical step-by-step field mapping and correcting procedure is as follows:

1. Establish the field dimensions to be corrected (degrees).
2. Assign half of the ROM address inputs to the X axis and half to the Y axis.
3. Draw a rectilinear address plot of X deflection degrees to Y deflection degrees using a granularity equal to the address bit granularity of the ROM.
4. Layout the acquisition counter Q logic waveforms (that will feed the ROM address inputs) in alignment with the appropriate axis on the X-Y plot.

5. For proper ROM programming, the ROM address inputs should reflect a logic number the same as produced by the acquisition counter for that specific area of the X-Y map.
6. Map the desired deflection field by moving the target to known positions within the FOV. Record the error output voltages. To optimize map repeatability, select map test positions displaced from correction change points.
7. Draw a field plot superimposed upon the address plot using smooth continuous curves.
8. If the target was positioned at address junctions, determine address centers by the intersection of lines drawn through diagonal junctions. Compare area centers to the ideal target position to establish the correction needed to align area centers. If the target was positioned at the address center, then a direct comparison can be made after plotting the error output voltages.
9. The correction granularity is determined by the number of bits of ROM output. The total angle error per axis divided by the maximum allotted correction bit equivalent number will establish the correction value for that axis.
10. Genrate a binary encoded-correction magnitude table.
11. Correlate a correction with each map address and enter into the ROM programming truth table.
12. A dynamic system of establishing correction requirements can be used during the mapping procedure by the insertion of external binary selected correction voltages. The corrections are added at each address until the desired error output voltage is obtained. This procedure, however, necessitates a map test position at each correction address.

It is noted that while all points in the FOV are correctable to a predetermined accuracy as previously described, target positions which lie on the junction of adjacent address areas (LSB change points(will produce a different error output voltage dependent upon the direction from which the junction is approached. For a target being tracked from boresight along the X axis at an angle of 2.5^{o}, the correction applied to the X axis error amplifier to the left of the junction corresponds to that of area 207 (Figure 3-12). However, if the same 2.5^{o} junction is approached from the right the correction will be that of area 191. As a result, different angle errors may be read out for the same target position when coincident with a correction junction. The angle readouts will differ an amount equal to the difference in the adjacent area corrections. It is noted, however, that each angle readout is accurate within the ±1 arch minute.

3.7.4 MMOS B Map

An uncorrected field map of MMOS B is shown in Figure 3-13. In comparing maps of MMOS A and MMOS B an improvement of ≈ 3 orders of magnitude in Y-axis distortion is shown in the MMOS B map, whereas the X axis shows some increased distortion. The improvement in overall map uniformity is the result of replacing the Cleveland Electronics Corporation deflection coil with one fabricated by Washburn Labs. The Washburn coil not only improved the overall field uniformity at a 2/1 increase in deflection sensitivity but also resulted in a 50% reduction in focus coil power. Due to the imbalance of X and Y distortions, 3 of the ROM's 8 output bits are used to correct the MMOS B Y-axis and 5 bits used to correct the X-axis. A LSB increment of 15 arc seconds is used as the basic correction unit.

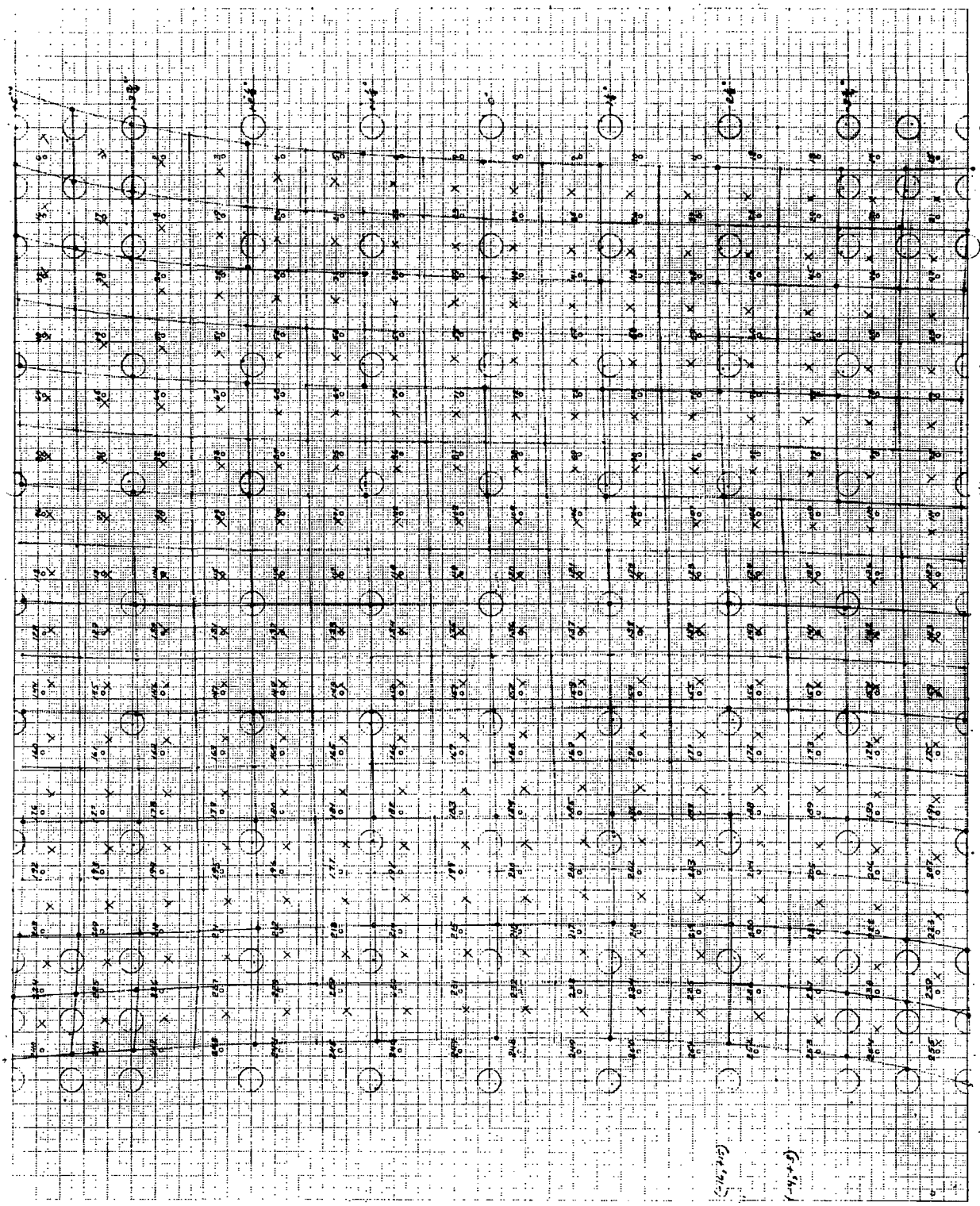

Figure 3-13. MMOS B Uncorrected Field Map

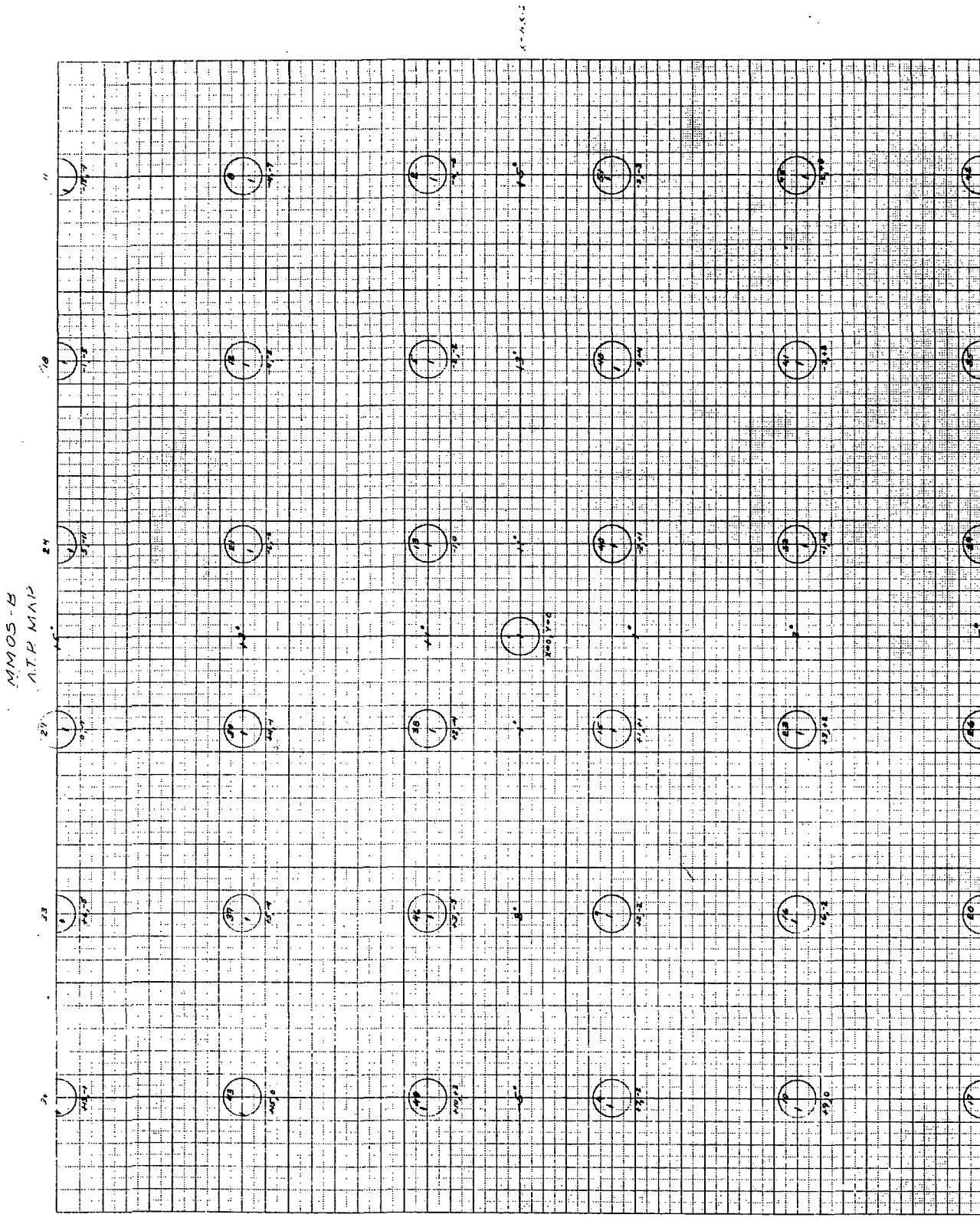

Figure 3-14. MMOS B Corrected Field Map

3.7.5 MMOS B Corrected Field Map

Figure 3-14 shows the resultant field map subsequent to correction. The map is one generated during the acceptance test procedure. A map containing 37 test positions was generated by target tracking over the 10^{o} x 10^{o} FOV. Error output voltages were recorded for target position combinations of $\pm 1^{o}$, 3^{o}, and 5^{o} in the X and Y axes. Ten error voltage samples were taken in X and Y at each test position. The raw data were then analyzed to establish a position for each of the 37 test points and a best fit gradient was selected for plotting the final map shown.

The circles surrounding the test points reflect the one arc minute tolerance specified for all points in the FOV. The resulting test points are plotted as short line segments to include the pointing accuracy drift encountered over a two-hour period previous to mapping. The pointing accuracy drift check was made subsequent to a 15-minute warmup period. The two-hour drift test revealed a drift of ±3.6 arc second in X and ±9 arc second in Y.

4.0 TESTING PROGRAM

Contained in this section are the results of formal Acceptance Tests on MMOS A and MMOS B. The results are from tests run at ITTG in April 1972 for MMOS A and April 1973 for MMOS B. A summary of performance parameters for MMOS B is given in Table 4-1.

TABLE 4-1

MMOS PERFORMANCE CHARACTERISTICS

Acquisition and Track	
Sensitivity	$+3^M$ A-O Target (Star, Beacon or Illuminated Target)
Target Discrimination	1^M Separation Greater than 0.5^o.
Acquisition Time	1 sec (for brightest target in 10^o x 10^o FOV)
Extended Target	5.7^o or less
Field-of-View Acquisition	10^o square
Field-of-View Instantaneous	11 arc minutes
Field-of-View Reacquisition	$\approx 1.25^o$ x 1.25^o
Accuracy (Relative to Mounting Pads)	1 arc minute (in 10^o x 10^o FOV); 3 arc minutes in XTAR
Turn-On Drift	<10 arc seconds
Noise Equivalent Angle (Jitter)	12 arc seconds (1 σ - for $+3^M$ target)
Tracking Loop Bandwidth	12 Hz
Error Signal Bandwidth	5 Hz
Beacon Modulation Sensitivity	15%
UV Radiometer	
Spectral Bandwidth	3700 - 3900 A^o
Scan	Single axis line scan; sawtooth - 10^o peak-to-peak; .2 Hz
Dynamic range	0 to 1.505×10^{-6} watts/cm^2/ster/A^o
Linearity	3% of measured voltage
Signal-to-Noise Ratio	1% of peak output voltage
Background	Sunlit clouds will not damage unit

TABLE 4-1 (Continued)

MMOS PERFORMANCE CHARACTERISTICS

MAP	
Dynamic Range	$+2^M$ Target to 10,000 ft-lamberts
Field	10^o square; 2.5^o square in LMT
Frame Rate	8 Hz; 30 Hz in LMT
Video Bandwidth	15 kHz
Uniformity	50% (worse case)
SIZE	6" dia. x 15" in.
WEIGHT	17.4 pounds
POWER	24.6 watts

APPENDIX A

ACCEPTANCE TEST

PROCEDURE

FOR

MULTI-MODE OPTICAL SENSOR - A

1.0 GENERAL

The Test Procedure supplements and becomes an Appendix to ITT Gilfillan Test Drawing 5522974.

1.1 Operating Conditions

The MMOS will be set up in a darkroom environment on an optical bench per Section 3.0 of the Test Plan. Unless otherwise specified, the tests will be made in a laboratory environment, with nominal line voltage, with a third magnitude star, with nominal output loads. At all times power is applied to the MMOS, a darkroom environment is implied. Whenever very accurate measurements are required, the various peripheral equipment such as the star simulator, should be on for two hours minimum prior to data taking.

1.2 Simulator Calibration

Prior to commencing into this procedure, the collimated star simulator intensity will have been calibrated per ITT Drawing 5522973 (Appendix B). The data from that procedure will be tabulated so that a star of +3, +2, +1, 0, or -1 visual magnitude can be presented to the MMOS.

The horizon simulator calibration will be made just prior to radiometer mode tests. The procedure is ITT Drawing 5522970 (Appendix C).

2.0 ALIGNMENT PROCEDURES

Prior to formal testing, a check of the test bed alignment will be made. Although not a part of the MMOS testing, it is a necessary step to insure the subsequent test results are valid.

2.1 Star Simulator Alignment (Test Plan Figure 4-1)

1. Place the Huet Optical Level on the granite table surface and set it to contain the surface reference. ✓
2. Place the level on the Moore table and shim as required to make parallel to the granite table within 1.6 arc minutes. ✓ <220sec
3. Mount the star simulator on the Moore rotary table. Positioning is not critical except that the front of the collimating lens should be approximately at the table axis of rotation to preclude vignetting of the MMOS lens by the collimating lens as the Moore table is rotated. ✓
4. Use an auto-collimator to align the Davidson Optronics D-616 mirrors prependicular to their base. ✓
5. Set the aligned mirror on the Moore table. Align an auto-collimator such that its line-of-sight is perpendicular to the mirror. ✓
6. Position the star (in the auto-collimator) to be aligned vertically with the auto-collimator. ✓

2.2 Star Simulator Calibration Data

Following is a tabulation from the simulator calibration procedure:

Visual Star Magnitude	Image Dissector Current	SIMULATOR	
		Filter Position	Bulb Current
5			
4	5.6 NA	5	840 MA
3	14.1 "	4	875 "
2	36.0 "	3	900 "
1	88.5 "	2	930 "
0	222. "	1	935 "
-1	560. "	0	940 "

2.3 Test Bed Alignment (Test Plan Figure 4-3)

1. Mount the MMOS on the Leitz table with the center of the lens approximately at the table axis of rotation to preclude vignetting of the MMOS lens by the collimating lens as the Leitz table is rotated. ✓

2. Set the Leitz table and the lower rotary table to approximately align the MMOS and star simulator. ✓

3. With the proper electrical interface per Test Plan Table 4-1, apply power to the MMOS. Use a 2^M star for alignment readings. ✓

4. With the MMOS tracking the star, monitor the X and Y outputs on an X-Y recorder. Rotate the Leitz table (θ) through 360^o. ✓

5. Vary the MMOS and/or Leitz table per Test Plan Figure 4-3 to null the X-Y outputs as a function of θ. ✓

6. At the optimum alignment record the peak to peak swing in X and Y for a rotation in θ of 360^o. Use a gradient of .00028 V/sec

   x = .0005 volts = .139 sec

   y - .001 volts = .278 sec

7. Set the Moore table vernier such that the angular readout is zero. ✓

8. Record the table readings and collimator readings which cannot be zeroed. ✓

   V_{leitz} = 3¼ min (coarse axis of the Leitz table)

   H_{sim} = .24665

   V_{sim} = .20570

   [readings of the horizontal and and vertical positions of a micrometer cross slide stage containing the pinhole source of the star simulator.]

2.4 MMOS Alignment (Test Plan Figure 4-4)

1. Rotate the star simulator from ρ_o so that the star image can be viewed in an auto-collimator. ✓

2. Align the auto-collimator vertically such that the star image is on its reference horizontal line. ✓

3. Translate the auto-collimator on the granite table to where it can auto-collimate on the roll axis surface of the MMOS reference mirror. ✓

4. Rotate the Leitz table in θ until the roll reference surface is perpendicular to the auto-collimator line-of-sight. ✓ see below

5. Record the Leitz table reading for θ. (angle at which variation in the X-output as a function of ρ is minimum) $\theta = 270^\circ$

6.* Without moving the auto-collimator vertical alignment, align a 90° mirror so that it is perpendicular to the auto-collimator line-of-sight. ____

7.* Place the mirror in the MMOS-star simulator line-of-sight per Test Plan Figure 4-4. ____

8.* Move the auto-collimator to align it to the star image reflected by the mirror. The boresight reference return should also be present in the auto-collimator. ____

9.* Align the MMOS in its Y-axis by varying the MMOS position (Y axis only) on the Leitz table until the vertical line return is within 5 arc seconds of its reference in the auto-collimator. ____

10.* Rotate the Leitz table 90° in the θ axis. ____

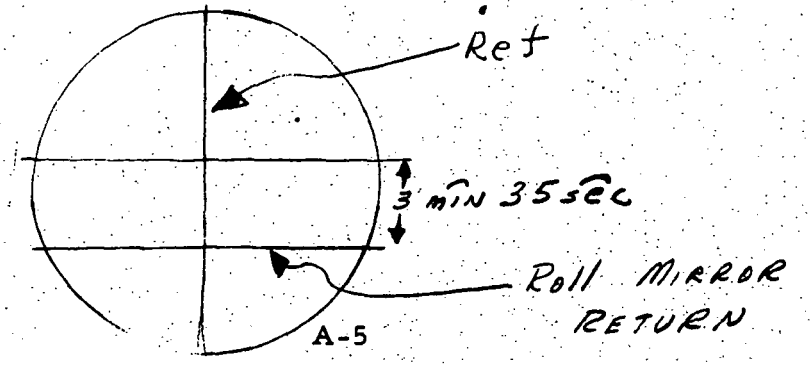

COMMENTS

ALIGNMENT PROCEDURE VARIATIONS

Difficulties encountered in aligning and setting the reference mirror prevented following the outlined procedure exactly. The mirror had been mounted and set on 4-17 but referencing the MMOS boresight to it could not be accomplished. Rather than delay Acceptance Tests, this alignment was postponed temporarily.

The initial mirror alignment was accomplished by autocollimating off the boresight reference mirror while rotating the MMOS in the θ angle and setting the mirror position to minimize shift of the reflected image. At the time it was felt that the alignment of mirror to electrical zero was within 1 minute of arc but it could not be proven.

During the Acceptance Tests, the boresight reference was taken as the MMOS electrical zero, ie., X error = Y error = 0.

On April 18, following the majority of tests, a check of the mirror alignment was again attempted and eventually accomplished. The procedure followed was essentially that outlined in the previous Sec. 2.4, items 6 - 11. It became evident that the alignment of the boresight reference surface to MMOS boresight was within 30 seconds of arc and could have been aligned to within 5 seconds of arc by resetting the tube-lens alignment internal to the MMOS. This was discussed with the NASA technical representative and it was decided to note the misalignment and not alter the MMOS internally. This was based on the fact that the field accuracy data had already been taken. Since an important aspect of the MMOS performance evaluation is correlation between this data and data from subsequent tests at NASA facilities, the number of changes between tests should be minimized.

The roll reference (90° side) is set as shown in the previous procedure. The boresight reference is as shown below:

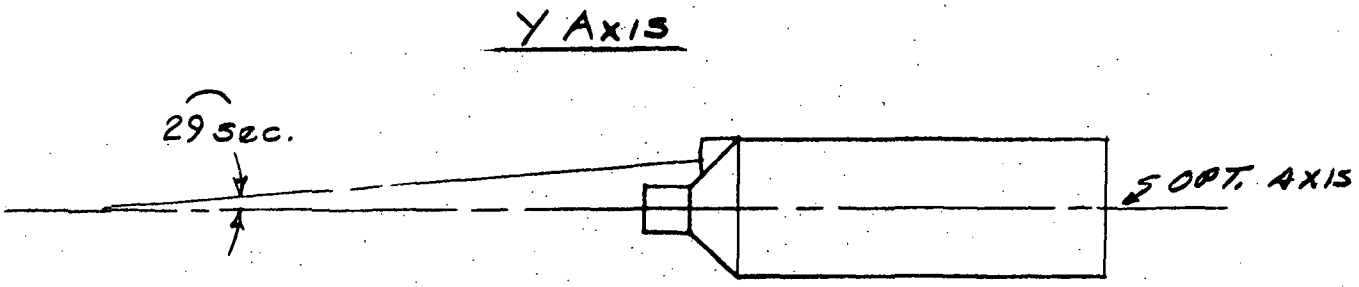

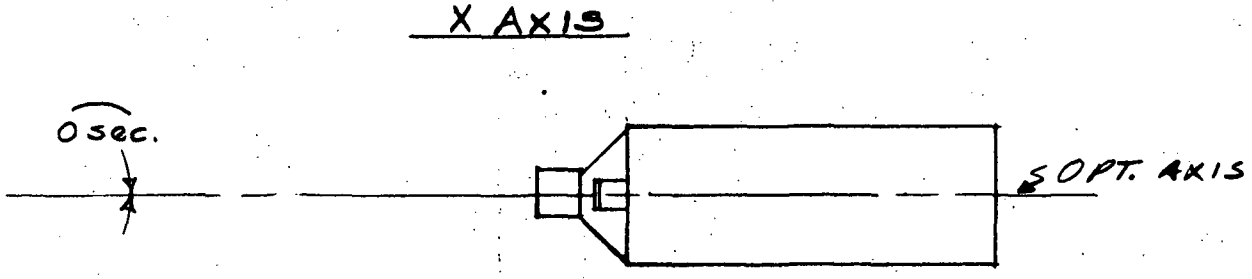

11.* Align the MMOS in its X-axis by varying the MMOS position (X axis only) on the Leitz table until the vertical line return is within 5 arc seconds of its reference in the auto-collimator. ____

12. If adjustments are required the entire Section 2.4 should be repeated. The final table angles are recorded. ____

ρ = 0

θ = 0

* SEE COMMENTS AFTER SEC. 2.5.

ITT WILL USE THE METHOD IN ITEMS 6 -11 TO MEASURE THE MIRROR BORESIGHT REFERENCE WITH RESPECT TO THE MMOS LINE OF SIGHT I.E. X = Y = 0 volt

2.5 MMOS Boresight Adjustment

1. With the MMOS in its aligned position, null the X and Y outputs by adjustment to the alignment screws near the front of the MMOS housing. ✓

2. Following adjustment, lock the screws to preclude any further adjustment. ✓

3. With the MMOS tracking the star at boresight (X = Y = 0) measure the HORIZON ANGLE output voltage to insure that it is 0 ± 0.010 volts. ✓

Hor. Angle 0

3.0 STAR TRACKING PERFORMANCE TESTS

3.1 Target Magnitude Calibration

Specification: Para. 3.2.1. The Sensor will meet all specifications when required to acquire and furnish error signals while observing stars and other targets having a visual magnitude of + 3 and brighter.

Method: With the star being tracked at the boresight axis, measure and record the TARGET MAGNITUDE voltage for the following star magnitudes.

TABLE 3.1

TARGET MAGNITUDE CALIBRATION

STAR MAGNITUDE	TARGET MAGNITUDE (Volts)
No Star	
4	+.480
3	+1.198
2	+2.310
1	+3.710
0	+4.670
-1	+4.950

4/18/72

3.2 Acquisition Field-of-View

Specification: Para. 3.2.2. The Sensor will have an effective field-of-view of at least $10^{\circ} \times 10^{\circ}$.

Method: The edge of the field-of-view is the angle at which a TARGET PRESENCE is first generated as the star is moved toward the MMOS boresight. Command the MMOS to the ACQ. mode. Rotate the simulator (ρ) so that the star is outside the AFOV. Then command the MMOS to the AUTO mode. Rotate the simulator to decrease ρ until a TARGET PRESENCE is attained. At this point record the value of ρ for each MMOS roll angle (θ). Record both the full and half AFOV angles.

2 Mag Star

TABLE 3-2

ACQUISITION FIELD-OF-VIEW

$10^{\circ} \times 10^{\circ}$ AFOV				
Roll Angle (θ)		Simulator Angle		
Leitz	MMOS	$+\rho$	$-\rho$	Spec.
0°	0°	$5^{\circ}18'$	$5^{\circ}10'$	$\geq 5.0^{\circ}$
45°	45°	$7^{\circ}10'$	$7^{\circ}12'$	$\geq 7.07^{\circ}$
90°	90°	$5^{\circ}7'$	$5^{\circ}9'$	$\geq 5.0^{\circ}$
135°	135°	$7^{\circ}11'$	$7^{\circ}14'$	$\geq 7.07^{\circ}$

($7^{\circ}4'$ -)

($7^{\circ}4'16''$)

$T = 92^{\circ}F$ TIME = 10:35

4/18/72

20° Dia. AFOV				
Roll Angle (θ)		Simulator Angle		
Leitz	MMOS	$+\rho$	$-\rho$	
0°	0°	$9^{\circ}18'$	$9^{\circ}54'$	
45°	45°	$8^{\circ}37'$	$10^{\circ}41'$	
90°	90°	$8^{\circ}30'$	$10^{\circ}20'$	
135°	135°	$9^{\circ}1'$	$10^{\circ}18'$	

3.3 Output Characteristics

Specification: Para. 3.2.4.1. The Sensor will have a maximum RSS error of less than one arc minute relative to the mounting pad. The value will be derived from the total pointing bias, tracking jitter values, and other error sources experienced when acquiring and tracking a third visual magnitude star.

Method: Data to determine specification compliance will be taken in several steps. Initially take data per the following Table 3-3A in order to calculate X and Y output gradient. Using a 2^M star, measure and record the X and Y outputs on an integrating digital voltmeter for angles tabulated in the table. Calculate the gradients from this data. Using the gradients, calculate the expected values of X and Y outputs for the 36 points of Test Plan Figure 5-1 and tabulate in Table 3-3B.

Using a 3^M star, measure the X and Y outputs for each of the 36 points on

a) a Dana Series 5400 digital voltmeter or a meter having an equivalent sampling time (meter will be connected to a printer and one sample taken).
b) an integrating digital voltmeter.

Record the instantaneous sample data in Table 3-3B. Compare the reading with the predicted reading. If the difference is greater than one arc minute, print out 50 independent samples at that angular position. The mean and variance at each point requiring 50 samples will be calculated. The accuracy criteria is satisfied if the sample mean + and - its variance is within one arc minute of the predicted value.

Results:

TIME = 13:45
TEMP = 99.5°F

Integrating Digital readouts

4-18-72 R.G. D.W.

TABLE 3-3A

ON AXIS OUTPUTS

	TABLE ANGLES		OUTPUTS (volts)	
	θ	ρ	X	Y
1	0	-3°	+2.959	+7
2	0	0	+2	+1
3	0	3°	+2.971	+6
4	45°	-4° 14' 34"	-2.967	-2.996
5	45°	0	+2	+2
6	45°	4° 14' 34"	+2.967	+3.006
7	90°	-3°	-4	-3.000
8	90°	0°	+1	0
9	90°	+3°	0	+3.008
10	135°	-4° 14' 34"	+2.962	-3.005
11	135°	0°	0	0
12	135°	4° 14' 34"	-2.971	+3.004

Gradient:

$$X = \frac{(\rho_5 + |\rho_{-5}|)}{60 \times 10} \quad \theta = 90^\circ \qquad Y = \frac{(\rho_5 + |\rho_{-5}|)}{60 \times 10} \quad \theta = 0^\circ$$

Based on Table 3-3B

X = 16.48 mV/min ⟷ Y = 16.68 mV/min

The gradient may be recalculated based upon measurements in Table 3-3B if closer registration of measured to predicted values is achieved. THE FINAL VALUES WERE BASED ON THE TABLE 3-3B DATA.

X GRAD = .989 mv/dg.
Y GRAD = 1.001 mv/dg.

4-18-73
RJ
DD

TABLE 3-3B
RANDOM ANGLE OUTPUTS

	TABLE ANGLES (deg min sec)		GYRO U. OUTPUTS (volts)					
			Measured		Predicted		Difference	
	θ	ρ	X	Y	X	Y	X (mv)	Y (mv)
1	0	0	+2	+3	0	0	+2	+3
2	11° 18' 36"	-5° 5' 56"	-4.933	-.998	4.945	1.001	-12	-3
3	11° 18' 36"	0	+3	+3	0	0	+3	+3
4	11° 18' 36"	5° 5' 56"	+4.938	+1.008	4.945	1.001	-7	+7

A-14

TABLE 3-3B

RANDOM ANGLE OUTPUTS

	TABLE ANGLES (deg min sec)		OUTPUTS (volts)					
			Measured		Predicted		Difference	
	θ	ρ	X	Y	X	Y	X(mv)	Y(mv)
5	18° 26' 6"	-3° 9' 44"	-2.965	-.990	2.967	1.001	-2	-11
6	18° 26' 6"	0	+2	+4	0	0	+2	+4
7	18° 26' 6"	3° 9' 44"	+2.973	+1.007	2.967	1.001	+6	+6
8	30° 57' 50"	-5° 49' 51"	-4.933	-2.998	4.945	3.003	-12	-5
9	30° 57' 50"	0	+2	+5	0	0	+2	+5
10	30° 57' 50"	5° 49' 51"	+4.943	+3.019	4.945	3.003	-2	+16

TABLE 3-3B

RANDOM ANGLE OUTPUTS

T = 101° F TIME = 1435

	TABLE ANGLES (deg min sec)		OUTPUTS (volts)					
			Measured		Predicted		Difference	
	θ	ρ	X	Y	X	Y	X (mv)	Y (mv)
✓11	45°	-7° 4' 16"	-4.942	-4.993	4.945	5.005	-3	-12
✓12	45°	-4° 14' 34"	-2.967	2992	2.967	3.003	+0	-11
✓13	45°	-1° 24' 51"	-.982	-.986	.989	1.001	-7	-15
✓14	45°	0	+3	+6	0	0	+3	+6
✓15	45°	1° 24' 51"	+.996	+1.011	.989	1.001	+7	+10
✓16	45°	4° 14' 34"	+2.967	+3.008	2.967	3.003	+0	+5
✓17	45°	7° 4' 16"	+4.958	+5.014	4.945	5.005	+13	+9

TABLE 3-3B

RANDOM ANGLE OUTPUTS

	TABLE ANGLES (deg min sec)		OUTPUTS (volts)					
			Measured		Predicted		Difference	
	θ	ρ	X	Y	X	Y	X (mv)	Y (mv)
18	59° 2' 10"	-5 49' 51"	-2.971	-5.000	2.967	5.005	+4	-5
19	59° 2' 10"	0	+2	+7	0	0	+2	+7
20	59° 2' 10"	5° 49' 51"	+2.979	+5.017	2.967	5.005	+12	+12
21	71° 33' 54"	-3° 9' 44"	-.989	-2.991	.989	3.003	+0	-12
22	71° 33' 54"	0	+2	+6	0	0	+2	+6
23	71° 33' 54"	3° 9' 44"	+1.000	+3.012	9.89	3.003	+12	+9

TABLE 3-3B

RANDOM ANGLE OUTPUTS

	TABLE ANGLES (deg min sec)		OUTPUTS (volts)					
			Measured		Predicted		Difference	
	θ	ρ	X	Y	X	Y	X (mv)	Y (mv)
V24	78° 41' 24"	-5° 5' 56"	-.993	-4.995	.989	5.005	+4	-10
V25	78° 41' 24"	0	+2	+7	0	0	+2	+7
V26	78° 41' 24"	5o 5' 56"	+.996	+5.016	.989	5.005	+7	+11
V27	101° 18' 36"	5° 5'56" ~~-5° 51'56"~~	+.983	-4.993	.989	5.005	-6	-12
V28	101° 18' 36"	0	+1	+8	0	0	+1	+8
V29	101° 18' 36"	5°5'56" ~~5° 51' 56"~~	-.980	+5.004	.989	5.005	-9	-1

TABLE 3-3B

RANDOM ANGLE OUTPUTS

	TABLE ANGLES (deg min sec)		OUTPUTS (volts)					
			Measured		Predicted		Difference	
	θ	ρ	X	Y	X	Y	X (mv)	Y (mv)
30	108° 26' 6"	-3° 9' 44"	+.991	-2.992	.989	3.003	+2	-11
31	108° 26' 6"	0	+1	+7	0	0	+1	+7
32	108° 26' 6"	3° 9' 44"	-.985	+3.014	.989	3.003	-4	+11
33	120° 57' 50"	-5° 49' 51"	+2.959	-4.996	2.967	5.005	-8	-9
34	120° 57' 50"	0	0	+8	0	0	0	+8
35	120° 57' 50"	5° 49' 51"	-2.963	+5.008	2.967	5.005	-4	+3

TABLE 3-3B

RANDOM ANGLE OUTPUTS

	TABLE ANGLES (deg min sec)		OUTPUTS (volts)					
			Measured		Predicted		Difference	
	θ	ρ	X	Y	X	Y	X(mv)	Y(mv)
36	135°	-7° 4' 16"	+4940	-4.994	4.945	5.005	-5	-11
37	135°	-4° 14' 34	+2.963	-2.997	2.967	3.003	-4	-6
38	135°	-1° 24' 51"	+.988	-.994	.989	1.001	-1	-7
39	135°	0	0	+8	0	0	0	+8
40	135°	1° 24' 51"	-.990	+1.010	.989	1.001	+1	+9
41	135°	4° 14' 34"	-2.970	+3.012	2.967	3.003	+3	+9
42	135°	7° 4' 16"	-4.945	+5.019	4.945	5.005	0	+14

TABLE 3-3B

RANDOM ANGLE OUTPUTS

TEMP = 101.5° F TIME = 15:25

	TABLE ANGLES (deg min sec)		OUTPUTS (volts)					
			Measured		Predicted		Difference	
	θ	ρ	X	Y	X	Y	X (mv)	Y (mv)
43	149° 2' 10"	-5° 49' 51"	+4.938	-2.997	4.945	3.003	-7	-4
44	149° 2' 10"	0	+2	+7	0	0	+2	+7
45	149° 2' 10"	5° 49' 51"	-4.943	+3.010	4.945	3.003	-2	+7
46	161° 33' 54"	-3° 9' 44"	+2.972	-.997	2.967	1.001	+5	-4
47	161° 33' 54"	0	+2	+7	0	0	+2	+7
48	161° 33' 54"	3° 9' 44"	-2.968	+1.011	2.967	1.001	+1	+10

TABLE 3-3B

RANDOM ANGLE OUTPUTS

	TABLE ANGLES (deg min sec)		OUTPUTS (volts)					
			Measured		Predicted		Difference	
	θ	ρ	X	Y	X	Y	X(m.z.)	Y(m.z.)
49	168° 41' 24"	-5° 5' 56"	+4.935	-.997	4.945	1.001	-10	-4
50	168° 41' 24"	0	+2	+8	0	0	+2	+8
51	168° 41' 24"	5° 5' 56"	-4.944	+1.007	4.945	1.001	-1	+6
52	0	0	+3	+9	0	0	+3	+9

X	Y
4945	5007
2907	3001
989	1001

Dana Readout

4-18-72

K.J. D.D.

TABLE 3-3C

RANDOM ANGLE OUTPUTS

TABLE ANGLES (deg min sec)		OUTPUTS (volts)					
		Measured		Predicted		Difference	
θ	ρ	X	Y	X	Y	X (mv)	Y (mv)
0	0	0	0				
11° 18' 36"	-5° 5' 56"	-4.929	-.995	4.945	1.001	-16	-6
11° 18' 36"	0	0	.002				
11° 18' 36"	5° 5' 56"	4.941	1.010	4.945	1.001	-4	+9

A-23

TABLE 3-3C

RANDOM ANGLE OUTPUTS

TABLE ANGLES (deg min sec)		OUTPUTS (volts)					
		Measured		Predicted		Difference	
θ	ρ	X	Y	X	Y	X(mv)	Y(mv)
18° 26' 6"	-3° 9' 44"	-2.965	-.994	2.967	1.001	-2	-7
18° 26' 6"	0	0	0				
18° 26' 6"	3° 9' 44"	2.968	1.006	2.967	1.001	+1	+5
30° 57' 50"	-5° 49' 51"	-4.935	-3.004	4.945	3.003	-10	+1
30° 57' 50"	0	+.003	0				
30° 57' 50"	5° 49' 51"	4.947	3.017	4.945	3.003	+2	+14

TABLE 3-3G

RANDOM ANGLE OUTPUTS

	TABLE ANGLES (deg min sec)		OUTPUTS (volts)					
			Measured		Predicted		Difference	
	θ	ρ	X	Y	X	Y	X(mv)	Y(mv)
11	45°	-7° 4' 16"	-4.941	-4.994	4.945	5.005	-4	-11
12	45°	-4° 14' 34"	-2.967	-2.994	2.967	3.003	0	-9
13	45°	-1° 24' 51" Recheck →	-.983 / -.983	-.986 / -.979	.989	1.001	-6 / -6	-15 / -22
14	45°	0	+.002	0			+2	0
15	45°	1° 24' 51"	.994	1.011	.989	1.001	+5	+10
16	45°	4° 14' 34"	2.970	3.008	2.967	3.003	+3	+5
17	45°	7° 4' 16"	4.959	5.015	4.945	5.005	+14	+10

TABLE 3-3C

RANDOM ANGLE OUTPUTS

	TABLE ANGLES (deg min sec)		OUTPUTS (volts)					
			Measured		Predicted		Difference	
	θ	ρ	X	Y	X	Y	X(mv)	Y(mv)
18	59° 2' 10"	-5 49' 51"	-2.971	-5.000	-2.967	-5.005	+4	-5
19	59° 2' 10"	0	0	+.004	0	0	0	+4
20	59° 2' 10"	5° 49' 51"	2.974	5.019	2.967	5.005	+7	+14
21	71° 33' 54"	-3° 9' 44"	-.991	-2.992	-.989	-3.003	+2	-11
22	71° 33' 54"	0	+.001	+.002	0	0	+1	+2
23	71° 33' 54"	3° 9' 44"	1.003	3.009	.989	3.003	+14	+6

TABLE 3-3C

RANDOM ANGLE OUTPUTS

	TABLE ANGLES (deg min sec)		OUTPUTS (volts)					
			Measured		Predicted		Difference	
	θ	ρ	X	Y	X	Y	X(mv)	Y(mv)
24	78° 41' 24"	-5° 5' 56"	-.994	-4.997	.989	5.005	+5	-8
25	78° 41' 24"	0	+.001	+.004			+1	+4
26	78° 41' 24"	5o 5' 56"	.996	5.011	.989	5.005	+7	+6
27	111° 18' 36"	-5° 51' 56"	.985	-4.991	.989	5.005	-4	-14
28	111° 18' 36"	0	0	0				
29	111° 18' 36"	5° 51' 56"	-.980	5.000	.989	5.005	-9	-5

TABLE 3-3C

RANDOM ANGLE OUTPUTS

	TABLE ANGLES (deg min sec)		OUTPUTS (volts)					
			Measured		Predicted		Difference	
	θ	ρ	X	Y	X	Y	X (mv)	Y (mv)
30	108° 26' 6"	-3° 9' 44"	.991	-2.997	.989	-3.003	+2	-6
31	108° 26' 6"	0	+.001	+.003	0	0	+1	+3
32	108° 26' 6"	3° 9' 44"	-.980	3.017	-.989	3.003	-9	+14
33	120° 57' 50"	-5° 49' 51"	2.956	-4.999	2.967	-5.005	-11	-6
34	120° 57' 50"	0	0	.003	0		0	+3
35	120° 57' 50"	5° 49' 51"	-2.965	5.007	-2.967	5.005	-2	+2

TABLE 3-3C

RANDOM ANGLE OUTPUTS

	TABLE ANGLES (deg min sec)		OUTPUTS (volts)					
			Measured		Predicted		Difference	
	θ	ρ	X	Y	X	Y	X(mv)	Y(mv)
36	135°	-7° 4' 16"	4.939	-4.990	4.945	-5.005	-6	-15
37	135°	-4° 14' 34	2.957	-2.991	2.967	-3.003	-12	-12
38	135°	-1° 24' 51"	.989	-.993	.989	-1.001	0	-8
39	135°	0	0	+.009	0	0	0	+9
40	135°	1° 24' 51"	-.991	1.009	-.989	1.001	+2	+8
41	135°	4° 14' 34"	-2.968	3.012	-2.967	3.003	+1	+9
42	135°	7° 4' 16"	-4.945	5.021	-4.945	5.005	0	+16

TABLE 3-3C

RANDOM ANGLE OUTPUTS

	TABLE ANGLES (deg min sec)		OUTPUTS (volts)					
			Measured		Predicted		Difference	
	θ	ρ	X	Y	X	Y	X(mv)	Y(mv)
43	149° 2' 10"	-5° 49' 51"	4.932	-2.996	4.945	-3.003	-13	-7
44	149° 2' 10"	0	+.001	+.003	0	0	+1	+3
45	149° 2' 10"	5° 49' 51"	-4.941	3.007	4.945	3.003	-4	+4
46	161° 33' 54"	-3° 9' 44"	2.968	-.996	2.967	-1.001	+1	-5
47	161° 33' 54"	0	+.002	+.007	0	0	+2	+7
48	161° 33' 54"	3° 9' 44"	-2.969	1.015	-2.967	1.001	+2	+14

TABLE 3-3C

RANDOM ANGLE OUTPUTS

	TABLE ANGLES (deg min sec)		OUTPUTS (volts)					
			Measured		Predicted		Difference	
	θ	ρ	X	Y	X	Y	X(mv)	Y(mv)
49	168° 41' 24"	-5° 5' 56"	4.936	-.992	4.945	-1.001	-9	-9
50	168° 41' 24"	0	0	+.003	0	0	0	+3
51	168° 41' 24"	5° 5' 56"	-4.940	1.003	-4.945	1.001	-5	+2
52	0	0	+.001	+.009	0	0	+1	+9

MMOS

FIELD LINEARITY PLOT / TABLE 3-3B

MMOS

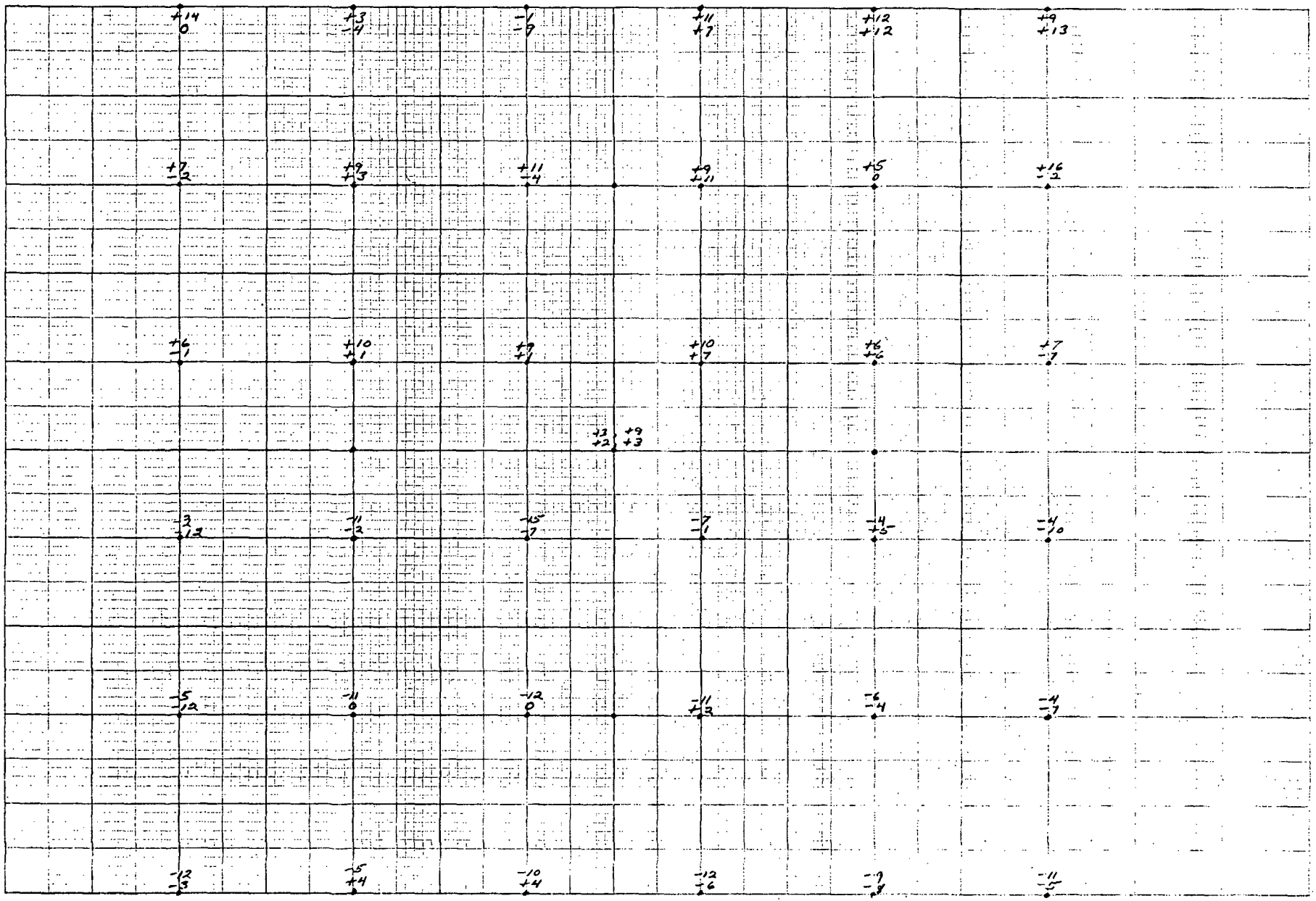

3.4 Tracking Noise Angle

Specification: no specific applicable reference; a component of output position error.

Method: With the MMOS tracking a 3^M star near boresight, record the X and Y outputs on a Sanborn recorder for one minute. Calculate the RMS noise angle by dividing the maximum negative to maximum positive peak of the recording by seven. Repeat the recording and calculation for 4^M and 2^M stars.

Results:

TABLE 3.4

NOISE ANGLE

STAR MAGNITUDE	OUTPUT					
	P - P (volts)		RMS (volts)		RMS ($\sqrt{sec}$)	
	X	Y	X	Y	X	Y
4	.031	.030	.0044	.0043	16.1	15.4
3	.022	.018	.0031	.0026	11.4	9.2
2	.014	.014	.0020	.0020	7.3	7.2
1	.0095	.0105	.0014	.0015	4.9	5.4
0	.0080	.0080	.0011	.0011	4.2	4.0

From Table 3.3A, the gradients:

X = 16.48mV/$\sqrt{min.}$ = .2747mV/$\sqrt{sec}$

Y = 16.68mV/$\sqrt{min.}$ = .2780mV/$\sqrt{sec}$

4/18/72

3.5 Acquisition Time

Specification: Para. 3.2.3.1

Acquisition of a star will be completed and error signals provided within 1.0 seconds after acquisition is commanded, where the target appears at any point in the $10^{o} \times 10^{o}$ field-of-view and may be moving at a rate relative to the Sensor as high as 0.5 degree per second. This performance will be demonstrated in at least 80% of the trials attempted with random selection of initial position and velocity.

Method: Use a Sanborn recorder to record 1) TARGET PRESENCE and 2) command to AUTO (removal of any command input). The acquisition time is the time interval between command to AUTO and generation of TARGET PRESENCE using a 3^{M} star as the target. Effect rates by manually slewing either the simulator (ρ) or the MMOS (θ). Determine the slew rate at which acquisition occurred by recording the X and Y outputs on another Sanborn recorder. Record a minimum of ten time intervals for random field positions.

Results:

TABLE 3-5

ACQUISITION TIME

	TRIAL	TIME	RATE
$\theta = 0°$	1	1 Sec	All @ 1.5°/sec
	2	1 Sec	
	3	1 Sec	
	4	1 Sec	
	5	1 Sec	
$\theta = 90°$	6	1 Sec	
	7	1 Sec	
	8	1 Sec	
	9	1 Sec	
	10	1 Sec	
$\theta = 45°$	11	1 Sec	
	12	1 Sec	
	13	1 Sec	
	14	1 Sec	
	15	1 Sec	
	16		
	17		
	18		
	19		
	20		

Spec. requires TIME ≤1.0 seconds for 80% of the trials.

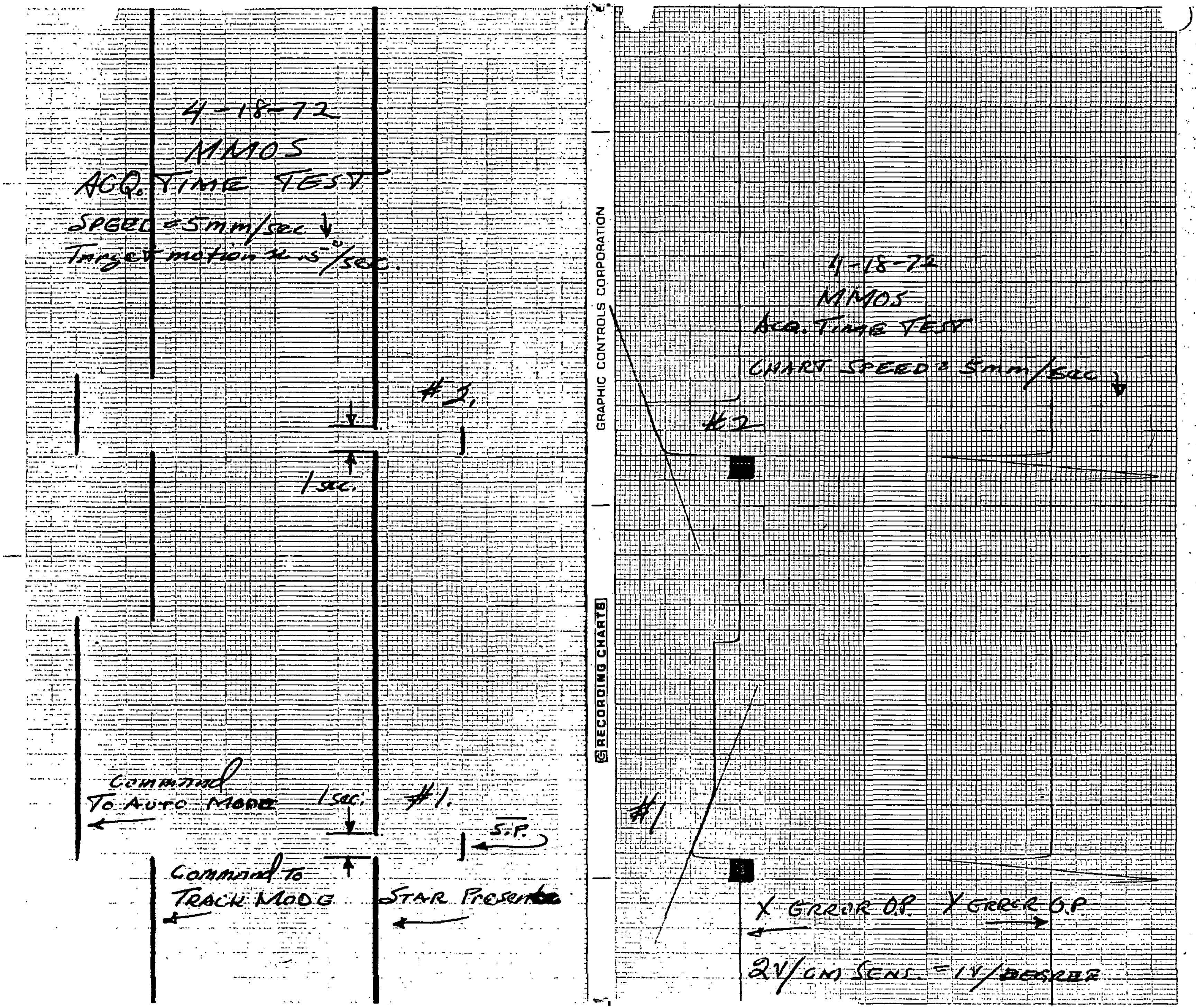
4-18-72
MMOS
ACQ. TIME TEST
SPEED = 5mm/sec
Target motion ≈ .5°/sec.
#2.
1 sec.
Command
To Auto Mode
1 sec.
#1.
S.P.
Command To
Track Mode
Star Present
GRAPHIC CONTROLS CORPORATION
RECORDING CHARTS
4-18-72
MMOS
ACQ. TIME TEST
CHART SPEED = 5mm/sec
#2
#1
X ERROR O.P.
Y ERROR O.P.
2V/CM SENS. = 1V/DEGREE

3.6 Star Selection

Specification: Para. 3.2.3: The Sensor must be capable of selecting the brightest target in the 10^{o} x 10^{o} field-of-view provided the magnitude difference is at least one and the angular separation at least 0.5 degrees.

Method: Remove the pinhole source plate from the simulator and replace with the plate containing two pinholes. Track one of the sources and set its intensity to a 3^{M} star by monitoring the TARGET MAGNITUDE. Repeat for the second source and set its intensity to be a 2^{M}. Now place both stars in the 10^{o} x 10^{o} AFOV and command the tracker to AUTO mode. Correct acquisition will be determined by turning off the brightest star to see if the MMOS returns to the ACQ. mode. Try several selection trials with various ρ's and θ's monitoring the TARGET MAGNITUDE to determine if correct selection has been accomplished.

Results:

STAR MAG. of		STAR SELECTED IN TRIAL		
#1	#2	1	2	3
4	3	3rd	3rd	3rd
2	3	2nd	2nd	2nd
2	1	1ST	1ST	1ST
0	1	0	0	0
0	-1	-1	-1	-1

4/18/72

3.7 Output Data Bandwidth

Specification: Para. 3.3.5. The Sensor output bandwidth will be no less than 5 Hz.

Method: For this test, move the MMOS from the Leitz table on to the Davidson Optical Bench. Mount the dynamic test source (CRT tube and prism) at the Davidson collimating lens focal plane. Apply a .1 Hz sine wave to one set of plates of the CRT. Set the sine wave amplitude to produce a ~~30~~ 5 arc minute (~~1.8~~ .08 volts) peak to peak swing in the appropriate MMOS output. Record on a Sanborn recorder the CRT input and MMOS output for discrete sweep frequencies of 0.1, 0.5, 1.0, 3.0, 5.0, 10.0 and 20.0 Hz. Repeat the measurements for the opposite MMOS channel. At 5 Hz the amplitude shall not be less than .707 of the amplitude measured at .5 Hz and the phase lag shall not be more than 45°.

TABLE 3.7 STAR MAG = 4.4 volts

MMOS BANDWIDTH

Input Frequency	OUTPUT			
	X		Y	
	Ampl.	Phase	Ampl.	Phase
0.1	15.5	0°	15.5	0°
0.5	15.5	-9°	15.3	-5°
1.0	15.0	-14°	15.0	-11°
3.0	14.7	-27°	14.0	-30°
5.0	13.2	-42°	12.2	-45°
10.0				
20.0				

3.8 Offset Voltage Capability

Specification: Para. 3.3.6. The Sensor must be capable of providing for control of the desired null point location by means of introducing two controlled voltage levels from an external source during operation in the OFFSET mode.

Method: Rotate the table to $\theta = 0$ and set ρ to 5^{o}. Measure and record the Y output. Apply approximately 5 volts to the Y OFFSET input and command the MMOS to the OFFSET mode. Measure the Y output. If it is not within .1 volts (.1 degree) of the initial reading, refine the Y OFFSET input and repeat a command sequence to OFFSET mode. Tailor the Y offset voltage until the Y output is within .1 volts of the Y output reading recorded during tracking. Once achieved, record the Y OFFSET voltage and calculate the transfer function in volts/degree. Rotate the MMOS to $\theta = 90^{o}$. Repeat the procedure outlined to determine the X OFFSET transfer function.

Results:

TABLE 3-8

OFFSET TRANSFER FUNCTION

CONDITION	Y (Volts)		X (Volts)	
	Output	Offset	Output	Offset
Star at Y = 5°				
Y Offset #1	-.980	-.989	////////	////////
#2	-1.980	-1.993	////////	////////
#3	-2.975	-2.978	////////	////////
#4	-3.985	-3.965	////////	////////
Star at X = 5°				
X Offset #1	////////	////////	-4.930	-4.933
#2	////////	////////	-3.942	-3.954
#3	////////	////////	-2.952	-2.913
#4	////////	////////	-1.973	-1.964

Y Offset T. F. = 1.0 V/degree

X Offset T. F. = 1.0 V/degree

CHECK: TRKING C-OFFSET

Star at X=Y=2.5°	X=-2.50	-2.48		
	Y=-2.55	-2.53		

3.9 X - Y Output Plot

Specification: no specific reference

Method: The object of this recording is to provide a composite graph of the X and Y outputs. Apply the X output to the horizontal and vertical channel of an X-Y recorder respectively. The recorder gain should be .5 volts/inch. Set ρ to 1^{o} and rotate θ through 360^{o}. Repeat for ρ in 1^{o} steps up to $\rho = 10^{o}$.

Results: Mark X-Y plot and include with test results.

NMOS 4-20-72
X-Y plot
D.W.
1 Volt
1 Volt
+X
-X
+Y
-Y
10°
20°
30°
40°
50°
60°
70°
80°
90°
← Constant θ from
0° to 360°

4.0 RADIOMETER PERFORMANCE TESTS

For the following tests, rotate the MMOS via the rotary table under the Leitz table to be aligned with the horizon simulator. If not already performed, calibrate the simulator intensity per drawing 5522970.

4.1 Zero Offset Output Voltage

Specification: Para. 3.2.6.2.1. The zero offset of the output voltage will be less than 0.1 precent of the full scale voltage.

Method: Command the MMOS to the RAD mode. With a cap on the MMOS lens, measure the HOR. INT. output.

Result:

HOR. INT. = .002 / .007 volts (S/B ≤ .005 volts)

MEASURED WITH MMOS AT 100°F; 2 HOUR WARMUP

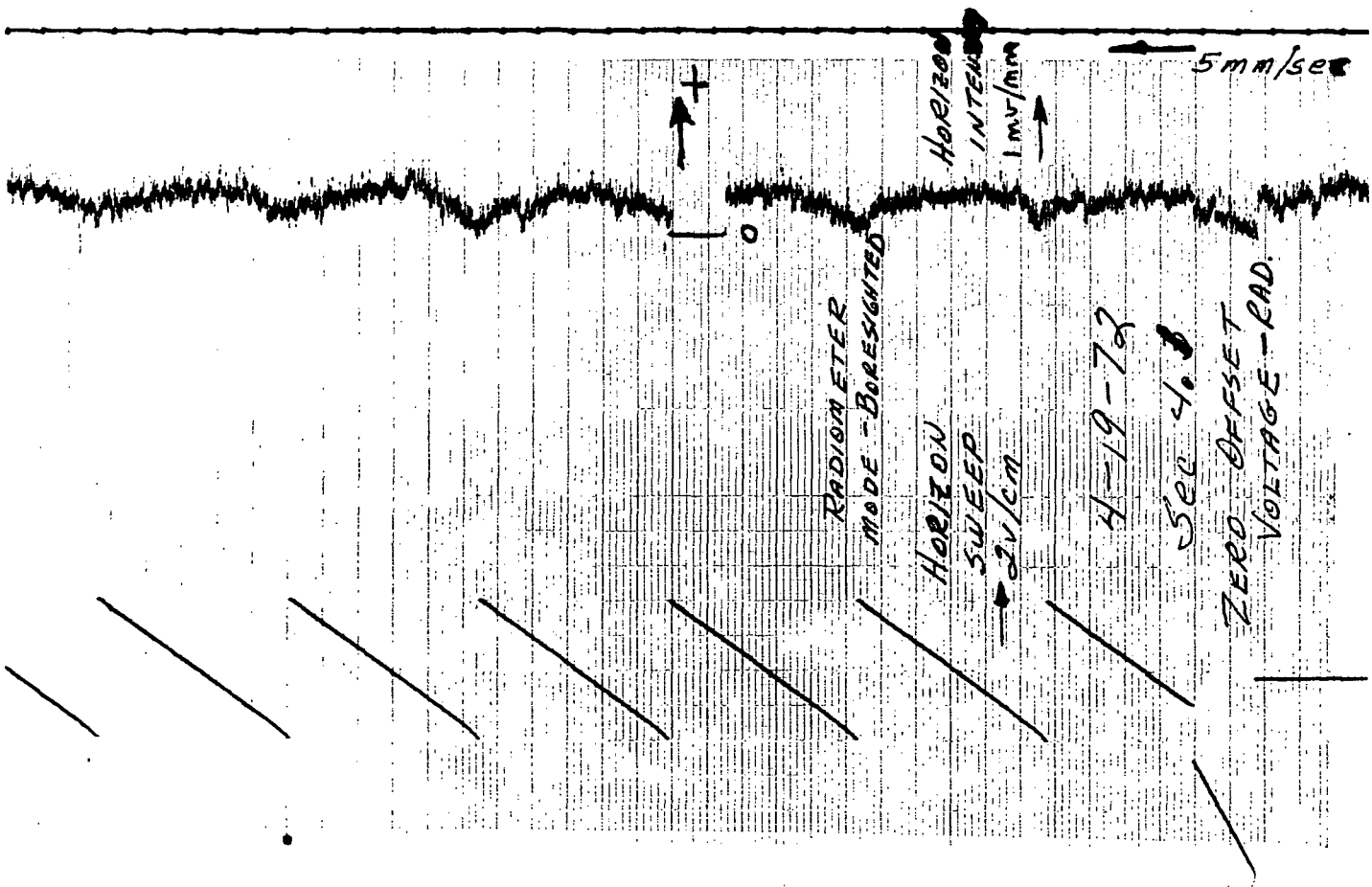

COMMENTS

The following three radiometer mode tests were made using a diffuse source whose light source was a D.C. supplied quartz iodide lamp. Initial test attempts using an A.C. supplied Xenon lamp failed due to a high content of power supply ripple and low frequency arc variation in the light output. Use of the D.C. powered quartz iodide lamp provided a source that allowed measurement of the performance without noticeable noise additions.

4.2 Horizon Intensity Ouput Uniformity

Specification: Para. 3.2.6.2.1 The horizon intensity output scale factor will be set at 5 volts for a peak radiance level of 1.505×10^{-6} watts cm^{-2} $ster^{-1}$ $angstrom^{-1}$.

Specification: Para. 3.2.6.2.1 The output voltage in the horizon measurement mode will be proportional to the radiance level within a linearity of 3% of the voltage measured at that point.

Method: Place a diffuse source larger than the MMOS collecting aperture as close as possible to the MMOS lens. The source should be previously calibrated to have a radiance of 1.505×10^{-6} watts cm^{-2} $ster^{-1}$ $angstrom^{-1}$. *

Method: Monitor the HOR. INT. output on the Dana 5400 Digital Voltmeter or equivalent. Set the meter printout speed at 15 readings per second. Command the MMOS to the RAD mode and record data for several scans.

Results: Using a 15 readings per second printout rate should provide approximately 75 readings for the entire scan of 10^{o}. This is a reading every 75 millisecond in time or every 8 arc minutes in angle. Tabulate the readings designating the number one reading at the top of the scan. All readings should be $5.25 \pm .25$ volts. Maximum variation between any two readings should not be greater than 6% using the average of the two extremes as the mean HOR. INT. output.

* A RADIANCE OF APPROXIMATELY 1/5 THIS VALUE WAS USED DUE TO THE INABILITY OF PRODUCING A UNIFORM SOURCE AT THE HIGHER LEVEL.

MIN. READING = 922 mv = -2.38%
MAX READING = 967 mv = +2.33%
Δ " = 45 mv
MEDIAN = 944 mv

READING		HORIZON INTENSITY		
Number	Horizon Angle (Approx)	Output M-Volts	Difference	
			Volts	%
1	+5°	957		
2		957		
3		956		
4		967		
5		962		
6		961		
7		957		
8	+4°	965		
9		967 *	MAXIMUM READING	
10		958		
11		956		
12		958		
13		965		
14		961		
15	+3°	965		
16		962		
17		952		
18		950		
19		961		
20		950		
21		955		
22	+2°	946		
23		961		
24		960		
25		953		

READING		HORIZON INTENSITY		
Number	Horizon Angle (Approx)	Output M-Volts	Difference	
			Volts	%
26		957		
27		946		
28		959		
29		955		
30	+1°	960		
31		953		
32		945		
33		943		
34		945		
35		945		
36		948		
37	0°	948		
38		943		
39		947		
40		941		
41		936		
42		950		
43		940		
44		935		
45	-1°	942		
46		932		
47		941		
48		941		
49		941		
50		938		

READING		HORIZON INTENSITY		
Number	Horizon Angle (Approx)	Output M-Volts	Difference Volts	Difference %
51		934		
52	-2°	934		
53		938		
54		931		
55		935		
56		924		
57		925		
58		931		
59		924		
60	-3°	936		
61		934		
62		942		
63		934		
64		931		
65		932		
66		936		
67	-4°	938		
68		937		
69		933		
70		929		
71		933		
72		940		
73		922 *	MINIMUM READING	
74		929		
75	-5°	926		

4.3 Horizon Intensity Signal-to-Noise Ratio

Specification: Para. 3.2.6.2.2. The peak to peak noise in the HOR. INT. output will not exceed 1% of the voltage for the radiance level of 1.505×10^{-6} watts cm^{-2} $ster^{-1}$ $angstrom^{-1}$.

Method: With the MMOS centered on the horizon target, ground the MMOS radiometer boresight pin (connector pin #4) such that there is no radiometer sweep and record the HOR. INT. output on a Sanborn recorder for one minute.

Results:

HOR. INT. noise = .050 Volt p-p (should be less than .050 V)

MEASUREMENT WAS MADE ON A-C COUPLED SANBORN RECORDER. MMOS WAS IN RAD. MODE AT BORESIGHT. HOR. INT. OUTPUT WAS 5 VOLTS.

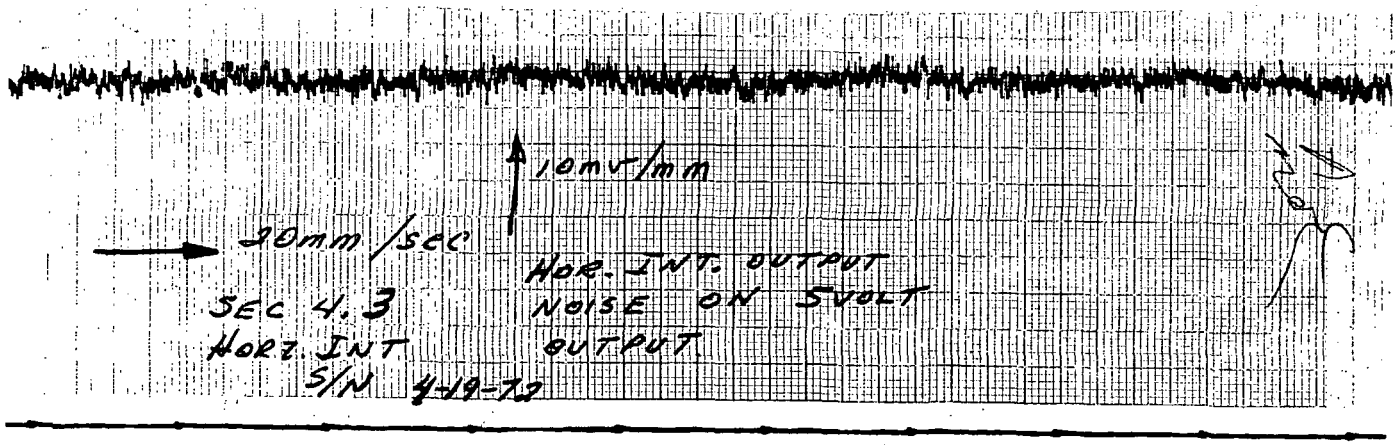

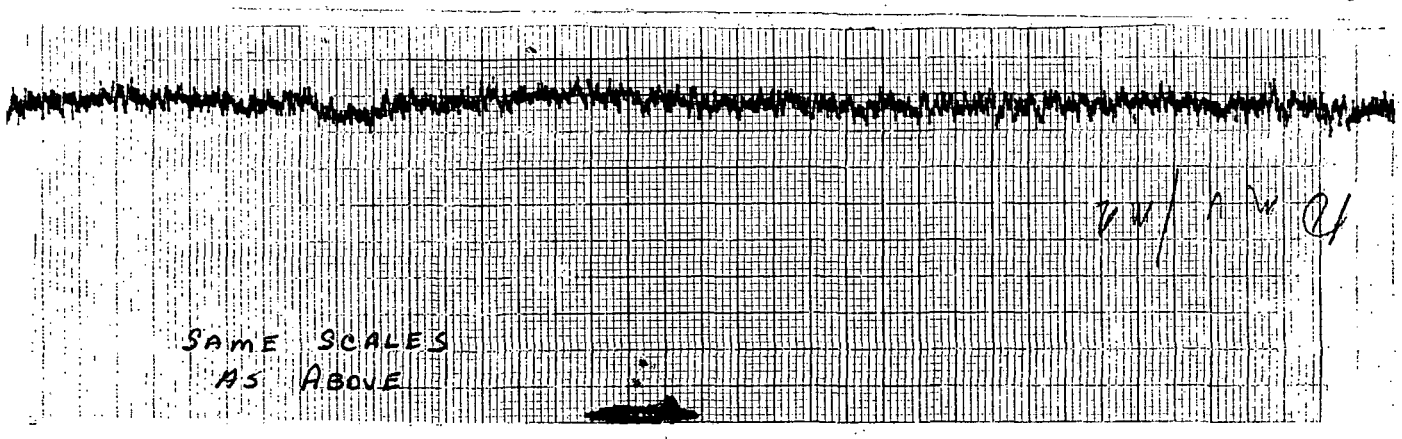

4.4 Horizon Intensity Output Linearity

Specification: Para. 3.2.6.2.1. The output voltage in the horizon measurement mode will be proportional to the radiance level within a linearity of 3% of the voltage measured at that point.

Method: Monitor the HOR. INT. and HOR. ANGLE on a Sanborn recorder. Center the collimated horizon target (approximately 2^{o} diameter) both horizontally and vertically in the MMOS field-of-view. Using a target intensity that produces approximately 5 volts on the HOR. INT. output at the center of the target, record the two outputs for several scans.

Result:

The objective is to observe the rise and fall of the HOR. INT. output as the transition from a light to dark portion of the target is crossed. It is noted that the horizon target need not be uniform for this test. Uniformity will not be checked in this test. The linearity of the output will be determined graphically from the Sanborn recording.

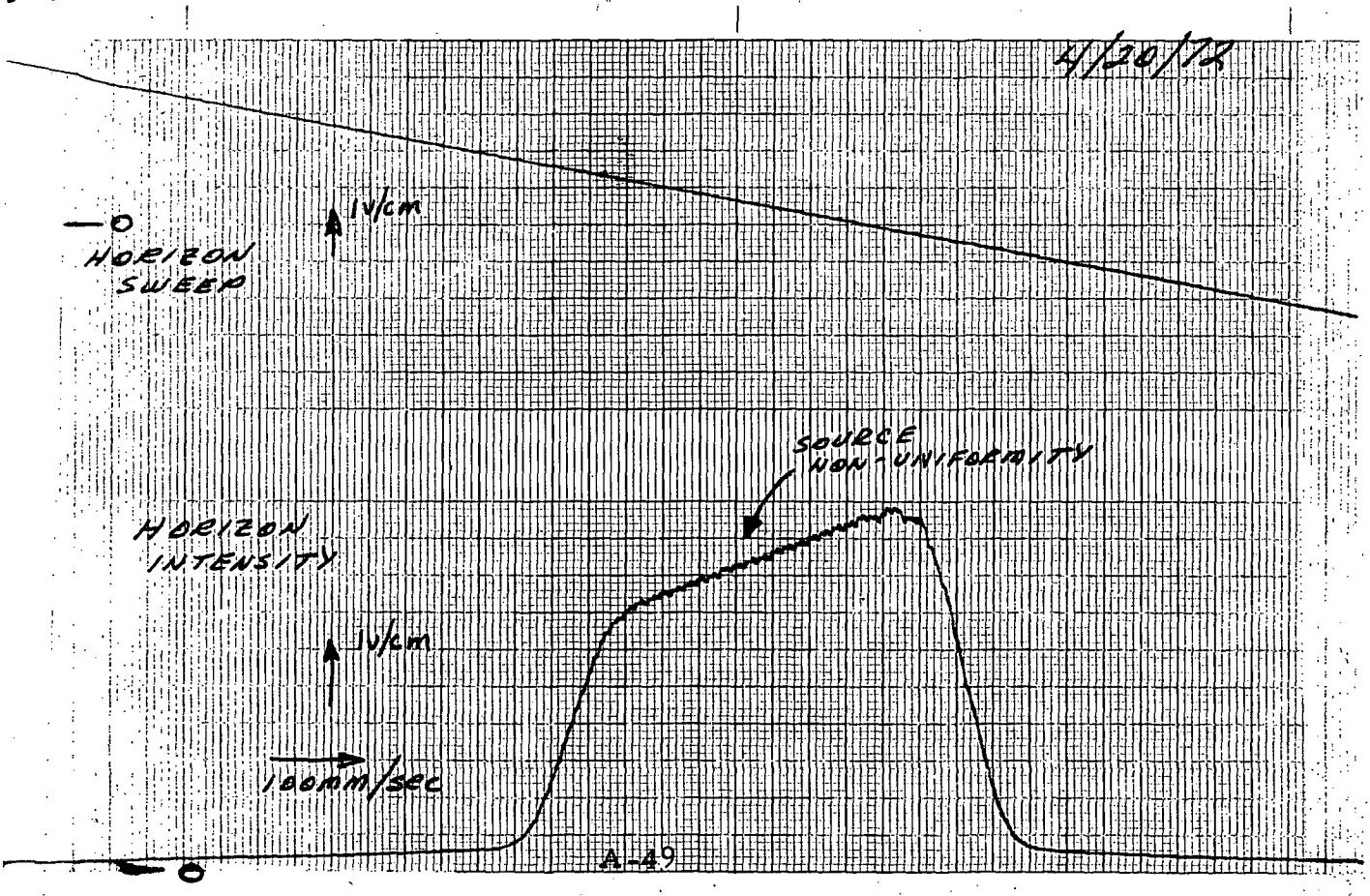

5.0 GENERAL PERFORMANCE TESTS

The objective of the following tests is to insure MMOS performance pertaining to overall operation, i.e., all modes of operation.

5.1 Bright Object Protection

Specification: Para. 3.3.3.1. A sun shutter and necessary activation circuitry to protect the Sensor from sun exposure is required. The activation speed must be sufficient for protection with a slew rate of 10 degrees/second between the Sensor and the sun exposure.

Method: Place a lens cap on the MMOS. Set the solar simulator in a mode to provide approximately one solar constant of energy. Monitor the MMOS SUN SHUTTER STATUS. Initially start with the solar beam at least 90° from the MMOS boresight. Rotate the MMOS slowly into the solar beam and record the angle at which the shutter is closed. Repeat this measurement twice. Now rotate the MMOS into the solar beam at approximately a 10 degree/second rate. Repeat this measurement twice. Since there are two sun sensors on the MMOS, rotate the MMOS about its boresight axis and repeat the measurements at 90° and 180°.

Results:

TABLE 5-1

SUN PROTECTION ANGLE

Sensor		Trial	Trip Angle	
			Static	Dynamic
#1	0°	1	93°	88°
#1	0°	2	93°	88°
#1	0°	3	93°	88°
#2	90°	1	83.5°	79°
#2	90°	2	83.5°	79°
#2	90°	3	83.5°	79°
#3	180°	1	81°	78°
#3	180°	2	81°	78°
#3	180°	3	81°	78°

5.1.1 Sun Sensor Threshold

Specification (no specific reference)

The sun exposure protection device will not preclude use of the Sensor in the RAD mode due to the horizon radiation.

Method: Place a lens cap on the MMOS. Place the MMOS in the collimated horizon beam of 1.5×10^{-6} watts/cm^2/ster/angstrom such that the sun sensors are illuminated. Turn on the MMOS and monitor the SHUTTER STATUS output. The shutter should not be activated by this illumination.

Results: THE SHUTTER DID NOT CLOSE WHEN ILLUMINATED BY THE COLLIMATED HORIZON SIMULATOR.

5.2 Mode Command Acceptance

Specification: Para. 3.3.6. A method of external mode selection will be provided. The method shall be capable of interrupting any automatic sequence and holding a mode regardless of target status.

Method: Most, if not all, of the mode commands will have been demonstrated during preceding performance tests. As a complete check command the MMOS into its various modes and check if STATUS outputs are correct per Table 5-2.

Results:

TABLE 5-2A

STATUS OUTPUTS

COMMAND	STATUS			
	ACQ	RE-ACQ	TRK	RAD
ACQ	H	L	L	L
RE-ACQ	L	H	L	L
TRK	L	L	H	L
RAD	L	L	L	H
NONE	H or L	H or L	H or L	L
No Star	H	L	L	L
Star	L	L	H	L
OFFSET	L	H or L	H or L	L
No Star	L	H	L	L
Star	L	L	H	L

TABLE 5-2B

STATUS LEVELS

STATUS OUTPUT	LEVEL **	
	High (5 ± 1 volt)	Low 0 ± 0.5 volt
ACQ	+3.45	+.12
RE-ACQ	+3.45	+.12
TRK	+3.45	+.12
RAD	+3.47	+.069
TARGET PRES.	+3.5	+.084 4/19
SHUTTER STATUS *	4.4 4/26	.60 4/26

* INITIAL READINGS FOR SHUTTER STATUS ON 4/19 WAS: HIGH 9.04V. AND LOW 14.48V.

A CIRCUIT MODIFICATION WAS MADE TO EFFECT THE VALUES SHOWN ABOVE.

** IT IS NOTED THAT THE HIGH LEVELS DO NOT EQUAL THE MINIMUM HIGH LEVEL. A REVIEW OF THE INTERFACE BY NASA SUGGESTED AN ADDITIONAL CRITERIA TO DETERMINE IF THIS WAS A PROBLEM. THE CRITERIA WAS: THE HIGH LEVEL MUST BE AT LEAST 3VOLTS INTO A 6KΩ LOAD. ALL OUTPUTS WERE TESTED AND FOUND TO SATISFY THIS CRITERIA.

5.3 Input Power

Specification: Para. 3.3.2. The Sensor total average power consumption will not exceed 15 watt.

Method: Set the input voltage to 28 VDC. Measure and record the input current for each mode.

TABLE 5.3

POWER CONSUMPTION

MODE	VOLTAGE	CURRENT	POWER
ACQ	28	940 MA.	26.3 W
RE-ACQ	28	935 MA	26.2 W
TRK	28	935 MA	26.2 W
RAD	28	940 MA	26.3 W

5.4 Input Line Variations

Specification: Para. 3.3.1. The MMOS will be capable of meeting all performance specifications while operating from a primary power source which has the following characteristics:

a) Nominal DC voltage of 28 VDC

b) Line variations (including normal transients) of 22 - 30 VDC.

c) Transient voltages of + 50 volts and -100 volts maximum amplitude, having a duration of 10 μ sec and a repetition rate of 10 pps.

d) Ripple voltage of 1.5 volts peak having frequency components from 20 Hz to 20 KHz.

The recovery time to specified performance for input level changes over a one second time interval from one DC level to another will be 0.7 second maximum where the input starting level can be at

a) a maximum voltage level of 32 volts or

b) a minimum voltage level of 21 volts.

Method and Results:

In each of the following set up the MMOS as in Sec. 3.4 for the X and Y output readings and as in Sec. 4.3 for the HOR. INT. readings.

A) Measure variations of the X output, Y output, and HOR. INT. output for the line voltage of 22 VDC and 30 VDC.

VOLTAGE	OUTPUTS		
	X	Y	HOR. INT.
22 VDC	+.004 V	-.006 V	5.6 V
30 VDC	+.004 V	-.006 V	5.6 V
28 VDC	+.004 V	-.006 V	5.6 V

B) Insert a 3 ohm power resistor into the input voltage line. Transformer couple to the resistor the output of a power amplifier (50 Hz -15 KHz BW). Apply a white noise source to the amplifier so that 1.5 volts peak signal is present on the power resistor. Note the MMOS operation with and without the line interference. Record X and Y outputs on Sanborn recorder to note any increase in noise angle. Measure variations in output as in (A)

	OUTPUTS		
	X	Y	HOR. INT.
No noise	15mV	17mV	50mV
White noise	16mV	16mV.	NO CHANGE

C) Replace the white noise generator with a square wave generator. Set the input to produce a 2 volt waveform at the resistor. Note the MMOS operation with and without the interference. The nominal voltage should be varied between 23 and 30 volts.

	OUTPUTS		
	X	Y	HOR. INT.
Without Sq. Wave	15mV	17mV	50mV
With Sq. Wave	16mV	17mV	NO CHANGE

APPENDIX B

ACCEPTANCE TEST

PROCEDURE

FOR

MULTI-MODE OPTICAL SENSOR - B

PERFORMED AT
ITT GILFILLAN
ON APRIL 25, 26, 27, 1973

ALL TESTS
WITNESSED BY:
Richard A. Deters ITTG
Charles E. Manry NASA/JSC

1.0 GENERAL

The Test Procedure supplements and becomes an Appendix to ITT Gilfillan Test Drawing.

1.1 Operating Conditions

The MMOS will be set up in a darkroom environment on an optical bench per Section 3.0 of the Test Plan. Unless otherwise specified, the tests will be made in a laboratory environment, with nominal line voltage, with a third magnitude star, with nominal output loads. At all times power is applied to the MMOS, a darkroom environment is implied. Whenever very accurate measurements are required, the various peripheral equipment such as the star simulator, should be on for two hours minimum prior to data taking.

1.2 Simulator Calibration

Prior to commencing into this procedure, the collimated star simulator intensity will have been calibrated per ITT Drawing 5522973 (Appendix B). The data from that procedure will be tabulated so that a star of +3, +2, +1, 0, or -1 visual magnitude can be presented to the MMOS.

All other simulator calibrations will be made just prior to tests of the operational modes using the particular simulator.

2.0 ALIGNMENT PROCEDURES

Prior to formal testing, a check of the test bed alignment will be made. Although not a part of the MMOS testing, it is a necessary step to insure the subsequent test results are valid.

2.1 Star Simulator Alignment (Test Plan Figure 4-1)

1. Place the Huet Optical Level on the granite table surface and set it to contain the surface reference. ✓ (a) ≃ 24 sec.
2. Place the level on the Moore table and shim as required to make parallel to the granite table within 1.6 arc minutes. (b) ≃ 25 sec (SEE BELOW
3. Mount the star simulator on the Moore rotary table. Positioning is not critical except that the front of the collimating lens should be approximately at the table axis of rotation to preclude vignetting of the MMOS lens by the collimating lens as the Moore table is rotated. ✓
4. Use an auto-collimator to align the Davidson Optronics D-616 mirrors prependicular to their base. ✓
5. Set the aligned mirror on the Moore table. Align an auto-collimator such that its line-of-sight is perpendicular to the mirror. ✓
6. Position the star (in the auto-collimator) to be aligned vertically with the auto-collimator. ✓

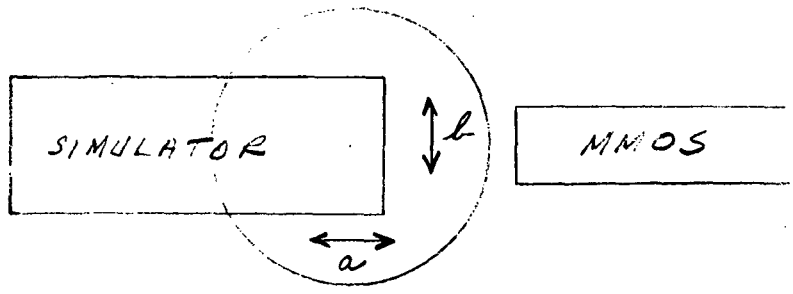

4-25-73
R. Deters

2.2 Star Simulator Calibration Data

Following is a tabulation from the simulator calibration procedure:

Visual Star Magnitude	Image Dissector Current	SIMULATOR	
		Filter Position	Bulb Current
5			
4	4.15 NA	5	835 MA
3	10.5 "	4	875 "
2	26.2 "	3	910 "
1	65.5 "	2	940 "
0	163. "	1	945 "
-1	415. "	0	970 "

4-25-73
R. Peters

2.3 Test Bed Alignment (Test Plan Figure 4-3)

1. Mount the MMOS on the Leitz table with the center of the lens approximately at the table axis of rotation to preclude vignetting of the MMOS lens by the collimating lens as the Leitz table is rotated. ✓

2. Set the Leitz table and the lower rotary table to approximately align the MMOS and star simulator. ✓

3. With the proper electrical interface per Test Plan Table 4-1, apply power to the MMOS. Use a 2^M star for alignment readings. ✓

4. With the MMOS tracking the star, monitor the X and Y outputs on an X-Y recorder. Rotate the Leitz table (θ) through 360^o. ✓

5. Vary the MMOS and/or Leitz table per Test Plan Figure 4-3 to null the X-Y outputs as a function of θ. ✓

6. At the optimum alignment record the peak to peak swing in X and Y for a rotation in θ of 360^o. Use a gradient of .00028 V/sec

   x = .006 volts = 21 sec

   y = .009 volts = 32 sec

7. Set the Moore table vernier such that the angular readout is zero. ✓

8. Record the table readings and collimator readings which cannot be zeroed. ✓

   V_{leitz} = 0° 1' (coarse axis of the Leitz table)

   H_{sim} = .25435 inch
   V_{sim} = .22995 inch

   [readings of the horizontal and and vertical positions of a micrometer cross slide stage containing the pinhole source of the star simulator.]

2.4 MMOS Alignment (Test Plan Figure 4-4)

* 1. Rotate the star simulator from ρ_o so that the star image can be viewed in an auto-collimator. ✓

2. Align the auto-collimator vertically such that the star image is on its reference horizontal line. ✓

3. Translate the auto-collimator on the granite table to where it can auto-collimate on the roll axis surface of the MMOS reference mirror. ✓

4. Rotate the Leitz table in θ until the roll reference surface is perpendicular to the auto-collimator line-of-sight. ✓

5. Record the Leitz table reading for θ. (angle at which variation in the X-output as a function of ρ is minimum) $\theta =$ 270°

6. Without moving the auto-collimator vertical alignment, align a 90° mirror so that it is perpendicular to the auto-collimator line-of-sight. ✓

7. Place the mirror in the MMOS-star simulator line-of-sight per Test Plan Figure 4-4. ✓

8. Move the auto-collimator to align it to the star image reflected by the mirror. The boresight reference return should also be present in the auto-collimator. ✓

9. Align the MMOS in its Y-axis by varying the MMOS position (Y axis only) on the Leitz table until the vertical line return is within 5 arc seconds of its reference in the auto-collimator. See page A-7A

10. Rotate the Leitz table 90° in the θ axis. ✓

* NOTE

The reference mirror alignment cube was mounted subsequent to the test procedure. The alignment relative to the boresight axis is shown in Table A-7A.

2.4 MMOS Alignment (Continued)

See page A-7A

11. Align the MMOS in its X-axis by varying the MMOS position (X axis only) on the Leitz table until the vertical line return is within 5 arc seconds of its reference in the auto-collimator.

12. If adjustments are required the entire Section 2.4 should be repeated. The final table angles are recorded. ρ = _____

θ = _____

MMOS-B

REFERENCE CUBE ALIGN.

ROLL AXIS

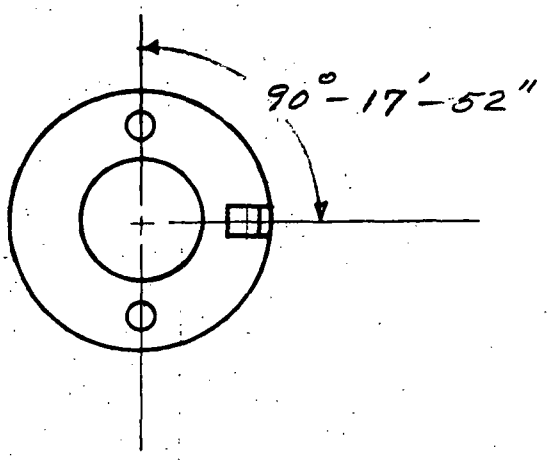

Y-AXIS

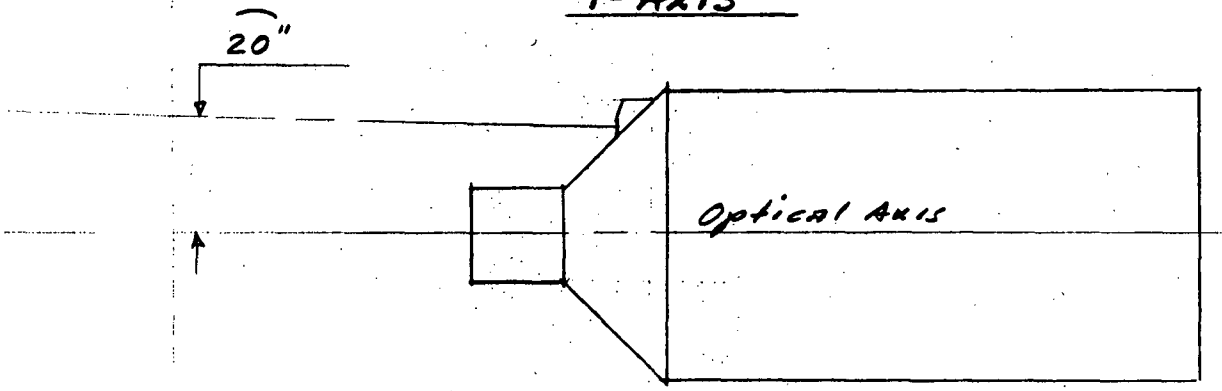

X-AXIS

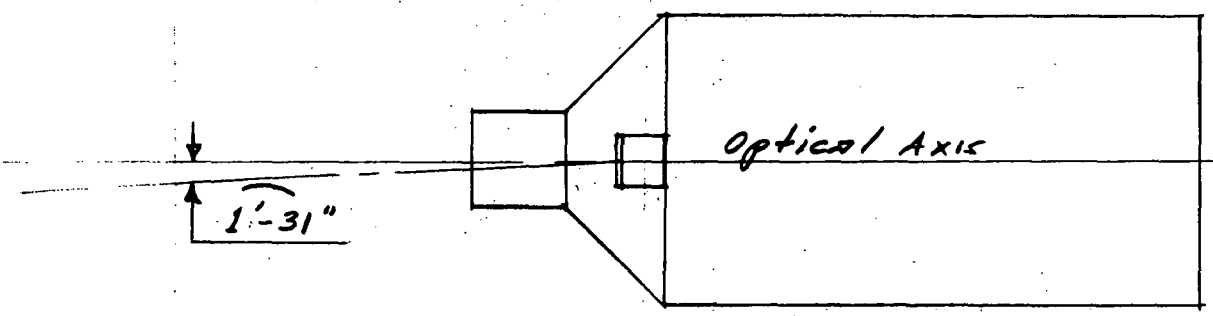

2.5 MMOS Boresight Adjustment

1. With the MMOS in its aligned position, null the X and Y outputs by adjustment to the alignment screws near the front of the MMOS housing. ✓

2. Following adjustment, lock the screws to preclude any further adjustment. ✓

3. With the MMOS tracking the star at boresight (X = Y = 0) measure the HORIZON ANGLE output voltage to insure that it is 0 ± 0.010 volts. ✓

Hor. Angle −.001V TO −.005V thru 2 hr. temp. test

3.0 STAR TRACKING PERFORMANCE TESTS

3.1 Target Magnitude Calibration

Specification: Para. 3.2.1. The Sensor will meet all specifications when required to acquire and furnish error signals while observing stars and other targets having a visual magnitude of + 3 and brighter.

Method: With the star being tracked at the boresight axis, measure and record the TARGET MAGNITUDE voltage for the following star magnitudes.

TABLE 3.1

TARGET MAGNITUDE CALIBRATION

STAR MAGNITUDE	TARGET MAGNITUDE (Volts)
No Star	+.05
4	+.25 MARGINAL TRACKING
3	+.81
2	+1.77
1	+3.00
0	+4.05
-1	+4.75

4-25-73
R. Peters

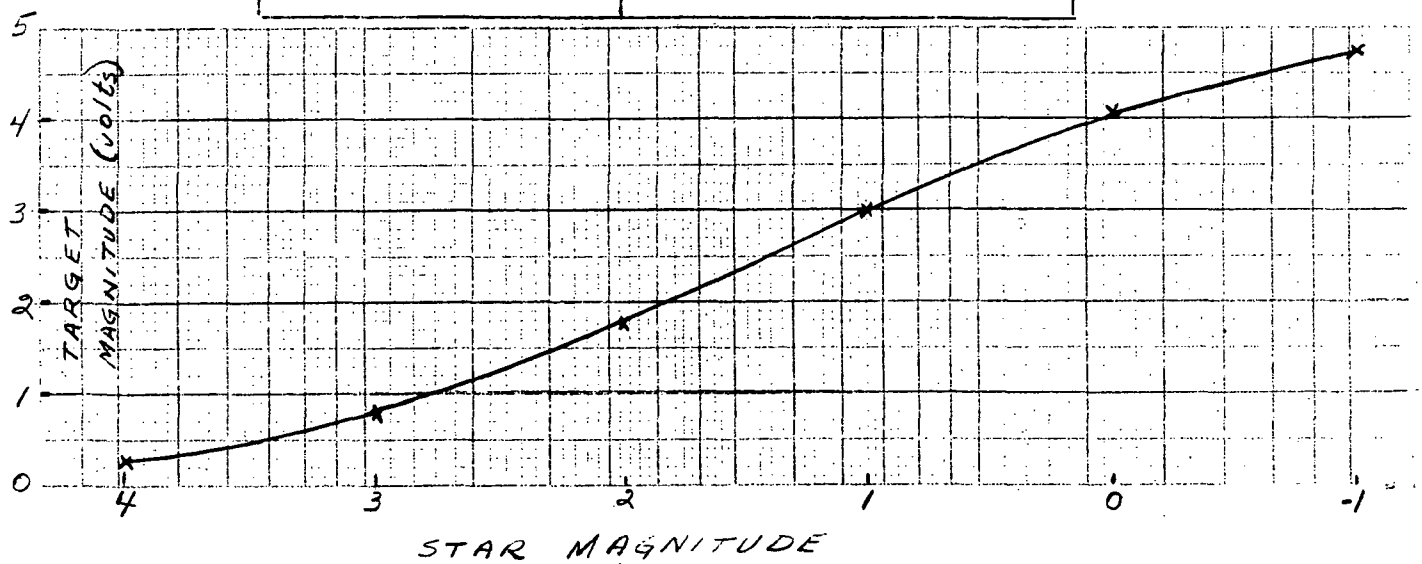

3.2 Acquisition Field-of-View

Specification: Para. 3.2.2. The Sensor will have an effective field-of-view of at least 10^{o} x 10^{o}.

Method: The edge of the field-of-view is the angle at which a TARGET PRESENCE is first generated as the star is moved toward the MMOS boresight. Command the MMOS to the ACQ. mode. Rotate the simulator (ρ) so that the star is outside the AFOV. Then command the MMOS to the AUTO mode. Rotate the simulator to decrease ρ until a TARGET PRESENCE is attained. At this point record the value of ρ for each MMOS roll angle (θ). Record both the full and half AFOV angles. Use a third magnitude star.

TABLE 3-2

ACQUISITION FIELD-OF-VIEW

10^{o} x 10^{o} AFOV					
Roll Angle(θ)		Simulator Angle			
Leitz	MMOS	+ ρ	- ρ	Spec.	
	0^{o}	$5^{o}3\frac{1}{2}'$	$5^{o}13'$	$\geq 5.0^{o}$	
	45^{o}	$7^{o}1'$	$7^{o}17'$	$\geq 7.07^{o}$	$(7^{o}4')$
	90^{o}	$5^{o}6'$	$5^{o}9'$	$\geq 5.0^{o}$	
	135^{o}	$7^{o}10'$	$7^{o}10'$	$\geq 7.07^{o}$	$(7^{o}4')$

4-25-73

3.3 Output Characteristics

Specification: Para. 3.2.4.1. The Sensor will have a maximum RSS error of less than one arc minute relative to the mounting pad. The value will be derived from the total pointing bias, drift after a 15 minute warmup, tracking jitter values, and other error sources experienced when acquiring and tracking a third visual magnitude star.

Method: Data to determine specification compliance will be taken in several stages.

A) For determination of time drift, take X and Y output readings for the 5 points in Table 3-3A at 15 minute intervals for a period of 2 hours. Use a 2^m star as the source and measure the outputs on an integrating digital voltmeter. The null point drift will be used as the basis for entire field translation. The drift of the other four points will be checked to insure that the drift is primarily a translation.

B) Following a 2 hour warmup, measure the X and Y outputs for the 36 points of Test Plan Figure 5-1. Use a 3^m star as the source. Record the outputs from an integrating digital voltmeter in Table 3-3B. Record one reading of the outputs from a Dana Series 5400 digital voltmeter in Table 3-3C.

C) From the data of Table 3-3B, calculate the optimum gradient for each of the X and Y outputs.

X = 16.867 mv/min 1.012 v/deg

Y = 16.700 mv/min 1.002 v/deg

Results: From Table 3-3A, calculate the time drift. Using the null point readings with the 2 hour reading as reference, record the variation about that reference for the time between 15 minutes and 2 hours.

X
+ 1 mv
- 1 mv

Y
+ 5 mv
- 0 mv

The time variation must be applied to each measured output reading of Table 3-3B. Using the gradients from (C) above, calculate the expected values of the X and Y outputs for the 36 test points. The difference between predicted output values and measured output values including the time drift must be less than 1 $\widehat{\text{min}}$.

NOTE

Data points for mapping taken from DANA DVM printout. See table 3-3C.

MM05-R

Res: $\Delta x = \pm 1$mv
$\Delta y = \pm 2.5$mv

4-26-73

A.T.P. TEMP. STAB. TEST

TABLE	θ	0° 45°		45°		45°		135°		135°		13.5°	
ANGLES	ρ	0°		-4° 14' 34"		4° 14' 34"		-4° 14' 34"		4° 14' 34"		0°	
FIELD	X	0°		+3°		-3°		-3°		+3°		0°	
ANGLES	Y	0°		+3°		-3°		+3°		-3°		0°	
OUTPUT (Volts)		X	Y	X	Y	X	Y	X	Y	X	Y	X	Y
TIME													
09:08	0	-1	+5	+3.029	+3.001	-3.029	-2.984	-3.030	+2.999	+3.025	-2.988	-3	+3
09:23	15	-1	-1	+3.028	+2.995	-3.029	-2.991	-3.031	+2.991	+3.024	-2.998	-4	-5
09:38	30	-1	-2	+3.027	+2.995	-3.030	-2.991	-3.030	+2.991	+3.024	-2.996	-5	-5
09:53	45	-2	0	+3.027	+2.994	-3.030	-2.989	-3.031	+2.993	+3.023	-2.997	-5	-4
10:08	60	-3	-1	+3.025	+2.992	-3.030	-2.990	-3.030	+2.990	+3.023	-2.998	-4	-6
10:23	75	-3	-2	+3.025	+2.993	-3.031	-2.992	-3.030	+2.988	+3.024	-3.000	-4	-8
10:38	90	-2	-3	+3.027	+2.991	-3.029	-2.992	-3.030	+2.988	+3.024	-3.001	-3	-9
10:53	105	-2	-4	+3.026	+2.991	-3.031	-2.995	-3.030	+2.986	+3.024	-3.004	-5	-11
11:08	120	-2	-5	+3.027	+2.990	-3.030	-2.996	-3.031	+2.984	+3.025	-3.008	-4	-13

X Δ 2mv Y Δ 5mv

4-26-73

TABLE 3-3A

DATA TAKEN VISUALLY FROM NLS D.V.M.

TABLE 3-3B

RANDOM ANGLE OUTPUTS

Start @ 11°.25

	TABLE ANGLES (deg min sec)		OUTPUTS (volts)					
			Measured		Predicted		Difference	
	θ	ρ	X	Y	X	Y	X	Y
1	0	0	0	-6				
2	11° 18' 36" -	5°54'4" -5° 5' 56"	+5.047	+.990				
3	11° 18' 36"	0	-1	-6				
4	11° 18' 36"	5° 5' 56"	-5.046	-1.002				

B-13

4-26-73

TABLE 3-3B

RANDOM ANGLE OUTPUTS

	TABLE ANGLES (deg min sec)		OUTPUTS (volts)					
			Measured		Predicted		Difference	
	θ	ρ	X	Y	X	Y	X	Y
5	18° 26' 6"	-3° 9' 44"	+3,030	+.994				
6	18° 26' 6"	0	-2	-8				
7	18° 26' 6"	3° 9' 44"	-3,025	-1.001				
8	30° 57' 50"	-5° 49' 51"	+5,046	+2.984				
9	30° 57' 50"	0	-3	-9				
10	30° 57' 50"	5° 49' 51"	-5,050	-3,000				

4-26-73

TABLE 3-3B

RANDOM ANGLE OUTPUTS

	TABLE ANGLES (deg min sec)		OUTPUTS (volts)					
			Measured		Predicted		Difference	
	θ	ρ	X	Y	X	Y	X	Y
11	45°	-7° 4' 16"	+5.040	+4.987				
12	45°	-4° 14' 34"	+3.028	+2.988				
13	45°	-1° 24' 51"	+1.007	+.992				
14	45°	0	-2	-9				
15	45°	1° 24' 51"	-1.012	-1.009				
16	45°	4° 14' 34"	-3.032	-3.000				
17	45°	7° 4' 16"	-5.051	-5.000				

4-26-73

TABLE 3-3B

RANDOM ANGLE OUTPUTS

	TABLE ANGLES (deg min sec)		OUTPUTS (volts)					
			Measured		Predicted		Difference	
	θ	ρ	X	Y	X	Y	X	Y
18	59° 2' 10"	10' 0" -5 49' 51"	+3.027	+4.986				
19	59° 2' 10"	0	-2	-11				
20	59° 2' 10"	5° 49' 51"	-3.031	-5.005				
21	71° 33' 54"	50' 16" -3° 9' 44"	+1.005	+2.983				
22	71° 33' 54"	0	-3	-11				
23	71° 33' 54"	3° 9' 44"	-1.014	-3.005				

4-26-73

TABLE 3-3B

RANDOM ANGLE OUTPUTS

	TABLE ANGLES (deg min sec)		OUTPUTS (volts)					
			Measured		Predicted		Difference	
	θ	ρ	X	Y	X	Y	X	Y
24	78° 41' 24"	-5° 5' 56"	+1,003	+4,983				
25	78° 41' 24"	0	-4	-11				
26	78° 41' 24"	5° 5' 56"	-1,013	-5,002				
27	101° 18' 36"	54'4" -5° 5' 56"	-1,012	+4.982				
28	101° 18' 36"	0	-3	-14				
29	101° 18' 36"	5° 5' 56"	+1,005	-5.007				

4-26-73

TABLE 3-3B

RANDOM ANGLE OUTPUTS

	TABLE ANGLES (deg min sec)		OUTPUTS (volts)					
			Measured		Predicted		Difference	
	θ	ρ	X	Y	X	Y	X	Y
30	108° 26' 6"	50'16" -3° 9' 44"	-1,016	+2,985				
31	108° 26' 6"	0	-4	-15				
32	108° 26' 6"	3° 9' 44"	+1,008	-3,012				
33	120° 57' 50"	10' 9" -5° 49' 51"	-3,031	+4,980				
34	120° 57' 50"	0	-5	-16				
35	120° 57' 50"	5° 49' 51"	+3,026	-5,010				

4-26-73

TABLE 3-3B

RANDOM ANGLE OUTPUTS

	TABLE ANGLES (deg min sec)		OUTPUTS (volts)					
			Measured		Predicted		Difference	
	θ	ρ	X	Y	X	Y	X	Y
36	135°	-7° 4' 16" (55'44")	-5.053	+4.983				
37	135°	-4° 14' 34 (45'26")	-3.031	+2.978				
38	135°	-1° 24' 51" (35'9")	-1.011	+.979				
39	135°	0	-4	-20				
40	135°	1° 24' 51"	+1.005	-1.017				
41	135°	4° 14' 34"	+3.025	-3.013				
42	135°	7° 4' 16"	+5.050	-5.015				

4-26-73

TABLE 3-3B

RANDOM ANGLE OUTPUTS

	TABLE ANGLES (deg min sec)		OUTPUTS (volts)					
			Measured		Predicted		Difference	
	θ	ρ	X	Y	X	Y	X	Y
43	149° 2' 10"	-5° 49' 51"	-5.056	+2.983				
44	149° 2' 10"	0	-1	-19				
45	149° 2' 10"	5° 49' 51"	+5.050	-3.018				
46	161° 33' 54"	-3° 9' 44" (50'16")	-3.028	+.980				
47	161° 33' 54"	0	-4	-19				
48	161° 33' 54"	3° 9' 44"	+3.022	-1.018				

4-26-73

TABLE 3-3B

RANDOM ANGLE OUTPUTS

TABLE ANGLES (dcg min sec)		OUTPUTS (volts)					
		Measured		Predicted		Difference	
θ	ρ	X	Y	X	Y	X	Y
99 168° 41' 24"	-5° 5' 56"	-5.049	+.984				
50 168° 41' 24"	0	-2	-21				
51 168° 41' 24"	5° 5' 56"	+5.050	-1.016				
52 0	0	-1	-10				

4-26-73

MM05-IS

FIELD MAP

USING AVE. DANA READINGS.

TABLE 3-3C

RANDOM ANGLE OUTPUTS

2nd cut Gradient X=1.012 Y=1.0018

1st Cut GRADIENT X=1.013 Y=1.002

	TABLE ANGLES (dcg min sec)		OUTPUTS (volts)					
			Measured		Diff. ~~Predicted~~		Difference	
	θ	ρ	X	Y	X	Y	X	Y
1	0	0	+1	-5				
2	11° 18' 36"	-5° 5' 56"	+5.056 +5.055	+.997 +.991	-4	-5	-9 mv	-5
3	11° 18' 36"	0	0 -1	0 -6			0	0
4	11° 18' 36"	5° 5' 56"	-5.067 -5.068	-1.000 -1.006	+7	-2	+2	-2

4-26-73

TABLE 3-3C

RANDOM ANGLE OUTPUTS

	TABLE ANGLES (deg min sec)		OUTPUTS (volts)					
			Measured		Diff. ~~Predicted~~		Difference	
	θ	ρ	X	Y	X	Y	X	Y
5	18° 26' 6"	-3° 9' 44"	+3.034	1.000 +.994	-2	-2	-5	-2
6	18° 26' 6"	0	0 0	0 -6			0	
7	18° 26' 6"	3° 9' 44"	(-3.038) ~~-3.048~~	-1.000 -1.006	+2	-2	(-1) ~~+8~~	-2
8	30° 57' 50"	-5° 49' 51"	+5.056 +5.054	+2.998 +2.990	-4	-7	-9	-8
9	30° 57' 50"	0	0 -2	0 -8			0	0
10	30° 57' 50"	5° 49' 51"	-5.069 -5.071	-3.005 -3.013	+9	0	+4	-1

B-23

4-26-73

TABLE 3-3G

RANDOM ANGLE OUTPUTS

	TABLE ANGLES (deg min sec)		OUTPUTS (volts)					
			Measured		Diff. ~~Predicted~~		Difference	
	θ	ρ	X	Y	X	Y	X	Y
11	45°	-7° 4' 16"	+5.048 +5.046	+5.002 +4.993	-12	-7	-17	-8
12	45°	-4° 14' 34"	+3.032 +3.030	+3.003 +2.994	-4	-2	-7	-3
13	45°	-1° 24' 51"	+1.011 +1.009	1.002 +.993	-1	0	-2	0
14	45°	0	0 -2	0 -9			0	0
15	45°	1° 24' 51"	-1.013 -1.015	-1.003 -1.012	+1	+1	0	+1
16	45°	4° 14' 34"	-3.042 -3.044	-3.003 -3.012	+6	-2	+3	-3
17	45°	7° 4' 16"	-5.070 -5.072	-5.014 -5.023	+10	+5	+5	+4

4-26-73

TABLE 3-3C

RANDOM ANGLE OUTPUTS

	TABLE ANGLES (deg min sec)		OUTPUTS (volts) Measured		Diff. ~~Predicted~~		Difference	
	θ	ρ	X	Y	X	Y	X	Y
18	59° 2' 10"	-5 49' 51"	+3.035 +3.033	+5.004 +4.994	-1	-5	-4	-6
19	59° 2' 10"	0	0 -2	0 -10			0	0
20	59° 2' 10"	5° 49' 51"	-3.043 -3.045	-5.014 -5.024	(15) +7 (25)	+6	+4	+6
21	71° 33' 54"	-3° 9' 44"	+1.006 +1.004	+2.996 +2.986	2.995 -6	-6	-7	-7
22	71° 33' 54"	0	0 -2	0 -10			0	0
23	71° 33' 54"	3° 9' 44"	-1.013 -1.017 -1.015	-3.007 -3.017	+3	+2	+2	+1

B-25

4-26-73

TABLE 3-3C

RANDOM ANGLE OUTPUTS

	TABLE ANGLES (deg min sec)		OUTPUTS (volts) Measured		Diff. ~~Predicted~~		Difference	
	θ	ρ	X	Y	X	Y	X	Y
24	78° 41' 24"	-5° 5' 56"	+1.007 +1.004	+4.998 +4.988	-5	-11	-6	-12
25	78° 41' 24"	0	0 -3	0 -10			0	0
26	78° 41' 24"	5° 5' 56"	-1.015 -1.018	-5.014 -5.024	+3	+5	+2	+4
27	101° 18' 36"	-5° 5' 56"	-1.012 -1.015	5.002 +4.989	0	-7	-1	-8
28	101° 18' 36"	0	0 -3	0 -13			0	0
29	101° 18' 36"	5° 5' 56"	+1.009 +1.006	-5.016 -5.029	-3	+7	-4	+6
			~~+1.009~~					

4-26-73

TABLE 3-3C

RANDOM ANGLE OUTPUTS

	TABLE ANGLES (deg min sec)		OUTPUTS (volts) Measured		Diff. ~~Predicted~~		Difference	
	θ	ρ	X	Y	X	Y	X	Y
30	108° 26' 6"	-3° 9' 44"	-1.016 -1.019	+3.004 +2.990	+4	-1	+3	-2
31	108° 26' 6"	0	-3	-14			0	0
32	108° 26' 6"	3° 9' 44"	+1.011 +1.008	-3.011 -3.025	-1	+6	-2	+5
33	120° 57' 50"	-5° 49' 51"	-3.042 -3.044	+5.004 +4.989	+6	-5	+3	-6
34	120° 57' 50"	0	-2	-15			0	0
35	120° 57' 50"	5° 49' 51"	+3.032 +3.030	-5.016 -5.031	-4	+7	-7	+6

4-26-73

TABLE 3-3C

RANDOM ANGLE OUTPUTS

	TABLE ANGLES (deg min sec)		OUTPUTS (volts)					
			Measured		Diff. ~~Predicted~~		Difference	
	θ	ρ	X	Y	X	Y	X	Y
36	135°	-7° 4' 16"	-5.073 -5.076	+5.003 +4.991	+13	-1	+8	-2
37	135°	-4° 14' 34	-3.041 -3.044	+3.001 +2.984	+5	-4	+2	-5
38	135°	-1° 24' 51"	-1.014 -1.017	+.998 +.981	+2	-4	+1	-4
39	135°	0	-3	-17			0	0
40	135°	1° 24' 51"	+1.010 +1.007	-1.003 -1.020	-2	+1	-3	+1
41	135°	4° 14' 34"	+3.033 +3.030	-3.007 -3.024	-3	+2	-6	+1
42	135°	7° 4' 16"	+5.062 +5.059	-5.020 -5.037	+2	+11	-5	+10

4-26-73

TABLE 3-3C

RANDOM ANGLE OUTPUTS

	TABLE ANGLES (deg min sec)		OUTPUTS (volts)					
			Measured		Diff. ~~Predicted~~		Difference	
	θ	ρ	X	Y	X	Y	X	Y
43	149° 2' 10"	-5° 49' 51"	-5.075 -5.077	+3.005 +2988	+15	0	+10	-1
44	149° 2' 10"	0	-2	-17			0	0
45	149° 2' 10"	5° 49' 51"	+5.058 +5.056	-3.013 -3.030	-2	+8	-9	+7
46	161° 33' 54"	-3° 9' 44"	-3.039 -3.041	+.999 +.982	+3	-3	0	-3
47	161° 33' 54"	0	-2	-17			0	0
48	161° 33' 54"	3° 9' 44"	+3.028 +3.026	-1.006 -1.023	-8	+4	-11	+4

4-26-13

TABLE 3-3C

RANDOM ANGLE OUTPUTS

	TABLE ANGLES (deg min sec)		OUTPUTS (volts)					
			Measured		Diff. ~~Predicted~~		Difference	
	θ	ρ	X	Y	X	Y	X	Y
49	168° 41' 24"	-5° 5' 56"	-5.070 -5.070	+1.005 +.985	+10	+3	+5	+3
50	168° 41' 24"	0	0	-20			0	0
51	168° 41' 24"	5° 5' 56"	+5.057 +5.057	-.999 -1.019	-3	-3	-8	-3
52	0	0	0	-9				

4-26-73

3.4 Tracking Noise Angle

Specification: no specific applicable reference; a component of output position error.

Method: With the MMOS tracking a 3^M star near boresight, record the X and Y outputs on a Sanborn recorder for one minute. Calculate the RMS noise angle by dividing the maximum negative to maximum positive peak of the recording by seven. Repeat the recording and calculation for 4^M and 2^M stars.

Results:

TABLE 3.4

NOISE ANGLE

STAR MAGNITUDE	OUTPUT					
	P - P (millivolts)		RMS (millivolts)		RMS ($\sqrt{sec}$)	
	X	Y	X	Y	X	Y
TAR. MAG = .49V X	30	33	4.29	4.71	15.2	16.9
3	20	21	2.86	3.00	10.2	10.8
2	10	9	1.43	1.29	5.1	4.6

4-25-73
R. Peters

From Table 3.3B, the gradients:

X = 16.867 mV/$\sqrt{min.}$ = .281 v/$\sqrt{sec}$

Y = 16.700 mV/$\sqrt{min.}$ = .278 v/$\sqrt{sec}$

3.5 Acquisition Time

Specification: Para. 3.2.3.1

Acquisition of a star will be completed and error signals provided within 1.0 seconds after acquisition is commanded, where the target appears at any point in the $10^{o} \times 10^{o}$ field-of-view and may be moving at a rate relative to the Sensor as high as 0.5 degree per second. This performance will be demonstrated in at least 80% of the trials attempted with random selection of initial position and velocity.

Method: Use a Sanborn recorder to record 1) TARGET PRESENCE and 2) command to AUTO from the LO MAP command. The acquisition time is the time interval between command to AUTO and generation of TARGET PRESENCE using a 3^{M} star as the target. Effect rates by manually slewing either the simulator (ρ) or the MMOS (θ). Determine the slew rate at which acquisition occurred by recording the X and Y outputs on another Sanborn recorder. Record a minimum of ten time intervals for random field positions.

Results:

TABLE 3-5

ACQUISITION TIME

TRIAL	TIME (SEC)	RATE (°/SEC)
1	.95	0
2	.95	"
3	.95	"
4	.95	"
5	.95	"
6	.95	"
7	.95	"
8	.95	"
9	.95	"
10	.95	"
11	.95	≃ .5
12	.95	"
13	.95	"
14	.95	"
15	.95	"
16	.95	"
17	.95	"
18	.95	"
19	.95	"
20	.95	"

Spec. requires TIME ≤1.0 seconds for 80% of the trials. 4-25-73
R. Deters

3.6 Star Selection

Specification: Para. 3.2.3: The Sensor must be capable of selecting the brightest target in the 10^{o} x 10^{o} field-of-view provided the magnitude difference is at least one and the angular separation at least 0.5 degrees.

Method: Remove the pinhole source plate from the simulator and replace with the plate containing two pinholes. Track one of the sources and set its intensity to a 3^{M} star by monitoring the TARGET MAGNITUDE. Repeat for the second source and set its intensity to be a 2^{M}. Now place both stars in the 10^{o} x 10^{o} AFOV and command the tracker to AUTO mode. Correct acquisition will be determined by turning off the brightest star to see if the MMOS returns to the ACQ. mode. Try several selection trials with various ρ's and θ's monitoring the TARGET MAGNITUDE to determine if correct selection has been accomplished.

Results:

STAR MAG. of		STAR SELECTED IN TRIAL			
#1	#2	1	2	3	
4	3	O.K.	O.K.	O.K.	4-25
2	3	O.K	O.K	O.K	4-25
2	1	O.K.	O.K	O.K	4-25
0	1	O.K	O.K	O.K	4-30
0	-1	O.K	O.K	O.K	4-30
					4-30

* See page A-35A

During tests on 4/25, correct star selection could not be accomplished for all conditions. Specifically, consistent star acquisition could not be demonstrated within 20 of the top of the full field. Investigation and an analysis resulted in a recommendation by ITTG to change a star selection circuit decay time constant to improve star acquisition and selection. NASA granted approval and the circuit change was made. Subsequent tests indicated proper acquisition and selection at all points in the full field.

B. Deters
5-16-73

3.7 Output Data Bandwidth

Specification: Para. 3.3.5. The Sensor output bandwidth will be no less than 5 Hz.

Method: For this test, move the MMOS from the Leitz table on to the Davidson Optical Bench. Mount the dynamic test source (CRT tube and prism) at the Davidson collimating lens focal plane. Apply a .1 Hz sine wave to one set of plates of the CRT. Set the sine wave amplitude to produce a 3 arc minute (0.05 volts) peak to peak swing in the appropriate MMOS output. Record on a Sanborn recorder the CRT input and MMOS output for discrete sweep frequencies of 0.1, 0.5, 1.0, 3.0, 5.0, 10.0 and 20.0 Hz. Repeat the measurements for the opposite MMOS channel. At 5 Hz the amplitude shall not be less than .707 of the amplitude measured at .5 Hz and the phase lag shall not be more than 45°.

TABLE 3.7

MMOS BANDWIDTH

Input Frequency	OUTPUT			
	X		Y	
	Ampl.	Phase	Ampl.	Phase
0.1	1.0	0°	1.0	0°
0.5	1.0	0°	1.0	0°
1.0	1.0	-13°	1.0	-13°
3.0	0.88	-38°	0.90	-38°
5.0	0.74	-49°	0.76	-49°
10.0	0.48	-98°	0.53	-98°
20.0	0.20		0.19	

4-25-73
R. Deters

3.8 Offset Voltage Capability

Specification: Para. 3.3.6. The Sensor must be capable of providing for control of the desired null point location by means of introducing two controlled voltage levels from an external source during operation in the OFFSET mode.

Method: Rotate the table to $\theta = 0$ and set ρ to 5^{o}. Measure and record the Y output. Apply approximately 5 volts to the Y OFFSET input and command the MMOS to the OFFSET mode. Measure the Y output. If it is not within .1 volts (.1 degree) of the initial reading, refine the Y OFFSET input and repeat a command sequence to OFFSET mode. Tailor the Y offset voltage until the Y output is within .1 volts of the Y output reading recorded during tracking. Once achieved, record the Y OFFSET voltage and calculate the transfer function in volts/degree. Rotate the MMOS to $\theta = 90^{o}$. Repeat the procedure outlined to determine the X OFFSET transfer function.

Results:

TABLE 3-8

OFFSET TRANSFER FUNCTION

CONDITION	Y (Volts)		X (Volts)	
	Output	Offset	Output	Offset
Star at Y = ~~8~~ 4°				
Y Offset #1		4	////////	////////
#2	−4.008	−4.20	////////	////////
#3	+4.004	+4.52	////////	////////
#4			////////	////////
Star at X = ~~8~~ 4°				
X Offset #1	////////	////////		4
#2	////////	////////	−4.047	−4.34
#3	////////	////////	+4.045	+4.58
#4	////////	////////		

Y Offset T. F. = 1.09 V/degree

X Offset T. F. = 1.11 V/degree

4-25-73

R. Deters

3.9 X - Y Output Plot

Specification: no specific reference

Method: The object of this recording is to provide a composite graph of the X and Y outputs. Apply the X output to the horizontal and vertical channel of an X-Y recorder respectively. The recorder gain should be .5 volts/inch. Set ρ to 1^{o} and rotate θ through 360^{o}. Repeat for ρ in 1^{o} steps up to $\rho = 10^{o}$.

Results: Mark X-Y plot and include with test results.

4.0 RADIOMETER PERFORMANCE TESTS

For the following tests, rotate the MMOS via the rotary table under the Leitz table to be aligned with the horizon simulator. If not already performed, calibrate the simulator intensity.

4.1 Zero Offset Output Voltage

Specification: Para. 3.2.6.2.1. The zero offset of the output voltage will be less than 0.1 precent of the full scale voltage.

Method: Command the MMOS to the RAD mode. With a cap on the MMOS lens, measure the HOR. INT. output.

Result:

HOR. INT. = +19 mV volts (S/B ≤ .005 volts)

4-27-73

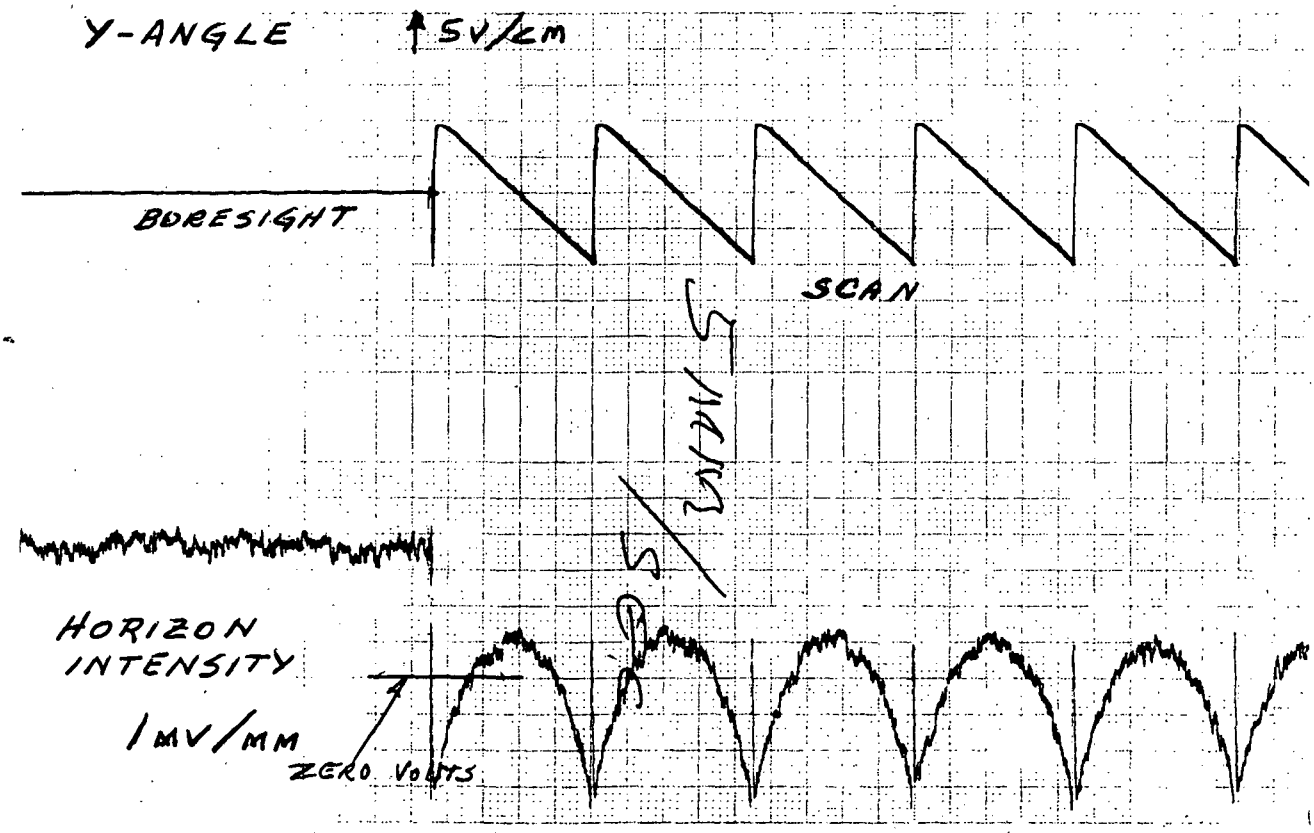

4.2 Horizon Intensity Ouput Uniformity

Specification: Para. 3.2.6.2.1 The horizon intensity output scale factor will be set at 5 volts for a peak radiance level of 1.505×10^{-6} watts cm^{-2} $ster^{-1}$ $angstrom^{-1}$.

@ .9 x 1.5μw/cm²/ster/ang:
5.2 V O.P.

Method: Set the source radiance to 1.505×10^{-6} watts cm^{-2} $ster^{-1}$ $angstrom^{-1}$.

Monitor the HOR. INT. output on the Dana 5400 Digital Voltmeter or equivalent. Set the meter printout speed at 15 readings per second. Command the MMOS to the RAD mode and record data for several scans.

Results: Using a 15 readings per second printout rate should provide approximately 75 readings for the entire scan of 10^{o}. This is a reading every 75 millisecond in time or every 8 arc minutes in angle. Tabulate the readings designating the number one reading at the top of the scan. All readings should be $5.25 \pm .25$ volts.

THE HOR. INT. OUTPUT WAS 5.2 volts FOR A RADIANCE LEVEL OF .9 THE PEAK RADIANCE LEVEL GIVEN ABOVE. THEREFORE THE HOR. INT. OUTPUT SCALE FACTOR IS 5.78 volts AT 1.505×10^{-6} WATTS · cm^{-2} · $STER^{-1}$ · $ANGSTROM^{-1}$

4-27-73
R Deters

SOURCE INTENSITY DECREASED FROM MAX. BY APPROXIMATELY 10 TIMES TO IMPROVE SOURCE UNIFORMITY.

READING		HORIZON INTENSITY		
Number	Horizon Angle (Approx)	Output M Volts	Difference	
			Volts	%
1	+5	576		
2		574		
3		577		
4		575		
5		577		
6		578		
7	+4	580		
8		579		
9		580		
10		579		
11		577		
12		578		
13	+3	578		
14		581		
15		586 (MAX)		
16		584		
17		586		
18		582		
19		581		
20	+2	581		
21		577		
22		578		
23		578		
24		578		
25		576		

4-27-73
R. Deters

READING		HORIZON INTENSITY		
Number	Horizon Angle (Approx)	Output m Volts	Difference	
			Volts	%
26	+1	569		
27		571		
28		566		
29		570		
30		567		
31		567		
32		564		
33	0	564		
34		562		
35		560		
36		559		
37		562		
38		561		
39		562		
40	-1	559		
41		557 (MIN)		
42		560		
43		560		
44		562		
45		558		
46		559		
47		559		
48		561		
49		561		
50	-2	563		

4-27-73
R. Peters

READING		HORIZON INTENSITY		
Number	Horizon Angle (Approx)	Output m Volts	Difference Volts	Difference %
51		562		
52		563		
53	-3	562		
54		564		
55		561		
56		561		
57		563		
58		563		
59		562		
60	-4	563		
61		563		
62		565		
63		564		
64		563		
65		561		
66		561		
67	-5°	562		
68				
69				
70	MIN. READING = 557 = -2.1%			
71	MAX. READING = 586 = +3.0%			
72	AV. READING = 569			
73				
74				
75				

4-27-73
R. Deters

4.3 Horizon Intensity Signal-to-Noise Ratio

Specification: Para. 3.2.6.2.2. The peak to peak noise in the HOR. INT. output will not exceed 1% of the voltage for the radiance level of 1.505×10^{-6} watts cm^{-2} $ster^{-1}$ $angstrom^{-1}$.

Method: With the MMOS centered on the horizon target, ground the MMOS radiometer boresight pin (connector pin #4) such that there is no radiometer sweep and record the HOR. INT. output on a Sanborn recorder for one minute.

Results:

HOR. INT. noise .046 Volt p-p (should be less than .050 V)

4-27-73
R Deters

5.0 GENERAL PERFORMANCE TESTS

The objective of the following tests is to insure MMOS performance pertaining to overall operation, i.e., all modes of operation.

5.1 Bright Object Protection

Specification: Para. 3.3.3.1. A sun shutter and necessary activation circuitry to protect the Sensor from sun exposure is required. The activation speed must be sufficient for protection with a slew rate of 10 degrees/second between the Sensor and the sun exposure.

Method: Place a lens cap on the MMOS. Set the solar simulator in a mode to provide approximately one solar constant of energy. Monitor the MMOS SUN SHUTTER STATUS. Initially start with the solar beam at least 90° from the MMOS boresight. Rotate the MMOS slowly into the solar beam and record the angle at which the shutter is closed. Repeat this measurement twice. Now rotate the MMOS into the solar beam at approximately a 10 degree/second rate. Repeat this measurement twice. Since there are two sun sensors on the MMOS, rotate the MMOS about its boresight axis and repeat the measurements at 90° and 180°.

Results:

TABLE 5-1

SUN PROTECTION ANGLE

Sensor		Trial	Trip Angle	
			Static	Dynamic
#1	0°	1	78°	77°
#1	0°	2	79°	77°
#1	0°	3	79°	77°
#2	~~90°~~ 270°	1	72°	70°
#2	~~90°~~ 270°	2	72°	70°
#2	~~90°~~ 270°	3	72°	69°
#3	180°	1	66°	65°
#3	180°	2	67°	65°
#3	180°	3	67°	65°

4-27-73
R. Deters

5.2 Mode Command Acceptance

Specification: Para. 3.3.6. A method of external mode selection will be provided. The method shall be capable of interrupting any automatic sequence and holding a mode regardless of target status.

Method: Most, if not all, of the mode commands will have been demonstrated during preceding performance tests. As a complete check command the MMOS into its various modes and check if STATUS outputs are correct per Table 5-2. Perform these tests in a darkroom environment. The STATUS level outputs will be loaded with 6K ohms to ground.

TABLE 5-2A

STATUS LEVELS

STATUS OUTPUT	LEVEL	
	High (3.5±5volt)	Low 0 ± 0.6 volt
ACQ	+3.32	+.13
RE-ACQ	3.42	.09
TRK	3.41	.10
RAD	3.29	.08
TARGET PRES.	3.32	.06
SHUTTER STATUS	4.18	0
BEACON PRES.	3.64	.12
LO MAP	3.64	.07
HI MAP	3.64	.11
X TAR	3.43	.13
LMT	3.33	.13
LGN	3.42	.13
ATTEN	3.39	.14
APERTURE	3.38	.13
U. V. FILTER	3.38	.14

4-26-73
R. Peters

TABLE 5-2B

COMMAND	STATUS OUTPUTS																							
	ACQ		RE-ACQ		TRK		RAD		LO MAP		HI MAP		X TAR		LMT		L-GN		UV FIL.		ATTEN		APER.	
RAD	L	✓	L	✓	L	✓	H	✓	L	✓	L	✓	L	✓	L	✓	H	✓	H	✓	L	✓	L	✓
LO MAP	H	✓	L	✓	L	✓	L	✓	H	✓	L	✓	L	✓	L	✓	L	✓	L	✓	L	✓	H	✓
HI MAP	H	✓	L	✓	L	✓	L	✓	L	✓	H	✓	L	✓	L	✓	H	✓	L	✓	H	✓	L	✓
X TAR	L	*	L	*	L	*	L	✓	L	✓	L	✓	H	✓	L	✓	L	✓	L	✓	L	✓	H	✓
LMT	L	✓	H	✓	L	✓	L	✓	L	✓	L	✓	L	✓	H	✓	H	✓	L	✓	H	✓	L	✓
NONE																								
NO STAR	H	✓	L	✓	L	✓	L	✓	L	✓	L	✓	L	✓	L	✓	L	✓	L	✓	L	✓	H	✓
STAR	L	✓	L	✓	H	✓	L	✓	L	✓	L	✓	L	✓	L	✓	L	✓	L	✓	L	✓	H	✓
OFFSET																								
NO STAR	L	✓	H	✓	L	✓	L	✓	L	✓	L	✓	L	✓	L	✓	L	✓	L	✓	L	✓	H	✓
STAR	L	✓	L	✓	H	✓	L	✓	L	✓	L	✓	L	✓	L	✓	L	✓	L	✓	L	✓	H	✓
RAD OFFSET	L	✓	L	✓	L	✓	H	✓	L	✓	L	✓	L	✓	L	✓	H	✓	H	✓	L	✓	L	✓

* CAN BE HIGH OR LOW DEPENDENT ON PRESENCE OR ABSENCE OF A TARGET

4-26-73
A. Dietz

5.3 Input Power

Specification: Para. 3.3.2. The Sensor total average power consumption will not exceed 15 watt.

Method: Measure and record the input current for each mode and each input voltage of Table 5.3

TABLE 5.3

POWER CONSUMPTION

MODE	VOLTAGE VOLTS	CURRENT AMPS	POWER WATTS
TRK	22	.990	21.78
	28	.845	23.66
	30	.800	24.00
RAD	22	.945	20.79
	28	.810	22.68
	30	.770	23.10
LO MAP	22	1.010	22.22
	28	.860	24.08
	30	.820	24.60
HI MAP	22	.945	20.79
	28	.810	22.68
	30	.770	23.10

4-26-73
R Peters

5.4 Input Line Variations

Specification: Para. 3.3.1. The MMOS will be capable of meeting all performance specifications while operating from a primary power source which has the following characteristics:

a) Nominal DC voltage of 28 VDC

b) Line variations (including normal transients) of 22 - 30 VDC.

c) Transient voltages of + 50 volts and -100 volts maximum amplitude, having a duration of 10 μ sec and a repetition rate of 10 pps.

d) Ripple voltage of 1.5 volts peak having frequency components from 20 Hz to 20 KHz.

The recovery time to specified performance for input level changes over a one second time interval from one DC level to another will be 0.7 second maximum where the input starting level can be at

a) a maximum voltage level of 32 volts or

b) a minimum voltage level of 21 volts.

Method and Results:

In each of the following set up the MMOS as in Sec. 3.4 for the X and Y output readings and as in Sec. 4.3 for the HOR. INT. readings.

A) Measure variations of the X output, Y output, and HOR. INT. output for the line voltage of 22 VDC and 30 VDC.

VOLTAGE	OUTPUTS X	Y	HOR. INT.
22 VDC	+.005	+.006	+.310 (IN TRK MODE)
30 VDC	+.005	+.006	+.310

ACQ & TRK. DEMONSTRATED

B) Insert a 3 ohm power resistor into the input voltage line. Transformer couple to the resistor the output of a power amplifier (50 Hz -15 KHz BW). Apply a white noise source to the amplifier so that 1.5 volts peak signal is present on the power resistor. Note the MMOS operation with and without the line interference. Record X and Y outputs on Sanborn recorder to note any increase in noise angle. Measure variations in output as in (A)

USED 3 mV STAR

	OUTPUTS X	Y	HOR. INT.
No noise	+.004	+.005	
White noise	+.004	+.005	

ACQ & TRK, DEMONSTRATED

C) Replace the white noise generator with a square wave generator. Set the input to produce a 2 volt waveform at the resistor. Note the MMOS operation with and without the interference. The nominal voltage should be varied between 23 and 30 volts.

USED 3 mV STAR

	OUTPUTS X	Y	HOR. INT.
Without Sq. Wave	+.004	+.006	
With Sq. Wave	+.004	+.006	

WITH THE SQ. WAVE ON THE LINE, THE FREQUENCY WAS VARIED BETWEEN 20 Hz - 20 Khz. A SLIGHT INCREASE IN OUTPUT NOISE ANGLE OCURRED AT 1.7 Khz. AT THIS FREQ. ACQUISITION AND TRACKING WAS DEMONSTRATED AT 23 AND 29 VOLTS DC INPUT.

6.0 PERFORMANCE TESTING (BEACON)

The source for all BEA mode tests is a 150w Xenon lamp. Attenuation of the beacon irradiance will be effected by means of an optical attenuator to simulate vacuum range, neutral density filters, and the MMOS lens iris. With no optical attenuation, the source will provide sufficient irradiance to cause automatic insertion of the attenuator and decrease of the dynode gain.

6.1 Source Calibration

Specification: none (This procedure will set the source irradiance)

Method: Place an optical attenuation of at least 10^5 times between MMOS and source. Also set the MMOS lens iris to its smallest opening prior to applying power. Following turn-on of the source and the MMOS, command the MMOS to AUTO mode. Open the iris as necessary to effect track lock. Upon successful tracking, move the tracker to null the X and Y outputs. Record the outputs on a Sanborn recorder. Using the TARGET MAGNITUDE indication, set the optical attenuation such that the irradiance at the MMOS is equivalent to a third magnitude star.

TARGET MAGNITUDE = .65 volts

Optical Attenuation: 5.4 ND

NOTE: At one time during tests using the Xenon source, measure its irradiance with a Pritchard photometer having an S-20 detector. Measure with a set of conditions, i.e., distance to source, optical attenuation, etc., so that the correlation between MMOS target magnitude indication and source irradiance can be checked.

PRITCHARD READING ON SOURCE AT SAME DISTANCE AND WITH SAME 5.4 N.D OPTICAL ATTENUATION WAS 1.6×10^{-6}.

$$H_S = (1.6 \times 10^{-6})(7.05 \times 10^{-8}) \frac{\text{METER}}{K}$$

$$= 1.13 \times 10^{-13} \text{ W/cm}^2$$

4-26-73
R. Peters

6.2 Sensitivity

Specification: Para. 3.2.8.1 - 3.2.8.4 - With a Xenon source equivalent to a +3mv or brighter Class G2 star, the MMOS performance values of sensitivity, acquisition time, and tracking accuracy will be the same as required for star tracking. The MMOS will have the capability of determining if the acquired and tracked target is a celestial object or a rendezvous beacon. This will be done by providing electronic circuitry which will detect the beacon modulation of 4.725 kHz and will activate a "beacon present" signal.

Method: Record the X and Y outputs during the following source conditions. Tabulate the noise angles in the following table from those recordings.

With an equivalent 3 mv target, increase the source modulation until a BEACON PRESENCE is recorded. Note and record the % modulation. Repeat this procedure using an equivalent 4 mv target.

SOURCE BASED ON SEC. 3.1	% MODULATION	TARGET MAGNITUDE VOLTAGE	OUTPUTS θ_N RMS (SEC)	
			X	Y
3.3mV ~~3mv~~	NONE	.65V	15.	12.
~~3mv~~ 3.3mV	(1.5 P-P / 5.8) 13%	1.45V	5.1	5.1
~~4~~ 2.2	NONE	1.55V	8.2	7.1
~~4~~ 2.2	(1.3 P-P / 5.8) 11%	2.00V	4.6	5.1

OPTICAL ATTEN WAS 5.0 N.D

4-26-73
R. Peters

6.3 Automatic Attenuation

Specification: Para. 3.2.9.4 - The MMOS will have a tube current sensing circuit which will be used to protect the anode portion of the tube from excessive currents. When the tube current exceeds a specified level to be determined by the contractor, the sensor will automatically insert into the optical path between the lens and the tube a neutral density filter or aperture with sufficient attenuation to prevent damage to the tube.

Method: Set the source to approximately the equivalent of a 3 mv star. Modulate the source such that a BEACON PRESENCE is indicated. Increase the source irradiance by removing optical attenuation. Monitor the TARGET MAGNITUDE and LO-MAP outputs as the irradiance is increased.

Record the outputs' levels at which the ATTEN status is gained. Also record the outputs' levels following the attenuator insertion. Continue to increase the source irradiance. Record the outputs' level just prior to and following gain of LOGN status.

EQUIV. STAR MAG	IRRADIANCE (EXTRAP-OLATED)	STATUS			MMOS OUTPUT	PRITCHARD DATA (NO MOD)	
		APER	ATTN	LOGN	TARGET MAG	READING	W/cm²
3		H	L	L			
	3.6 N.D.	H	L	L	2.95 NO 3.76 MOD	7.3×10^{-5}	5.15×10^{-12}
	3.4 N.D	L	H	L	.76 NO .90 MOD		
	1.0 ND	L	H	L	5.40 NO 5.76 MOD	1.3×10^{-2}	9.17×10^{-10}
	1.0 ND	L	H	H	2.20 NO 2.48 MOD		

4-26-73
R. Deters

7.0 PERFORMANCE TESTING (X-TAR)

The horizon simulator source will be used for these tests. Apertures and neutral density filters will be used to effect proper source dimensions and irradiance. The diffuse source brightness should be calibrated for 1,000 ft-lamberts.

7.1 Source Calibration

Specification: none (This procedure will set the source irradiance and reference null).

Method: Place an aperture of 0.010" diameter or less over the simulator diffuse source. Initially attenuate the optical signal by a factor of 10^6 using neutral density filters. Allow the MMOS to acquire and track in the AUTO star tracking mode. Remove filters as required to effect tracking. Position the target such that the outputs (X, Y) = (0, 0). Vary the optical attenuation until the intensity is that of a 2.0 ± 1.0 visual magnitude.

From Test Section 3.1

STAR MAG	TARGET MAGNITUDE (Volts)
3	+.81
2	+1.77
1	+3.00

A. Record the following:

TAR. MAG = 1.00 Volts

OPTICAL ATTEN. = 3.0 N.D.

4-26-73
R. Peters

B. Remove the aperture from the diffuse source and replace it with the 0.5^{o} aperture. Command the MMOS to the X-TAR mode. Note the following: ATTEN BECOMES POSITIVE

TARGET MAGNITUDE = 4.42 Volts

C. Remove optical attenuation gradually so that the ATTEN and LO GN status become positive. Remove all attenuation so that the MMOS is tracking the 1,000 ft-lambert source.

Note the following:

TARGET MAGNITUDE = 4.39 Volts

X ERROR = -.010 Volts

Y ERROR = +.125 Volts

4-26-73
R. Peters

7.2 Accuracy

Specification: Para. 3.2.7. The target for evaluation of the MMOS will be a fully diffused sphere with an angular dimension of 5.73° maximum. The MMOS will track the target with an accuracy of three arc minutes RSS.

Method: Use the source characteristics determined in Test Sec. 7.1(D) Record the X and Y outputs on a Sanborn recorder. With the MMOS commanded to the X TAR mode, demonstrate acquisition and tracking. Record the output voltages as a function of target size as it is increased to 4° diameter maximum. Note and record the minimum target size which can be tracked. Tabulate the following from the recordings. The AC RMS is the P-P divided by seven.

Target Diameter Angular Size	OUTPUTS							
	X				Y			
	DC		AC(RMS)		DC		AC(RMS)	
	mv	MIN	mv	Sec	mv	MIN	mv	Sec
4°	-.043	-2.55	NEG		+.054	3.23	NEG	
3°	-.048	-2.85			+.058	3.47		
2°	-.057	-3.38			+.035	2.10		
1°	-.040	-2.37			+.045	2.69		
0.5° (Min)	-.010	-.59			+.125	7.49		
0.5° REPEAT	-.012	-.71			+.120	7.71		

NOISE ANGLE (AC) IS NEGLIGIBLE COMPARED TO 270 Hz CROSS SCAN COMPONENT OF 60 mv P-P.

4-27-73

7.3 Tracking Performance

Specification: none

Method: Demonstrate acquisition and tracking of an irregular or asymmetrical target. Produce these targets by altering the variable aperture mask.

Comments:

1) HALF MOON (4°)
2) CROSS (4°)
3) SLIT (.5° x 4°)

ACQUISITION AND TRACKING WAS DEMONSTRATED ON THE THREE TARGETS.

4-27-73

8.0 PERFORMANCE TESTING (HI MAP, LO MAP, AND LMT)

The horizon simulator source will be used for all these tests except 8.1 and 8.2. Aperture plates and/or masks will be used to effect various targets. The MMOS output information will be observed on the Tektronix 604 Display Monitor. The X-ANGLE, Y-ANGLE, and LO VIDEO or HI VIDEO will be applied to the display monitor horizontal, vertical and Z-axis inputs respectively.

8.1 LO VIDEO Transfer Function - LO MAP

Specification: Para. 3.2.9.2. The radiant intensity analog voltage from the MMOS will be scaled according to the Specification column in the table below.

Method: Use the calibrated star simulator. With the MMOS in the AUTO mode, acquire, track, and boresight a third magnitude star. Command the MMOS to the LO MAP mode. Measure and record the LO VIDEO for the following star magnitudes.

STAR MAGNITUDE	LO VIDEO (Volts)	
	MEASURED	SPECIFIED
4	.2	< 0.25
3	.5	0.5
2	1.2	1.26
1	2.5	3.15
0.5	3.5	5.00
0	5.6	> 5.50
-1	9v	> 5.50

4-27-73

8.2 LO VIDEO Uniformity - LO MAP

Specification: Para. 3.2.9.3. The radiant intensity analog voltage shall be linearly dependent upon the input radiant intensity with a maximum deviation of ±15%.

Method: Set the star simulator to approximately a ~~first~~ 0 mag. magnitude star. Measure and record the LO VIDEO for the various positions in the LO MAP field-of-view tabulated below.

POSITION		LO VIDEO (Volts)
X	Y	
0	0	5.6 V
0	+2.5	4.5 V
0	+5.0	2 V
0	-2.5	4.4 V
0	-5.0	2.0 V
+2.5	0	4.0 V
+5.0	0	1.5 V
-2.5	0	4.2 V
-5.0	0	3.0 V
0	0	5.0 V (REPEAT)

4-27-73

8.3 HI VIDEO Transfer Function - HI MAP

Specification: Para. 3.2.9.2. The radiant intensity analog voltage gradient from the MMOS will be 0.5 volts per 1,000 ft-lamberts with 5.0 volts equal to 10,000 ft-lamberts.

Method: Calibrate the horizon simulator to provide a source brightness of 10,000 ft-lamberts. Command the MMOS to the HI MAP mode. Measure and record in the table below the HI VIDEO for various brightness levels. Optically attenuate the source to produce brightness levels down to 1,000 ft-lamberts.

SOURCE		HI VIDEO (Volts)	
FILTER	BRIGHTNESS* (ft-ℓ)	MEASURED	SPECIFIED
None	10,000	4.8V	5.00
.2 ND	6,310	2.85V	3.15
.4	3,981	1.65	1.99
.6	2,512	1.10	1.26
.8	1,585	.6	.79
1.0	1,000	.4	.5

4-27-73

* The 10,000 ft-ℓ brightness is calibrated. All others will be based on the neutral density filter transmission.

8.4 HI VIDEO Output Uniformity - HI MAP

Specification: Para. 3.2.9.3. The radiant intensity analog voltage shall be linearly dependent upon the input radiant intensity with a maximum deviation of ±15%.

Method: Set the source brightness to approximately 5,000 ft-lamberts. Observe the HI VIDEO output at various positions in the field-of-view. Note the source uniformity to insure that it does not contribute to any output variations.

COMMENTS: SHOWN BELOW IS THE HI MAP FIELD WITH HI-VIDEO READINGS AT RESPECTIVE POSITIONS ON THE FIELD.

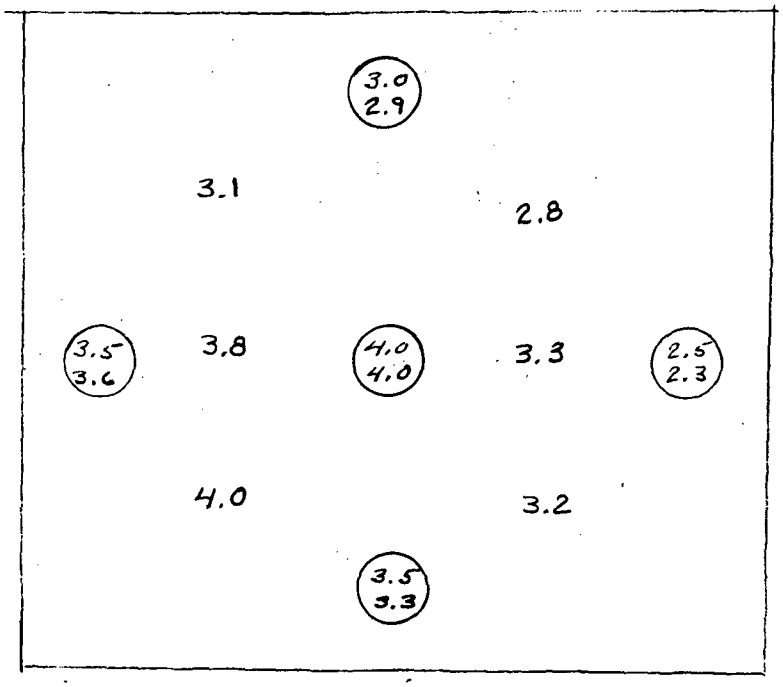

8.5 Automatic Over-Exposure Protection

Specification: Para. 3.2.9.4. The MMOS will have a tube current sensing circuit which will be used to protect the anode portion of the tube from excessive currents. When the tube current exceeds a specified level to be determined by the contractor, the sensor will automatically insert into the optical path between the lens and the tube a neutral density filter or aperture with sufficient attenuation to prevent damage to the tube. In the case of the LO MAP mode, activation of the neutral density filter by the current sensing circuit will also switch the mode to HI MAP mode, and latch it in this mode until overridden by an external command.

Method: Place an optical attenuation of approximately 10^6 times between the source and the MMOS. Command the MMOS to the LO MAP mode. Increase the source brightness by removing optical filters. Note the brightness at which the LO MAP status is lost and ATTEN status gained. Continue increasing the source brightness. Note the brightness at which the LO GN and HI MAP status are gained.

SOURCE		STATUS			
FILTERS	BRIGHTNESS	LO MAP	ATTEN	LO GN	HI MAP
		H	L	L	L
4.6 ND	.55 FL	L	H	L	L
2.0	8.6	L	H	H	H
0	8300	L	H	H	H

4-27-73

8.6 Display Monitor Presentation

Specification: Para. 3.2.9, 3.2.10. The MMOS will have a map mode of operation to provide graphical data for a CRT display. During operation in the map mode, the sensor will continuously scan its entire field-of-view and will provide a linear analog voltage output representative of the target scene average radiant intensity in each sequential position of the instantaneous field-of-view. During this time the sensor will also provide output voltages representing the center position of the instantaneous field-of-view for each element.

Method: Use various source patterns over the diffuse source. Command the MMOS to the desired mode and note the resultant display on the monitor.

Comments: THE DISPLAY MONITOR WAS UTILIZED IN THE MAJORITY OF TESTS IN THIS ATP. DUE TO AN INHERENT DELAY IN THE BUILDUP OF PHOSPHORESENCE IN THE DISPLAY MONITOR, THE RC CIRCUIT SHOWN WAS USED IN THE X ANGLE LINE TO THE DISPLAY MONITOR

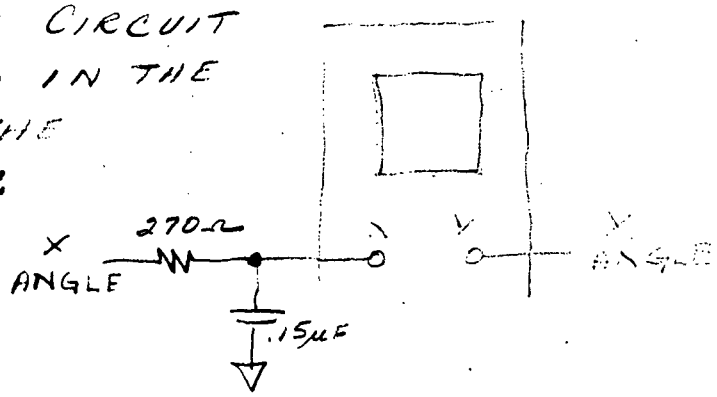

DISPLAY MONITOR
DELAY
CORRECTION

4-27-73
R. Deters

8.7 Landmark Track Scan Offset

Specification: Para. 3.2.10. In the landmark tracking mode, the two pointing command voltages will be scaled at 1.0 volts per degree with a range of from +5 volts to -5 volts. The pointing commands existing at the time that each reacquisition scan is initiated will be sampled and held throughout that scan. Any pointing commands arriving after the reacquisition scan has been initiated will be ignored until the next scan initiation.

Method: Command the MMOS to the LMT mode. Apply offset voltages to the X and Y OFFSET inputs. Note the gimballing of the LMT field-of-view about the total MAP field-of-view as a function of the offset voltage.

Comments:

THE LMT MODE WAS DEMONSTRATED BY OBSERVANCE OF THE LMT SCAN ON THE DISPLAY MONITOR. THE MANNER BY WHICH THE LMT SCAN IS LIMITED WITHIN THE 10° x 10° FIELD WAS DEMONSTRATED AND IS SHOWN BELOW.

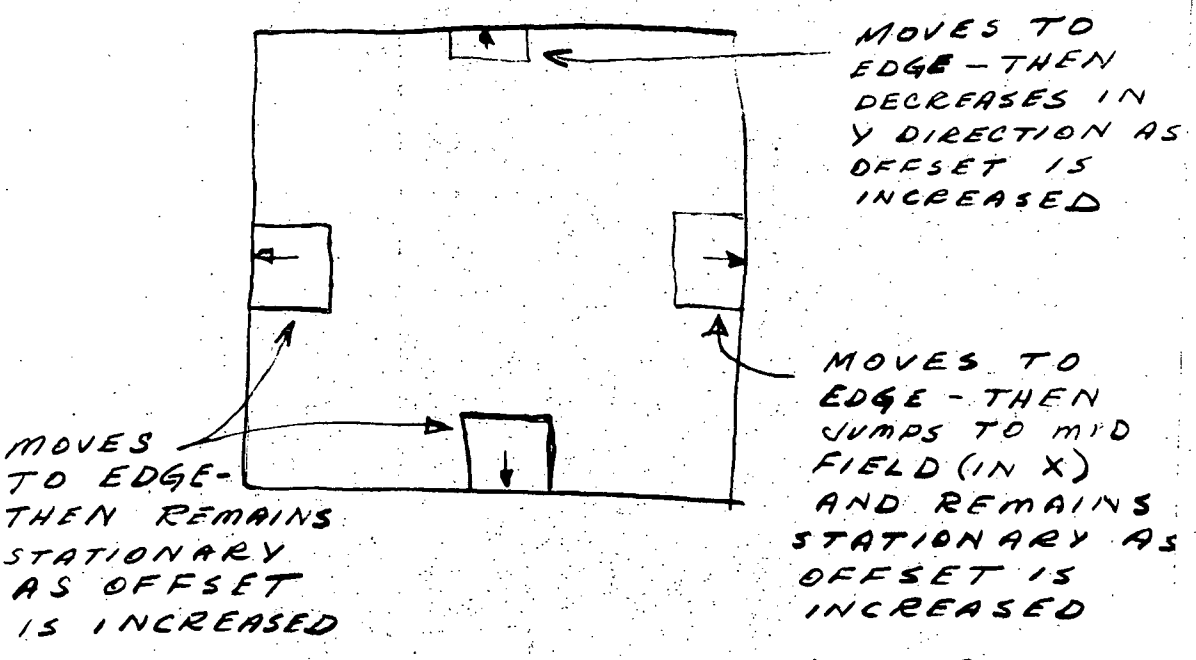

4-27-73

A ORIGINAL ISSUE	REVISIONS		
LTR	DESCRIPTION	DATE	APPROVED

5522973

SHEET NO.	1	2	3	4	5	6	7	8	9	10	11	12	13	14	15	16	17	18	19	20	21	22	23	24	25
ISSUE LTR.																									

NEXT ASSEMBLY USED ON	73-69402				

CONTRACT	ITT Federal LABORATORIES SAN FERNANDO, CALIF., U.S.A. A DIVISION OF INTERNATIONAL TELEPHONE AND TELEGRAPH CORPORATION
DWN Ann Kotz	
CKD R. A. Lo... 9/7/71	STAR SIMULATOR - MMOS CALIBRATION PROCEDURE
APPD	
ITTFL	SIZE A · CODE IDENT. NO. 90348 · 5522973
	SCALE · SHEET

1. SCOPE

1.1 The specification pertains to the procedure of simulating stellar targets with laboratory sources for testing the Multi-Mode Optical Sensor (MMOS). It involves establishing the standard, transferring from the standard to a lab test simulator, and extrapolating for the magnitude range desired.

2. GENERAL INFORMATION

2.1 The standard will be the NASA OAO star simulator which utilizes lamps calibrated by NBS. This [illegible] source calibrated to provide the irradiance of a second magnitude Class AO star at a distance D_{OAO} which is a parameter of the particular star simulator lamp used.

2.2 The transfer device will be the multiplier phototube (S-20) and optics of a MMOS.

2.3 The magnitude range needed for MMOS tests is -1 to +3. These simulations will be made with an ITT A/OD collimated source.

3. EQUIPMENT

- NASA OAO Star Simulator
- Multi-Mode Optical Sensor
- ITT A/OD Collimated Star Source
- Voltmeter
- Ammeter

4.0 STANDARD CALCULATION

4.1 A tabulation of the following curves are required:

a) Absolute Spectral Response Class AO Star
b) Absolute Spectral Response NASA OAO Star Simulator
c) Relative S-20 Spectral Response of the MMOS phototube.
d) Relative Optics Spectral Characteristics

4.2 The following product sums using the tabulations above are required:

a) Star and S-20 plus Optics
b) Simulator and S-20 plus Optics

DRAWING NO. 5522973

PREPARED BY	DATE	SIZE	CODE IDENT. NO.	
CHECKED BY	DATE	A	90348	5522973
				SHEET 2 of 8

4.3 The NASA OAO star simulator produces an illuminance equivalent to that of a second visual magnitude star at a distance D_{OAO} from the source. The correcting formula for the particular S-20 response is then:

$$m_{OAO} = 2 + 2.5 \log \frac{\text{STAR X(S-20 + Optics)}}{\text{SS X(S-20 + Optics)}}$$

4.4 If the distance D_o between the simulator and MMOS is other than D_{OAO}, a correction factor of the distance ratio squared must be added to the above formula.

$$m_o = 2 + 2.5 \log \frac{\text{STAR X(S-20 + Optics)}}{\text{SS X(S-20 + Optics)}} - 5 \log \frac{D_{OAO}}{D_o}$$

5.0 MMOS CALIBRATION

5.1 Mount MMOS at a distance of 15 feet or greater from the SS such that it can be adjusted vertically and horizontally.

5.2 NASA OAO SS must be operated in accordance with its operating instructions.

5.3 With no deflection currents to the MMOS, center it on the SS star by maximizing the tube output current.

5.4 Maximize the current by varying optical focus and MMOS position.

5.5 Record both D_o and I_o as this is the standard star of magnitude m_o.

6.0 -1 to +3 MAGNITUDE RANGE CALCULATION

6.1 Construct a graph with I as a $\log_{10}$ function and m as a linear function. The function should be a line passing through (I_o, m_o) with a slope of 2.51 (largest I corresponding to brightest star, i.e. - m's).

PREPARED BY	DATE	SIZE	CODE IDENT. NO	
		A	90348	5522973
CHECKED BY	DATE			SHEET 19

ITTFL DIE(S)-V REV 4/61

DRAWING NUMBER 5522973

7.0 DATA TRANSFER

7.1 Mount MMOS in line with the ITT A/OD collimated star source.

7.2 Vary filter position & source current to provide the various tube output currents corresponding to the desired magnitudes from the graph of Sec. 6.1.

7.3 Tabulate the current and filter positions for the various magnitudes.

Federal LABORATORIES
SAN FERNANDO, CALIF., U.S.A.
A DIV. OF INT. TEL. & TEL. CORP.

PREPARED BY	DATE	CODE IDENT. NO.	DWG.	5522973
CHECKED BY	DATE	90348	A SIZE	SHEET 4 of 9

NASA OAO 68 Lamp #

D_{OAO} = 26.8"

F4012 Tube; S/N 067204

(STAR)(S-20 + Optics) = .2274

SOURCE (S-20 + Optics) = .2133

RATIO = 1.0661

m_{OAO} = 2 + 2.5 log 1.0661

= 2 + 2.5 (.0278)

= 2.0695

D_o = 16'

I_o = 68 NA

$m_o = 2.0695 - 5 \log \frac{D_{OAO}}{D_o}$

= 2.0695 - 5 (.22401)

m_o = 2.0695 - 1.12

= .95

(I_o, m_o) = (68 NA , .95)

PREPARED BY	DATE	SIZE	CODE IDENT. NO.	5522973
CHECKED BY	DATE	A	90348	SHEET 1 of 9

TABLE 4.1 a

ABSOLUTE SPECTRAL IRRADIANCE
SAOV SECOND MAGNITUDE - CLASS AOV

(Angstroms)	W(pw/ft^2/10mu	(Angstroms)	W(pw/ft^2/10mu)
		5500	5.41
		5600	5.12
3000	4.73	5700	4.86
3100	4.64	5800	4.59
3200	4.56	5900	4.48
3300	4.47	6000	4.27
3400	4.39	6100	4.08
3500	4.30	6200	3.89
3600	4.19	6300	3.70
3700	4.20	6400	3.52
3800	7.92	6500	3.36
3900	10.70	6600	2.94
4000	11.26	6700	3.03
4100	9.02	6800	2.91
4200	10.91	6900	2.80
[illegible]	10.99	[illegible]	[illegible]
4400	9.76	7100	2.60
4500	9.23	7200	2.50
4600	8.70	7300	2.41
4700	8.20	7400	2.29
4800	7.77	7500	2.20
4900	7.12	7600	2.11
5000	6.97	7700	2.06
5100	6.62	7800	1.99
5200	6.30	7900	1.90
5300	5.99	8000	1.84
5400	5.70	8100	1.79
		8200	1.74
		8300	1.98
		8400	1.88
		8500	1.80

TABLE 4.1-b

ABSOLUTE SPECTRAL IRRADIANCE
NASA OAO STAR SIMULATOR AT D_{OAO}

(Angstroms)	W(pw/ft^2/10mu)	(Angstroms)	W(pw/ft^2/10mu)
		5500	5.90
		5600	5.63
3000	0.00	5700	5.49
3100	0.00	5800	5.09
3200	0.00	5900	4.56
3300	0.00	6000	4.15
3400	0.00	6100	3.75
3500	0.01	6200	3.62
3600	0.64	6300	3.75
3700	1.47	6400	3.62
3800	2.65	6500	3.35
3900	4.82	6600	2.95
4000	7.25	6700	2.68
4100	9.38	6800	2.68
4200	10.40	6900	2.68
4300	10.90	7000	2.95
4400	10.60	7100	3.62
4500	10.00	7200	4.29
4600	9.25	7300	5.09
4700	8.17	7400	5.90
4800	7.64	7500	6.97
4900	7.10	7600	7.37
5000	6.57	7700	7.84
5100	6.16	7800	8.31
5200	5.76	7900	8.65
5300	5.90	8000	8.98
5400	5.90	8100	9.32
		8200	9.65
		8300	10.33
		8400	11.00
		8500	11.55

PREPARED BY	DATE	CODE IDENT. NO. 90348	DWG. A SIZE	5522 973
CHECKED BY	DATE			SHEET 7 of 9

TABLE 4.1-c

RELATIVE SPECTRAL RESPONSE
P4012 S/N 067204

(Angstroms)	I/Io	(Angstroms)	I/Io
		5500	45.0
		5600	43.5
3000	8.0	5700	41.5
3100	37.0	5800	40.0
3200	50.0	5900	38.5
3300	57.0	6000	37.0
3400	62.0	6100	35.5
3500	66.0	6200	34.0
3600	70.0	6300	32.5
3700	72.0	6400	31.5
3800	74.0	6500	30.0
3900	74.0	6600	29.0
4000	73.0	6700	28.0
4100	72.0	6800	27.0
4200	69.0	6900	26.0
4300	67.0	7000	24.5
4400	65.0	7100	23.5
4500	63.0	7200	22.5
4600	61.0	7300	21.0
4700	60.0	7400	20.0
4800	58.0	7500	18.5
4900	56.0	7600	17.0
5000	54.0	7700	15.0
5100	52.0	7800	13.7
5200	50.0	7900	12.0
5300	49.0	8000	10.5
5400	47.0	8100	9.0
		8200	7.5
		8300	6.0
		8400	5.0
		8500	3.7

PREPARED BY	DATE	CODE IDENT. NO. 90348	DWG. A SIZE	5522973
CHECKED BY	DATE			SHEET 8 of 9

TABLE 4.1-G

RELATIVE SPECTRAL RESPONSE
MMOS LENS - ANGENIEUX 2.0 INCH f/0.95

(Angstroms	T/To	(Angstroms)	T/To
		5500	
		5600	
3000		5790	
3100		5800	
3200		5900	
3300		6000	
3400		6100	
3500		6200	
3600		6300	
3700		6400	
3800		6500	
3900		6600	
4000		6700	
4100		6800	
4200		6900	
4300		7000	
4400		7100	
4500		7200	
4600		7300	
4700		7400	
4800		7500	
4900		7600	
5000		7700	
5100		7800	
5200		7900	
5300		8000	
5400		8100	
		8200	
		8300	
		8400	
		8500	

PREPARED BY DATE

CHECKED BY DATE

CODE IDENT. NO. 90348 | DWG. A SIZE | 5522973

SHEET 9 of 9

S/N 067204 8/31/72

61 0.30000004E 04 SAOV-AEROBEE
61 0.30000004E 04 F4012 S/N 06720
61 0.30000004E 04 MMOS LENS
51POINTS DELTA= 10.0000 INTEGRAL= 0.22741284E 06

S/N 067204 8/31/72

61 0.30000004E 04 S SS DETERS
61 0.30000004E 04 F4012 S/N 06720
61 0.30000004E 04 MMOS LENS
51POINTS DELTA= 10.0000 INTEGRAL= 0.21329131E 06